Research of Noise and Vibration Analysis for Structures Involving Transfer Path and Sound Source

HILMI BIN HELA LADIN

2015

Research of Noise and Vibration Analysis for Structures Involving Transfer Path and Sound Source

Doctoral Thesis

By

HILMI BIN HELA LADIN

Supervised by Prof. Nobutaka TSUJIUCHI

Doshisha University

2015

TABLE OF CONTENTS

CHAPTER 1

Introduction

1.1. Background

In the advancement of industrial machineries and transportation today, considerable emphasis is being put to place to merge the technological advancement with the aspects of daily life comfort. Rising demands of a more eco-friendly technology have motivated manufacturing industries to discover and develop new methods to improve their product. Thus, various works have been done in order to improve the suitability of industrial machineries and transportation to the environment around us. Besides that, not only are industries working to develop a more eco-friendly technologies, but the rising of global prices on natural resources which leads to the increased cost in production, forced industries as well as researchers to develop more efficient methods in order to reduce production costs and time, improve reliability, safety and overall value.

Industrial sectors, for example, rely heavily on internal combustion engines such as diesel engines and gas engines as the power source of their machineries. The efficiency of diesel engine was used as the power sources for various machines such as agricultural machines, construction machines and emergency power generators. However, heavy industrial machineries as well as transportation machines are often the main source of the pollutions problems particularly noise and vibration pollution. Therefore, the demands to improve these technologies have become the main focus or researchers around the globe.

In recent years, the noise and vibration pollution issues are still being observed, particularly in Japan, environmental issues are taken very seriously. Therefore regulations and laws regarding the guidelines and restrictions for the noise and vibration radiations from industries as well as transportations are being revised every year. The Japanese Ministry of the Environment conducted fiscal surveys to investigate the percentages of complaints by noise and vibration sources as shown in Figure 1.1 and Figure 1.2. Based on the figures, it is understood that most of the complaints are from the noises and vibrations that came from construction works and factory plants. These are the places that most of the heavy machines are involved where the noises and vibrations come from engines, heavy loading, and so on. Therefore, extensive researches are being conducted to improve these sectors, as the demands for better environment for the society and workers are still rising.
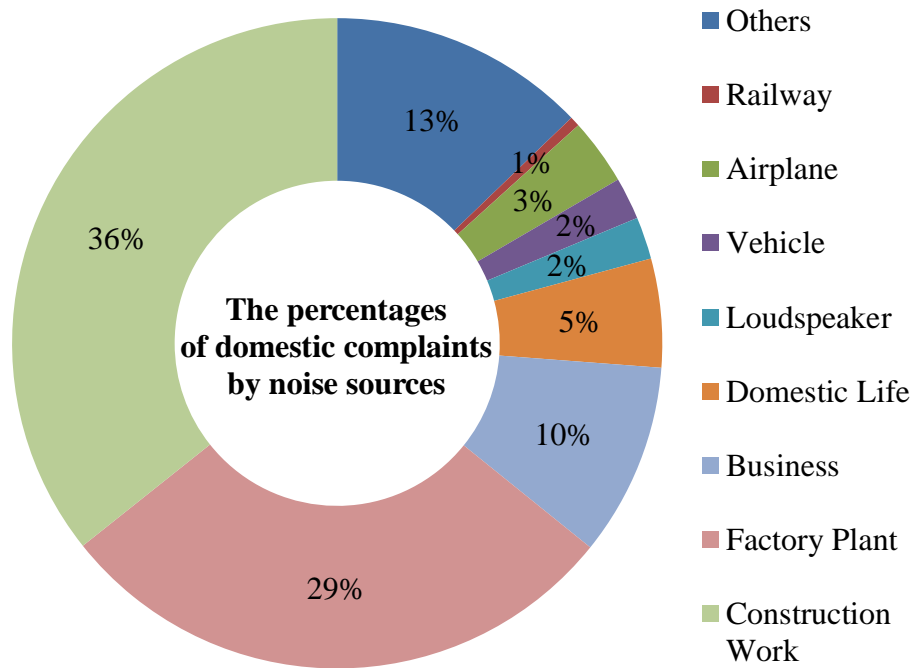
Figure 1.1 The percentages of domestic complaints by noise sources (The results of noise regulation law enforcement survey for fiscal 2013 by the Japanese Ministry of the Environment)
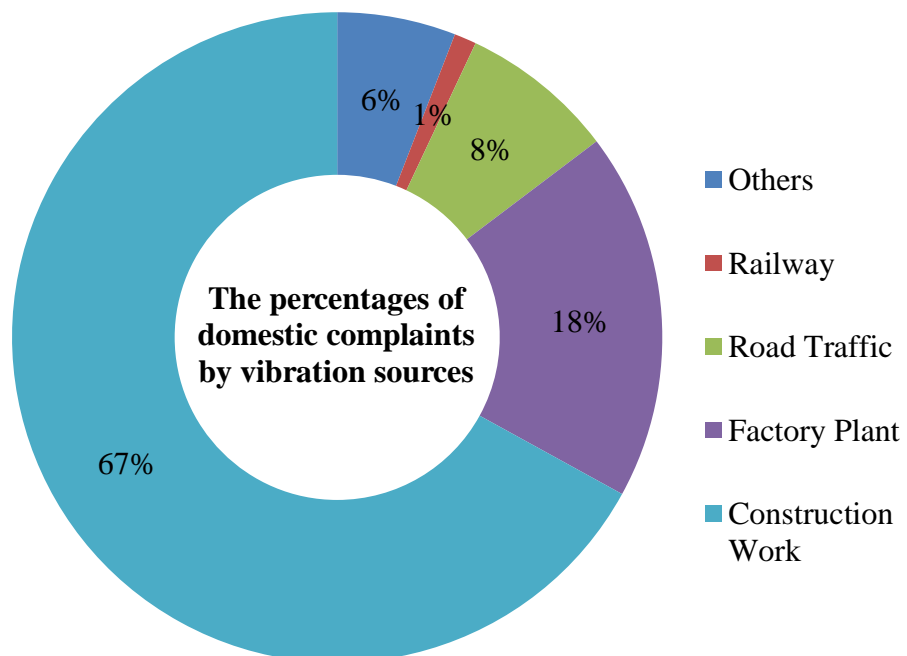
Figure 1.2 The percentages of domestic complaints by vibration sources (The results of vibration regulation law enforcement survey for fiscal 2013 by the Japanese Ministry of the Environment)

Noise and vibration sources can be classified into airborne, structure-borne and fluid-borne noise. The noise that is emitted directly from machines causing the air particles to vibrate and produce noise is called airborne noise, while the noise emitted by the vibration from machines that transferred along structures is called structure-borne noise. Besides that, there is also fluid-borne noise, which will not be the focus of this research.

There are several conventional methods to reduce airborne noise. The most common method to reduce airborne noise is through noise insulation using sound insulation materials such as glass wool placed between panels. Even though this method is an established base in civil engineering involving double walls or double panels of a room[1], it is not a practical method for machineries as it will increase the size and weight thus increasing costs and will be less efficient. On the other hand, one of the conventional methods to reduce structure-borne noise involves applying damping treatment with damping materials on the structures involved. However, the effectiveness of damping treatments depends upon design parameters such as choice of damping materials, locations and size of the treatment[2]. Therefore, more efficient ways to reduce noise and vibration in machines are gaining attention amongst researchers and industries.

In order to realize this, are to develop new and improved methods particularly developing experimental and analytical simulation techniques. These techniques could improve the noise and vibration reduction efficiency by pre-modification analysis and prediction, thus reducing the need of extensive trial and error during experiments and structural modifications, which will reduce production costs and time.

1.2. Literature Review and Research Objective

In an industrial machines, internal combustion engine are commonly used as the main power source because of its efficiency. However, the drawbacks of using these engines are the high radiation of noise and the vibration that transferred along the structure of the machines.

In order to reduce the level of noise produced from the engine, modifications need to be done on the engine or the structure of the machine itself. As stated in 1.1, numerical simulation technique is needed in order to predict and simulate noise radiation beforehand, so that only certain parts of the structure needed to be focused on for the modification. Moreover, other than the main noise source which in this example is the engine, the noise source from the vibration of structure needed to be accurately identified. Vibration measurement technique using accelerometers are the simplest method to measure the surface vibration of a structure which could identify the noise radiation. However, there is possibility the surface vibration does not contribute significantly to the noise radiation due to the fact that surface vibration below coincidence frequency is a poor radiator[3]. Thus, this will cause unnecessary modification for noise reduction. Therefore, an effective method called inverse numerical acoustic analysis which can identify the surface vibration of a sound source

from measured field point sound pressures and calculated transfer function by boundary element method, could be applied[3][4].

In inverse numerical acoustic analysis (INA), the surface vibration of sound source is identified by obtaining the pseudo inverse matrix of the transfer function. This is because the number of sound source vibration points for identification are often larger than the sound pressure measurement points, thus the transfer function matrix is rarely a regular matrix[5]. However, the problems faced by this method are that the calculation error of pseudo inverse matrix and sound pressure measurement error can have a significant influence on the identification result. Furthermore, when the vibration of a machine structure is calculated, the identification result using inverse numerical acoustic analysis does not obtain high accuracy because of noise-emitting sources in the form of airborne noise. Although good identification could be achieved with structure-borne noise[6][7], different approach is needed to identify the sound source when dealing with airborne noise. Besides that, sound pressure measurement points selection technique is needed to reduce the effect of airborne noise error. A square lattice shape arrangement of measurement points is common in inverse numerical acoustic analysis, and recently circular shape arrangement[8] was also introduced. However, when it comes to dealing with more complex structure, different approach is needed which can adapt to the change of radiation concentration in complex structure.

Noise and vibration prediction method using Finite Element Method (FEM) and Boundary Element Method (BEM) are effective for low frequency range. However, in order to analyze structure-borne noise and vibration it is necessary to consider the overall audible frequency range including the high frequency range noise and vibration which Statistical Energy Analysis (SEA) is known to be effective. SEA method which was first introduced in the 1960's by Lyon et.al, as a response prediction method for acoustic and vibration system of aerospace sector, is an effective method to predict high frequency range of noise and vibration[9]. In order to predict the vibration, it is necessary to estimate the SEA parameters called damping loss factors (DLF) and coupling loss factors (CLF). The loss factors could be experimentally estimated by conducting excitation tests on a single subsystem[10-13]. However, for a complex structures, it is difficult to estimate the loss factors by conducting single subsystem excitation tests. Therefore, Power Injection Method (PIM) was proposed where it is possible to evaluate the loss factors for complex structures even when all the subsystems are connected together[14]. When conducting the analysis, a system is divided into simplified subsystems in order to estimate the parameters accurately. In addition, because the numbers of measurement points affects the accuracy of parameters estimation and vibration prediction, multiple points of vibration measurements are carried out during experiments. However, there is no guidance in determining specific measurement points. In addition, when there was a structural modification on a subsystem, parameters had to be estimated again on the entire system, thus increasing the number of experiments that needs to be conducted.

In SEA, previous research established an external input power identification technique for simple and practical structure using finite element method[15-17]. The results of the

energy analysis models were excellent in cases with unclear input force locations. The identification of input powers was found to be effective and quantitatively accurate if the location and number of excitation and response points could be appropriately distributed within the subsystem. In regards to input power, the relation between sound power in a car interior and structural input power on the car body have been discussed[18]. To realize low noise in the car interior, component engineering was required in order to identify the structural input power accurately. However, SEA is ineffective when dealing with multiple components. On the other hand, transfer path analysis (TPA) is based on estimation of a frequency response function (FRF) between the excitation points and response points. Identifying the input forces is trivial when their locations are obvious. The response contributions of transfer paths can then be evaluated after identifying the vibration and noise sources. TPA has been employed in several previous research studies on identifying input forces where a novel approach was proposed that used an apparent-mass matrix instead of a matrix inversion method to improve the accuracy of input identification[19]. To improve the accuracy of SEA results, research has also been conducted in which the input power in SEA is calculated by utilizing the force predicted by TPA[20]. However, a study comparing the input powers and contribution rates determined by SEA and TPA are still in working progress.

From the discussions based on the existing literature above, it is clear that in spite of extensive research effort, many new areas are still to be discovered regarding the best approach in noise and vibration analysis for structures especially involving sound source identification and transfer path of vibration contribution. These new areas can be broadly divided as the following questions;

1. How do we approach the sound source identification involving airborne noise for complex structures?

2. How do we approach in estimating damping loss factor when the structure have been modified?

3. Could we merge two effective structural dynamics analysis method which is SEA and TPA in order to solve the dynamics of a complex structure?

Based on the above statement, our research objective is to develop new approaches from the existing experimental and analysis technique of noise and vibration for structures, in order to improve their efficiency and reliability of noise and vibration reduction. Firstly, to specify the sound source, after verifying that good accuracy was achieved in sound source identification from structure-borne excitation using INA, we needed to establish the effect of airborne noise on the accuracy of sound source identification. Thus, new approaches are proposed to reduce the identification error by using different boundary condition and new placement technique of sound pressure measurement points. Secondly, we establish the new approach in vibration analysis and prediction of structure-borne noise using SEA. We proposed a damping loss factors estimation technique which can determine the damping loss factors of a modified structure. Thirdly, in order to effectively solve the dynamics of complex structures, we establish the possibility of combining the theory of TPA and SEA by proposing

comparison method. After verifying the comparison method in numerical analyses, the new method is taken to application on real structure by in order to verify the validity on real world application. These issues will be discussed in this dissertation.

1.3. Thesis Structure

In the first chapter, the background of this research regarding the pursuit of improving the environment particularly noise and vibration pollution was emphasized. The literature review and objective of this research are mentioned which is to develop new approaches from the existing experimental and analysis technique of noise and vibration for structures, in order to improve their efficiency and reliability of noise and vibration reduction.

In the second chapter, the development airborne of noise and vibration analysis and prediction technology using inverse numerical acoustic analysis is mentioned. The verification of the influence of airborne noise on sound source identification and vibration prediction accuracy is mentioned. In order to tackle this problem, new approach in the placement of sound pressure measurement technique is also described.

In the third chapter, the development of vibration analysis method for damped structure using statistical energy analysis method is mentioned. This chapter focused on structure-borne noise and vibration analysis, while verifying the influence of the number of vibration measurement points on the vibration response prediction. Moreover, the proposal of damping loss factors estimation method for modified structure which is represented by damped structure is described.

In the fourth and fifth chapter, the development of comparison method of statistical energy analysis and transfer path analysis is mentioned. As a basic study to compare both of these methods, an evaluation method is proposed to compare SEA and TPA for multiple excitation input sources and transfer path contributions between excitation sources and evaluation points. The validity of the proposed method is verified from numerical analyses and experimental verification using real structure.

Lastly, in the sixth chapter, the conclusions obtained in this research and the suggestions for future work are mentioned.

References

[1] Fahy F. J., 1985, Sound and Structural Vibration – Radiation, Transmission and Response, Academic Press Ltd, London.

[2] Subramanian, S., Surampudi, R., Thomson, K., Vallurupalli, S., 2003, "Optimization of Damping Treatment for Structure Borne Noise Reduction," SAE Technical Paper, (2003-01-1592).

[3] Williams, E. G., 1999, Fourier Acoustics – Sound Radiation and Nearfield Acoustical Holography, Academic Press Ltd, London.

[4] Gardner, B. K. and Bernhard, R. J., 1988, "A Noise Source Identification Technique Using an Inverse Helmholtz Integral Equation Method," Journal of Vibration and Acoustics, ASME, **110**(1), pp. 84-90.

[5] Tournour, M., Brux, P., Mas, P., Wang, X., McCulloch, C., and Vignassa, P., 2003, "Inverse Numerical Acoustics of a Truck Engine," SAE Technical Paper, (2003-01-1692).

[6] Kobayashi, A., 2011, "Verification of Coverage of Inverse-numerical Acoustic Analysis," Proceedings of the 29th IMAC A Conference on Structural Dynamics, **9**, pp. 73-80.

[7] Hilmi, H. L., Koizumi, T., Tsujiuchi, N., Maruo, K., and Uehara, H., 2013, "Construction of Sound Source Model of Gas Engine Using Inverse-Numerical Acoustic Analysis," Proceedings of the 5th International Operational Modal Analysis Conference, pp. 370-377.

[8] Nakano, Y., and Yoshimura, T., 2013, "Precision Improvement of Identification of the Sound Source by Inverse Acoustic Analysis (In Japanese)," Transactions of the JSME©, **79**(801), pp. 1495-1504.

[9] Lyon, R. H., and DeJong, R. G., 1995, Theory and Application of Statistical Energy Analysis, Butterworth-Heinemann, Boston.

[10] Lai, H.-Y., 2007, "Experimental Comparison of Test Methods for Structure-borne Sound Power Measurement," SAE Tech. Pap., (2007-01-2169).

[11] Bolduc, M., Atalla, N., and Wareing, A., 2005, "Measurement of SEA Damping Loss Factor for Complex Structures," SAE Tech. Pap., (2005-01-2327).

[12] Pocha, J., 1977, "Acoustic Excitation of Structures Analyzed by the Statistical Energy Method," AIAA J., **15**(2), pp. 175-181.

[13] Crocker, M. J., and Price, A. J., 1969, "Sound transmission using statistical energy analysis," J. Sound Vib., **9**(3), pp. 469-486.

[14] Bies, D. A., and Hamid, S., 1980, "In situ determination of loss and coupling loss factors by the power injection method," J. Sound Vib., **70**(2), pp. 187-204.

[15] Kuroda, K., and Yamazaki, T., 2013, "A Study on Comparison between Input Powers and Contribution Rates from Statistical Energy Analysis and Transfer Path Analysis on a Mechanical Structure," Journal of System Design and Dynamics, **7**(4), pp. 504-515.

[16] Kuroda, K., Yamazaki, T., Hilmi, H. L., and Koizumi, T., 2013, "Comparison between Input Powers and Contribution Rates from Energy Analysis and Transfer Path Analysis on Thin-Walled Plane Frame Structures," Proceedings of 15th Asia Pacific Vibration Control Conference, pp. 1326-1330.

[17] Kuroda, K., Yamazaki, T., 2012, "Comparison of SEA and TPA for Input Source and Contribution Rates," The Proceedings of 41st International Congress on Noise Control Engineering, pp. 8307-8318.

[18] Kadomatsu, K., and Iwanaga, Y., 2002, "Vibro-Acoustic Transfer Function and Driving-Point Conductance for Vehicle Body (in Japanese)," Transactions of the Japan Society of Mechanical Engineers. C, **68**(676), pp. 3561-3565.

[19] Kobayashi, S., and Yoshimura, T., 2009, "Identification of Excitation Force Spectra Using Apparent-Mass Matrix (in Japanese)," Transactions of the Japan Society of Mechanical Engineers. C, **75**(753), pp. 1500-1507.

[20] David, C., Herrin, W. D., Harvind, R., and Jiantie, Z., 2011, "Obtaining Structure-Borne Input Power for a SEA Model of an Earthmoving Machine Cab," SAE Technical Paper, 2011-01-1732.

CHAPTER 2

Development of Airborne Noise and Vibration Analysis Using Inverse Numerical Acoustic Analysis Method

2.1. Introduction

In the pursuit for noise reduction of machine structure, in many cases it is necessary to identify the sound source of the unwanted noise. Typically, in sound source identification the vibration is generally measured with accelerometers or transducers. However, the difficulties of mounting accelerometers on the surface of hot structures such as an engine or measuring vibration of a thin plate structure where mounting accelerometers could affect the measurement results, needed to be taken into consideration. In order to overcome these difficulties, an effective method called inverse numerical acoustic analysis which can predict the surface vibration of a sound source from measured field point sound pressures and calculated transfer function by boundary element method, could be applied[1][2].

In inverse numerical acoustic analysis (INA), the surface vibration of sound source is identified by obtaining the pseudo inverse matrix of the transfer function. This is because the number of sound source vibration points for identification are often larger than the sound pressure measurement points, thus the transfer function matrix is rarely a regular matrix[3]. However, the problems faced by this method are that the calculation error of pseudo inverse matrix and sound pressure measurement error can have a significant influence on the identification result.

Furthermore, when the vibration of a machine structure is calculated, the identification result using inverse numerical acoustic analysis does not obtain high accuracy because of various factors. One of the factors that need to be considered is the noise-emitting source's form in the form of structure-borne and airborne.

In this chapter, we aim to verify the influence of airborne noise on the accuracy of vibration identification using INA. We focused on an oil pan model which represents a component that is susceptible to the combustion noise (airborne) and the vibration from the engine (structure-borne). On previous work[4][5], we verified that with structure-borne excitation, we achieved good agreement on the vibration identification of sound source. But with airborne noise excitation there were different trends in vibration energy level especially for low frequency region[6].

Moreover, in order to reduce the effect of error from the airborne noise during measurement, we proposed a placement technique of sound pressure measurement points using space filling design from the design of experiments. Microphones arrangement in sound pressure measurement is generally in square lattice shape. Nakano et.al proposed and verified in simulation that by arranging sound pressure measurement points in circular shape it was possible to reduce the influence of measurement error and thus stabilizes the analysis[7]. The arrangement of an arbitrary numbers of sound pressure measurement points could be determined using space filling design. In addition, the advantage of using space filling design is that it can effectively estimate the vibration of sound source with different aspect ratio[8]. The proposed technique is verified with simulation and experiment.

2.2. Inverse Numerical Acoustic Analysis Theory

The relation between sound pressure and surface vibration can be written as the following equation:

$$\{p\} = [H]\{v\} \tag{2.1}$$

where $\{p\}$ is the vector of sound pressure at m field points, $\{v\}$ is the vector of normal velocity at n surface points of the sound source, and $[H]$ is the $m \times n$ transfer function matrix set up by the Boundary Element Method (BEM).

Inverse-numerical acoustic analysis is the inverse problem of solving Equation (2.1) for the unknown $\{v\}$ given the vector of measured sound pressure $\{p\}$. Surface vibration velocity $\{v\}$ can be obtained by the matrix inversion method. However, the inverse matrix of the matrix $[H]$ cannot always be obtained because $[H]$ is not usually a regular matrix. Instead of the inverse matrix, the pseudo inverse matrix is widely used in sound source identification, as in the following equation:

$$\{v\} = [H]^+\{p\} \tag{2.2}$$

where $[H]^+$ is a pseudo inverse matrix of $[H]$.

In calculation of a pseudo inverse matrix, singular value decomposition was applied. By using a singular matrix, the transfer function matrix can be written as the following equation:

$$[H] = [V][\Sigma][U]^H \tag{2.3}$$

where $[V]$ and $[U]$ are an $m \times m$ unitary matrix and an $n \times n$ unitary matrix satisfying $[V]^H[V] = [U]^H[U] = I$, and $[\Sigma]$ is a diagonal matrix containing the singular values of [H] in non-increasing order. The total number of singular values is $\min(m, n)$, generally m. Here superscript H means the complex conjugate transposition.

From Equation (2.3), the pseudo-inverse matrix of [H] can be obtained as follows:

$$[H]^+ = [U][\Sigma]^+[V]^H \tag{2.4}$$

In this calculation, the pseudo-inverse matrix is sensitive to $[\Sigma]^+$. Generally $[H]$ is ill conditioned, so that $[\Sigma]$ contains small values. This results in $[\Sigma]^+$ containing huge values and $[H]^+$ becomes unreliable. To avoid this problem, huge terms of $[\Sigma]^+$ are set to zero. A criterion for dropping small singular value is called Tolerance. Tolerance is defined as follows:

$$Tolerance = \sigma_i/\sigma_1 \tag{2.5}$$

where σ_1 is the maximum singular value in the singular matrix $[\Sigma]$ and σ_i is the minimum singular value in the singular matrix$[\Sigma]$. Tolerance is determined from the L-curve criterion, which is based on a plot of the result norm versus the corresponding residual norm in a log-log scale.

In this paper, the surface normal velocity $\{v\}$ is given as follows:

$$\{v\} = [U]\begin{bmatrix} 1/\sigma_1 & 0 & & \cdots & & 0 \\ 0 & \ddots & & & & \\ & \ddots & 1/\sigma_i & \ddots & \ddots & \vdots \\ \vdots & \ddots & & 0 & & \\ & & & \ddots & \ddots & 0 \\ 0 & & \cdots & & 0 & 0 \end{bmatrix}[V]^H\{p\} \tag{2.6}$$

Therefore, it is important to select the appropriate tolerance because a small tolerance causes large errors because of huge inverse matrix values and a large tolerance causes large errors because of information loss [9][10].

2.3. Experimental Verification of Sound Source Model Identification Using Inverse Numerical Acoustic Analysis Method

2.3.1. Experimental Conditions
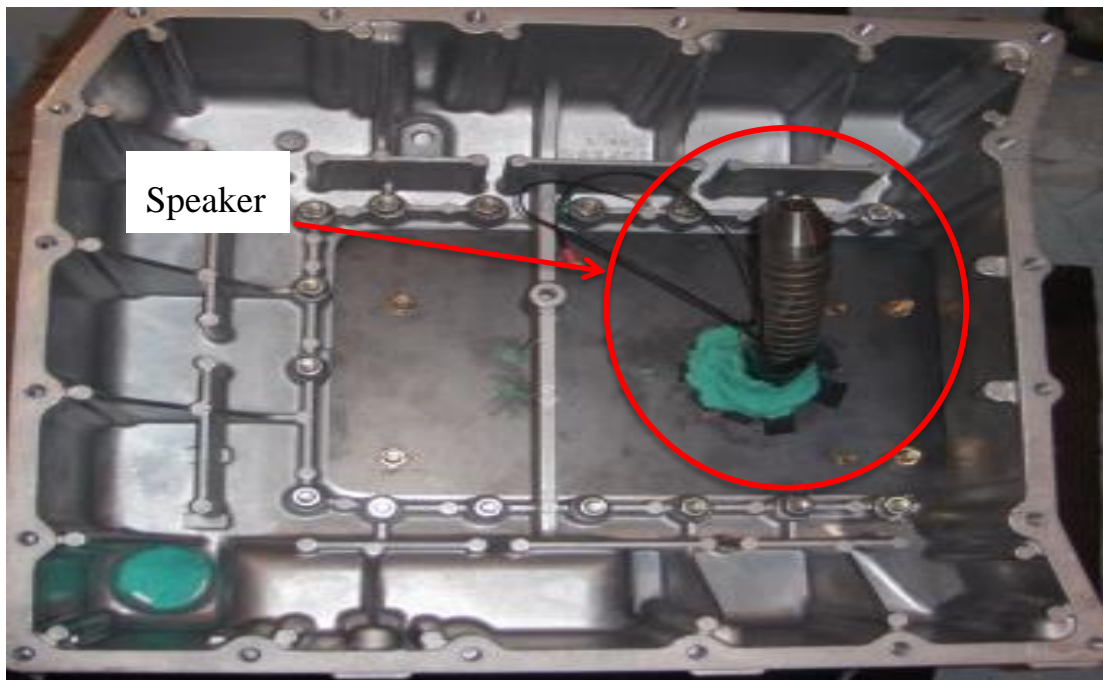
Figure 2.1 Oil pan inside view for speaker test (upper) and shaking test (lower)

Figure 2.1 shows the oil pan used as the experimental target. The oil pan (440x405x225mm) is made of aluminium with average thickness of 4mm. The speaker test using a volume speaker and shaking test using F3 shaker, was done in a semi-anechoic room. The input frequency region was 400-2000Hz, and it was excited by a random signal. In this study, to identify the surface vibration of the oil pan, we had to measure sound pressure from only the oil pan. Therefore, to avoid transmitting the vibration downward, the oil pan was fixed to an iron plate, and an isolation rubber was installed. Moreover, to prevent sound leakage, clay and pugging were installed.

2.3.2. Radiated Sound Pressure Measurement
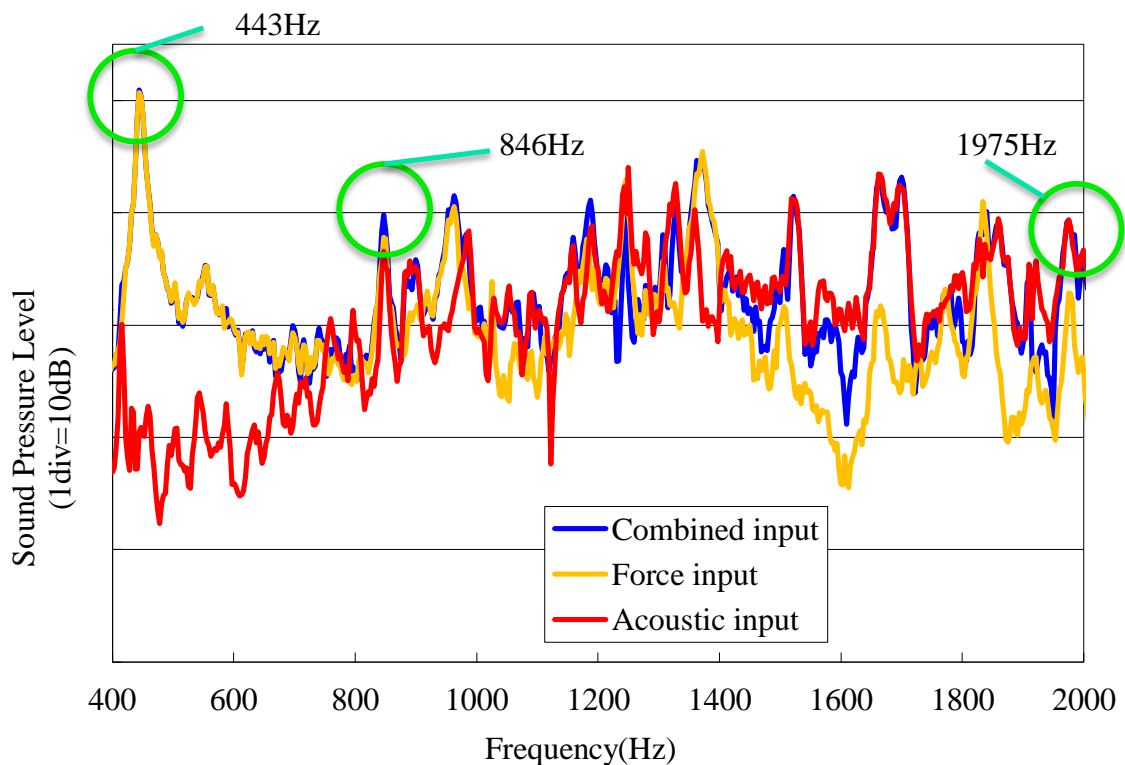
Figure 2.2 Average sound pressure level

To determine the frequency of an analytical object, we measured radiated sound pressure from the oil pan at frequency region of 400-2000Hz using Bruel & Kjaer microphones. Measurement points were five points located on a hemisphere of 500mm radius, centered on the oil pan. Figure 2.2 shows the mean-square averaged sound pressure level of all measurement points. Consequently, to verify the influence of airborne noise and structure-borne noise, we focused on low frequency region where the effect of structure-borne noise is largest, mid-frequency, and high-frequency region where the effect of airborne noise is largest. The frequency values which we are going to focus on are 443Hz, 846Hz and 1975Hz.

2.3.3. Identification of Sound Source

To calculate inverse-numerical acoustic analysis, the boundary element model (BE model) of the sound source and field-point-mesh (FPM) of sound measuring point are created. We used the experimental results of sound pressure and input them into the FPM. Then, we calculate surface vibration produced by the sound source using INA. In addition, we measured sound source surface vibration directly to verify the identification result. The software that we used for this analysis is LMS Virtual Lab.

BE model of oil pan is shown in Figure 2.3. The length of each element was approximately 25mm. The number of nodes and elements were 1262 and 1290, respectively.
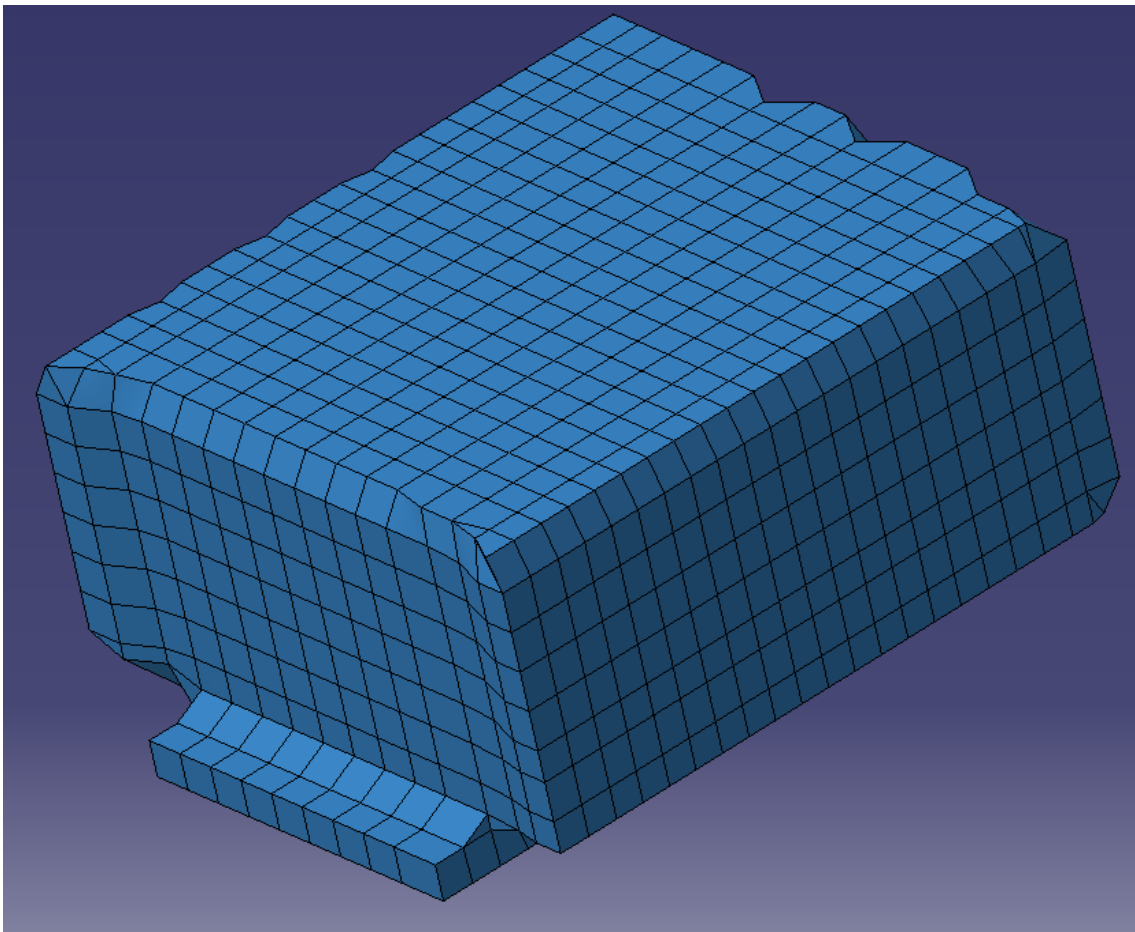
Figure 2.3 Boundary element model of the oil pan

For the inverse-numerical acoustic analysis, we measured sound pressure around the oil pan. Figure 2.4 shows the position of the measurement point. The measurement point is a plane placed 60mm from the oil pan's surface. We measured sound pressure in five directions (top, right, left, back and front of the oil pan). The measurement point's pitch was 30mm, and we measured the sound pressure of 798 points in total. We measured sound pressure by using one point on the surface as a reference point.
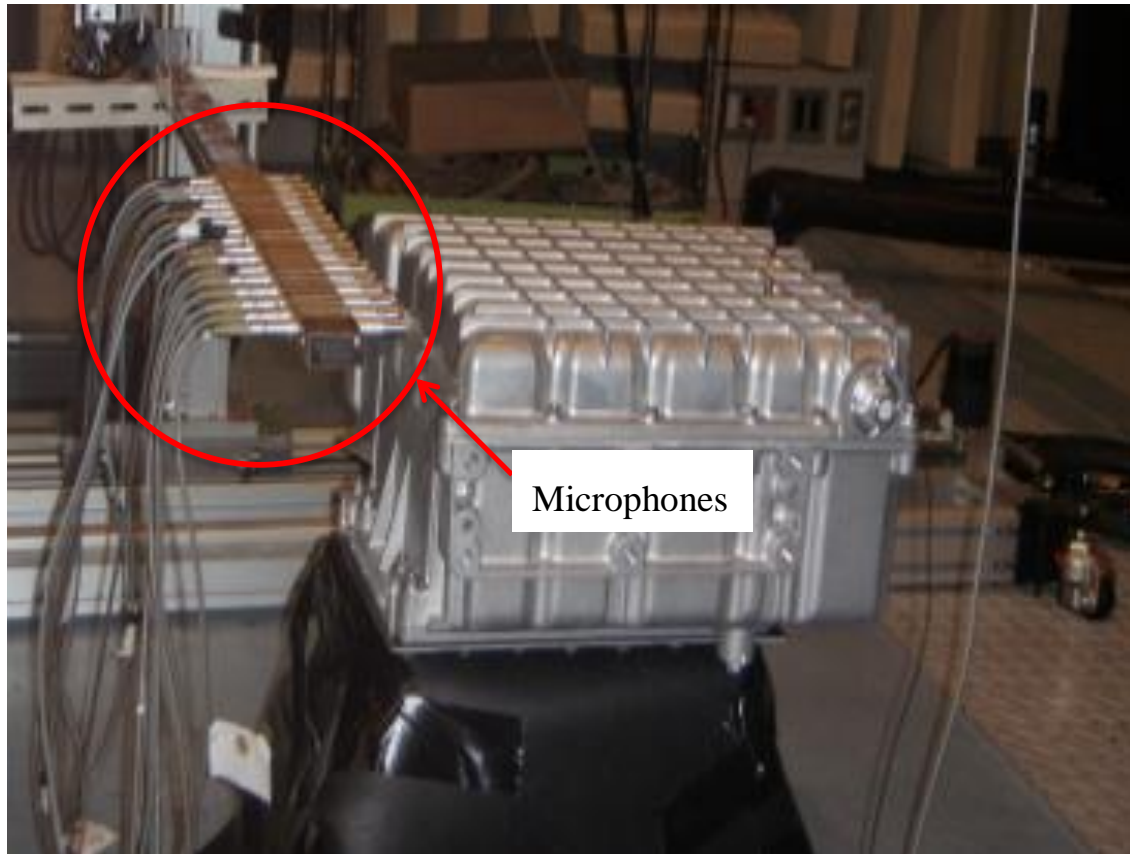
Figure 2.4 Position of microphones as measurement points

To verify the accuracy of identification results by using INA, the oil pan's surface vibration was measured using Polytec's 3-dimension laser Doppler.

The identification result was verified by comparing it with the measurement results. The identification in each input situation of 443Hz, 846Hz and 1975Hz is shown in Figure 2.5, Figure 2.6 and Figure 2.7 respectively. We focused on the surface vibration of the top side where the vibration distributions are more obvious.
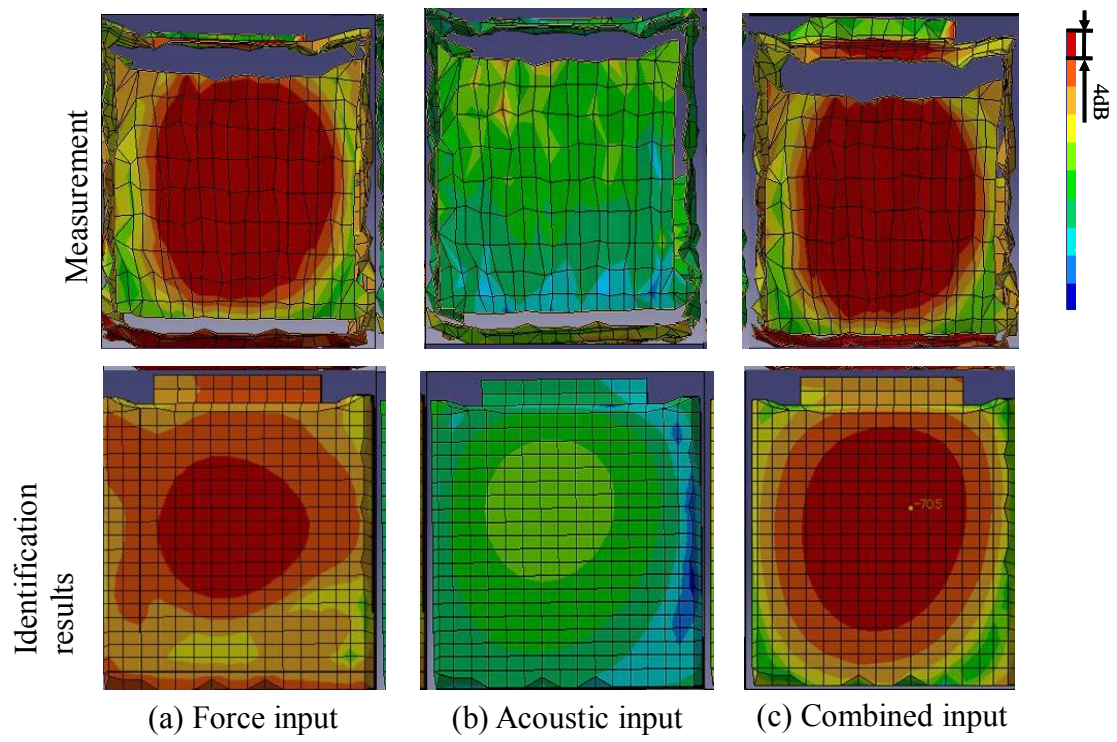
Figure 2.5 Sound source surface vibration at 443Hz
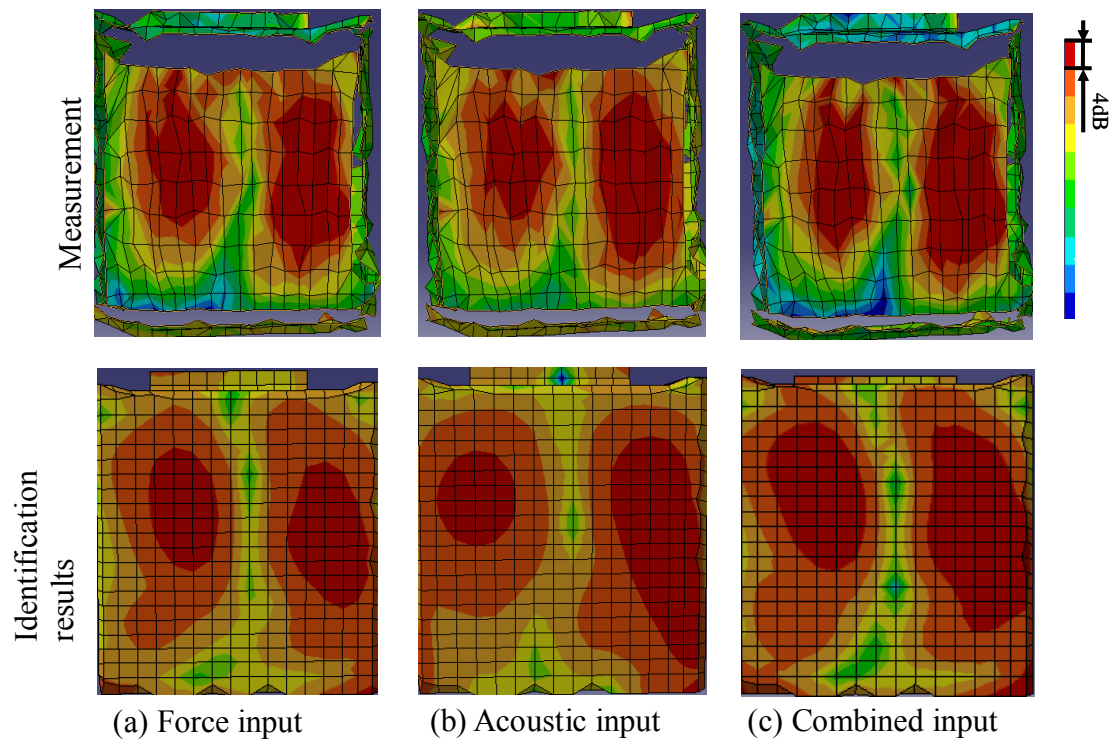
Figure 2.6 Sound source surface vibration at 846Hz
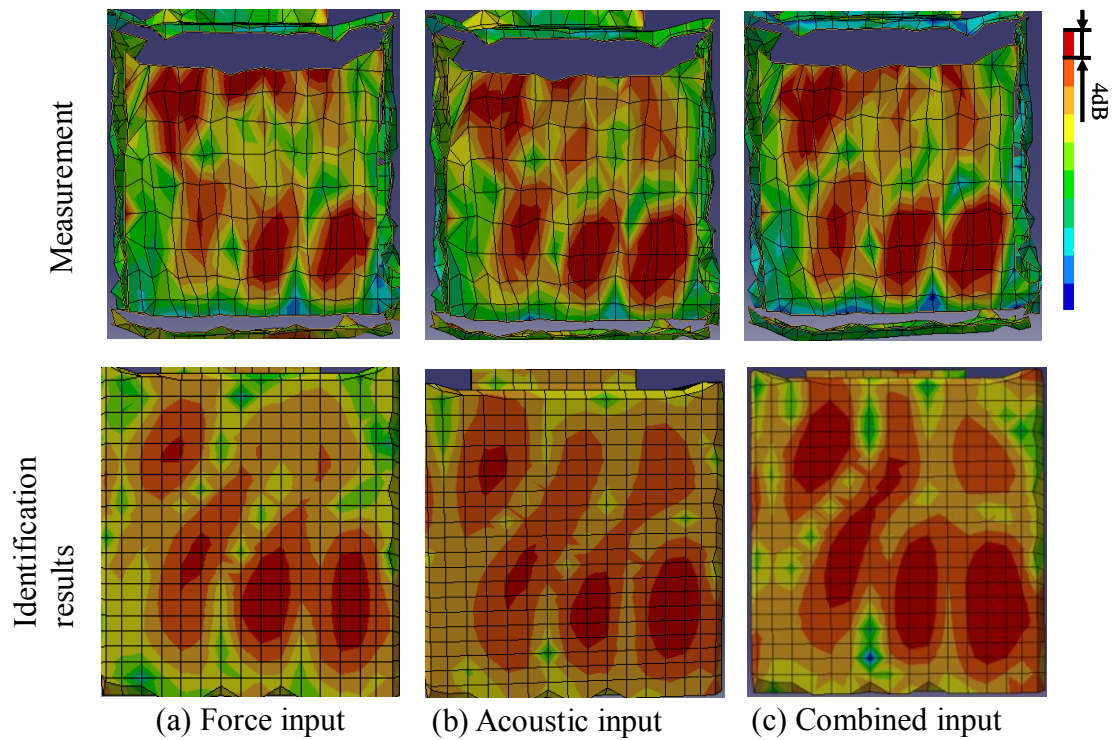
Figure 2.7 Sound source surface vibration at 1975Hz

At 443Hz, results for force input show similar trends in vibration distribution, but for the acoustic input the actual measurement does not show any vibration mode compared to the identified results. However, in other frequency values, the measured and identified results show similar trends. In conclusion, there is a certain condition involving airborne noise that will affect the accuracy of the identified sound source. The factor will be discussed in the next section.

2.3.4. Experimental Verification for Acoustic Input

To verify the influence of airborne noise on the accuracy of INA, we conducted a speaker test (acoustic input) with similar experimental conditions as stated in previous section. Figure 2.8 shows the averaged sound pressure level of 5 measurement points. Consequently, to verify the influence of airborne noise, we focused on 423Hz, 579Hz, 798Hz, 838Hz, 873Hz, 901Hz.

To verify the accuracy of identification results by using inverse-numerical acoustic analysis, the oil pan's surface vibration was measured using accelerometer on 9 points with a reference point as shown in Figure 2.9. The identification result was verified by comparing it with the measurement results.
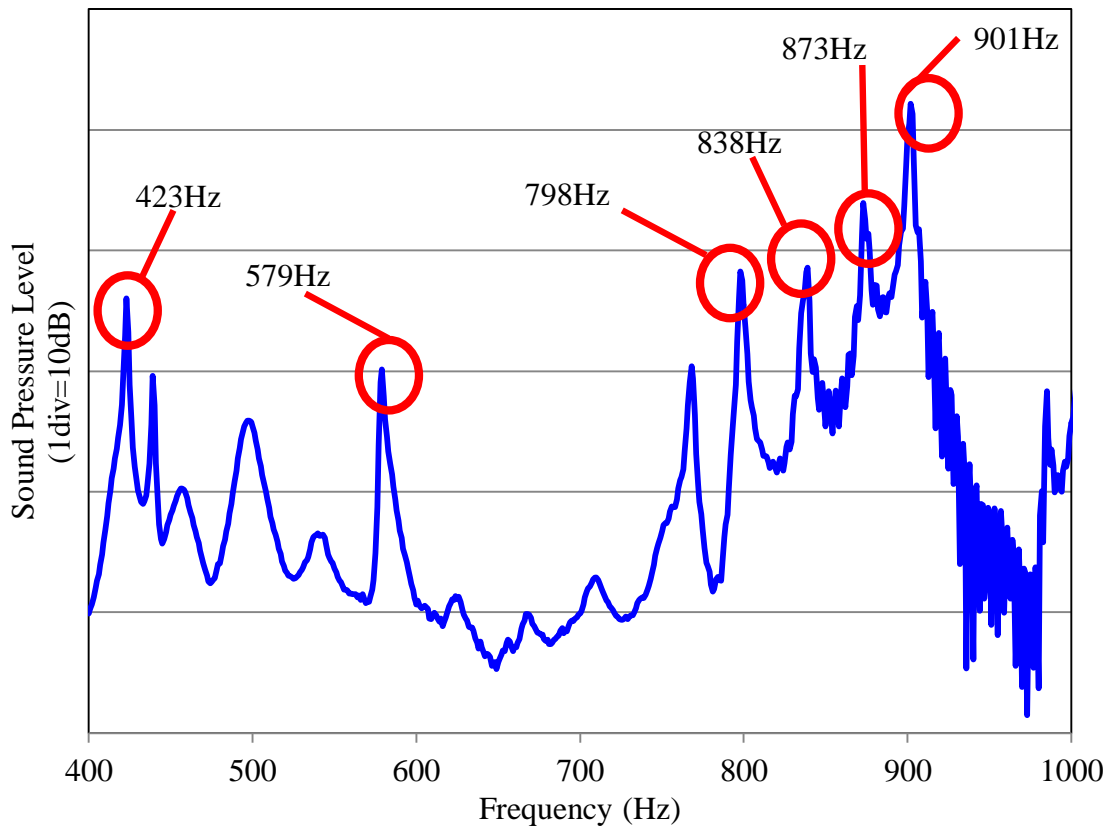
Figure 2.8 Average sound pressure level
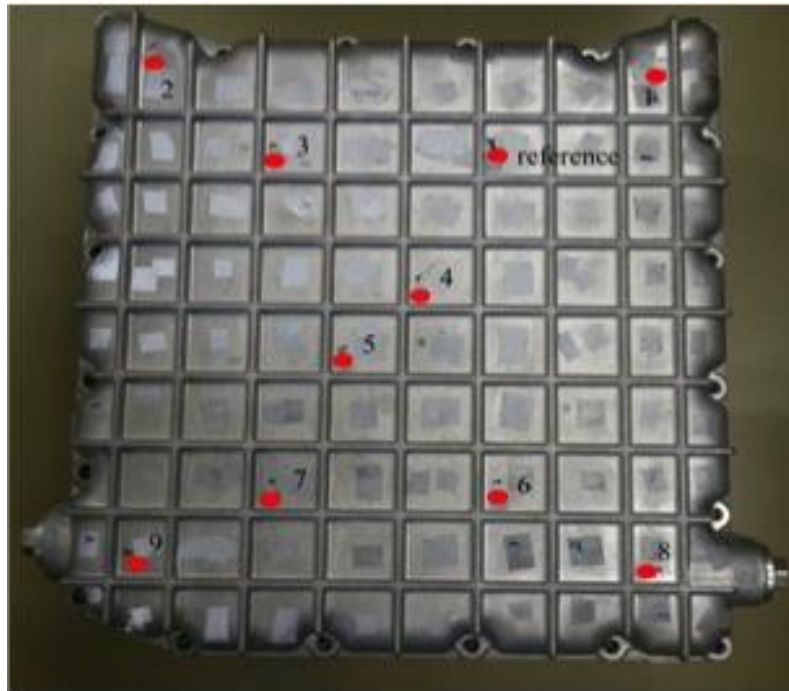
Figure 2.9 Vibration measurement view

18

Table 2.1 Comparison between identification and measurement results for surface vibration acceleration

Frequency [Hz]	Correlation Coefficient	Identification/Measurement
423	0.79	1.23
579	0.80	1.14
798	0.87	1.17
838	0.84	1.12
873	0.86	1.10
901	0.87	0.97

Table 2.1 shows the vibration energy ratio between the identification and measurement results and the correlation coefficients of vibration distribution. Based on Table 2.1 we could identify that the identification and measured results have similar trends in vibration distribution. However, the vibration energy ratio shows that the identification results show larger vibration energy than the actual vibration measurements.

2.3.5. Sound Pressure Prediction

To verify the accuracy of the sound source model, we used the identified vibration to predict the sound pressure on five points of a hemisphere of 500mm and 1000mm radius centered on the oil pan using BEM, and compared it with the actual sound pressure measurements as shown in Figure 2.10 and Figure 2.11 respectively. The comparisons of averaged prediction values and averaged actual measurement values of each input method are shown in Figure 2.12 and Figure 2.13. Table 2.2 and Table 2.3 shows the sound pressure values and error between measurements and prediction values. According to Table 2.2 and Table 2.3, the prediction values and the actual measurement values of each input method correspond within a margin of error of below 3 dB at 500mm and 4 dB at 1000mm of measurement radius.

From these results, we verified that the prediction results shows good agreement with the measurement results and the accuracy of noise prediction would decrease according to the measurement radius.

Moreover, when the identified vibration results were applied as the boundary condition for the prediction of sound pressure, the prediction values of sound pressure in each input have good agreement with the actual measured values.

Therefore in general, in order to predict the sound pressure of sound sources, we verified that it is more suitable to use the identified vibration results rather than the actual vibration measurement results as the boundary condition.
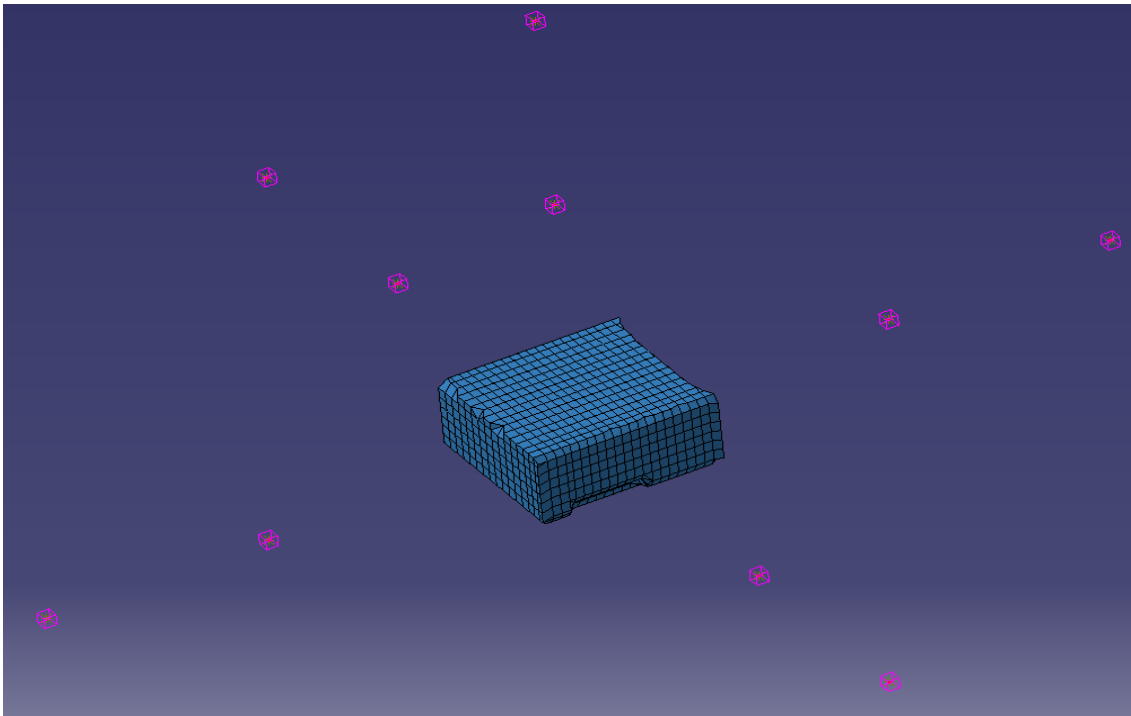
Figure 2.10 Field point measurement of BE model at 500mm radius
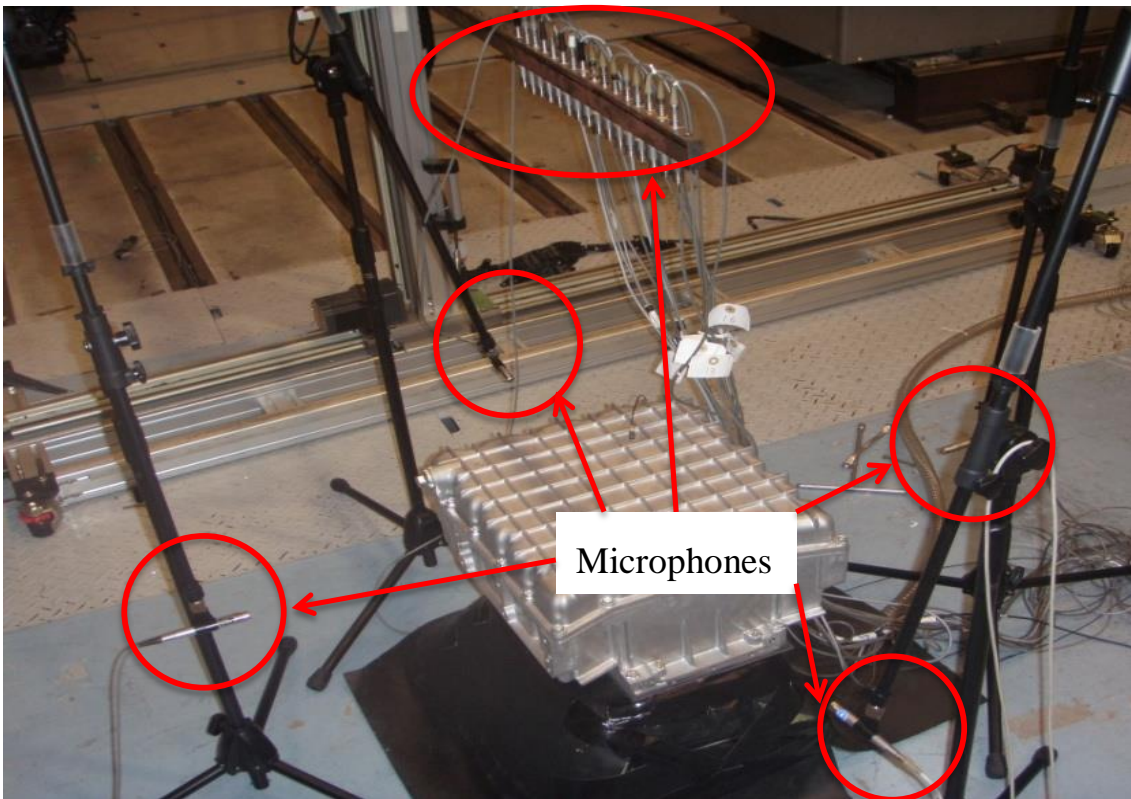
Figure 2.11 Position of measurement points at 500mm radius
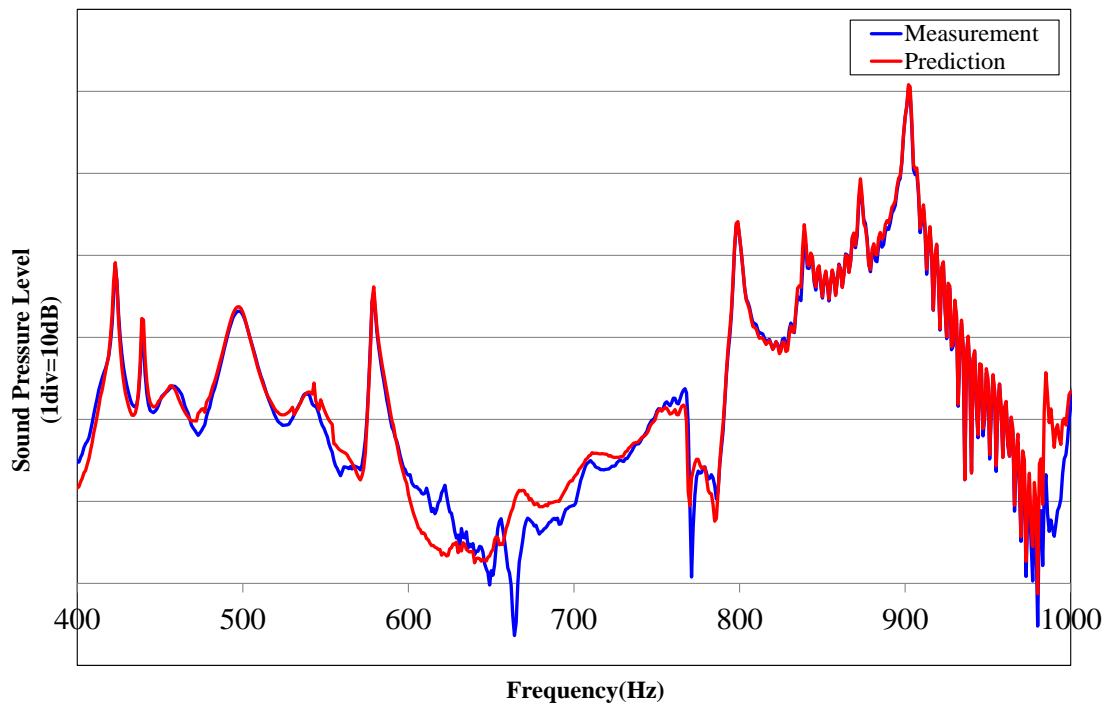
Figure 2.12 Comparison of sound pressure level between measurement and prediction results at 500mm radius
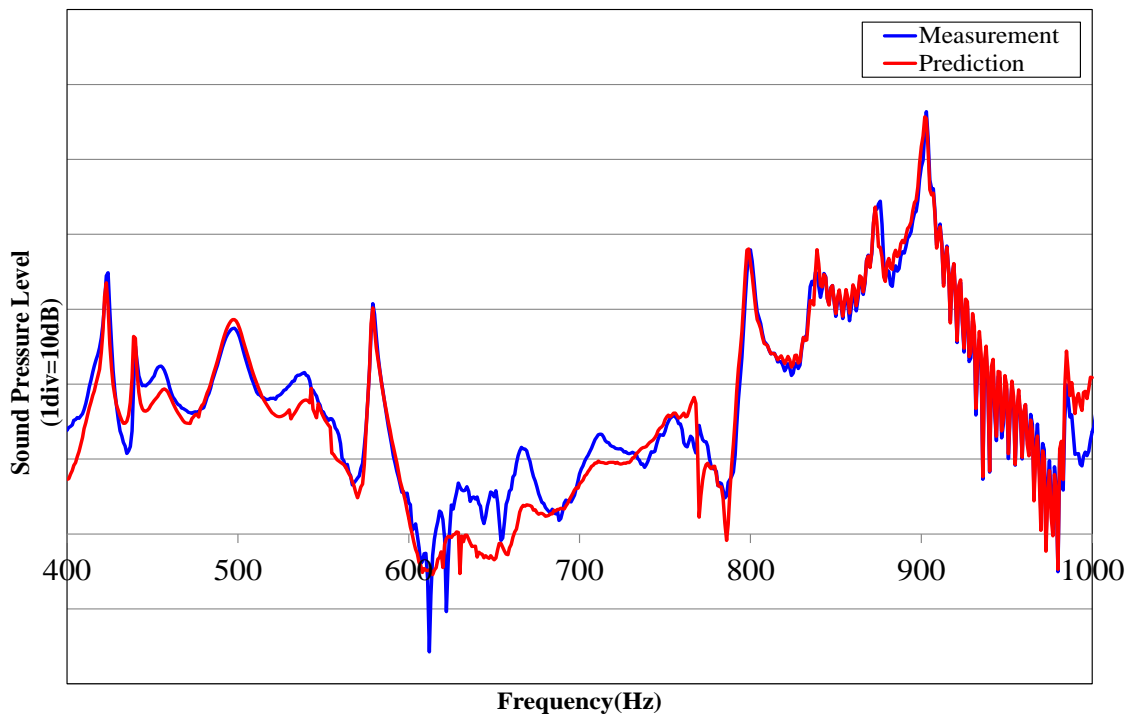
Figure 2.13 Comparison of sound pressure level between measurement and prediction results at 1000mm radius

22

Table 2.2 Sound pressure of target frequency at 500mm

Frequency (Hz)	Measurement (dB)	Prediction (dB)	Error (dB)
423	38.81	39.56	0.75
579	35.49	36.28	0.79
798	43.65	43.90	0.25
838	38.42	40.82	2.40
873	48.25	49.36	1.11
901	58.23	58.21	0.02

Table 2.3 Sound pressure of target frequency at 1000mm

Frequency (Hz)	Measurement (dB)	Prediction (dB)	Error (dB)
423	34.47	34.07	0.40
579	30.75	30.54	0.21
798	34.47	37.90	3.43
838	34.93	35.12	0.19
873	43.56	43.69	0.13
901	49.88	53.06	3.18

2.4. Placement Technique of Measurement Points for Optimization of Inverse Numerical Acoustic Analysis Method

2.4.1. Theory of Acoustic Transfer Function

2.4.1.1. Acoustic transfer function

In our study, we consider the sound source as planar surface, and the acoustic transfer function $[H]$ is determined. In planar surface consisting of infinitesimal area elements, the area elements are considered as emitting monopole sound source. The potential velocity of the emitting sound wave from the monopole sound source $\emptyset$ can be written as follows;

$$\emptyset = \frac{Q}{2\pi r} e^{j(\omega t - kr)} \tag{2.7}$$

where ω is angular frequency, k is wave numbers, r is the distance between sound source and measurement point, and Q is the volume velocity.

When sound pressure P and excluded volume velocity V are,

$$P = \rho \frac{\partial \emptyset}{\partial t} = j\omega\rho \frac{Q}{2\pi r} e^{j(\omega t - kr)} \tag{2.8}$$

$$V = Q e^{j\omega t} \tag{2.9}$$

the transfer function of the points with distance r from the planar element and ΔS which means fine area on the planar surface that has one monopole sound source can be written as the following equation [11];

$$H = \frac{P}{V} \Delta S = \frac{j\Delta S \omega \rho}{2\pi r} \exp\left(-\frac{j\omega r}{c}\right) \tag{2.10}$$

2.4.1.2. Space filling design

Space filling design, one of the classes of surrogate modeling, is an optimal design method to calculate the design variables. The purpose of this method is to be arranged the design variables as balanced as possible within a space, thus it is expected that it is an effective measurement points placement method for inverse acoustic analysis. We introduced the most typical space filling design. We consider the problem of arranging the number of n points $\mathbf{x}_i = (x_{i1}, \cdots, x_{is}), (i = 1, \cdots, n)$ for a s-dimensional space[12][13].

2.4.1.2.1. _Sobol sequence_

Sobol sequence is one of low-discrepancy sequence, which is used for the numerical integration inside unit hypercube.

2.4.1.2.2. *Maximin design*

A design is called a maximin distance design if it maximizes the minimum inter-site distance:

maximize min $d(\mathbf{x}_i, \mathbf{x}_j)$

where $d(\mathbf{x}_i, \mathbf{x}_j) = \left\{ \sum_{k=1}^{s} (x_{ik} - x_{jk})^2 \right\}^{\frac{1}{2}}$ (2.11)

2.4.1.2.3. *Latin hypercube design*

Latin hypercube design is the most popular experimental design technique. In a Latin hypercube design, each factor has as many levels as there are runs in the design. When a Latin hypercube design with *m* points in *s*-dimensional space is constructed, each of the *s*-dimensional space is divided into *m* levels from the lower bound to the upper bound of the factor. Each design point is allocated in the level one by one of one factor.

2.4.1.2.4. *Uniform design*

The L_p discrepancy is a measure of the difference between the empirical cumulative distribution function of an experimental design and the uniform cumulative distribution function. A design is called uniform design if it minimizes the centered L_2 discrepancy CL_2.

$$
\begin{aligned}
CL_2 = \left(\frac{13}{12}\right)^2 &- \frac{2}{n} \sum_{i=1}^{n} \prod_{k=1}^{s} \left(1 + \frac{1}{2}|x_{ik} - 0.5|^2\right) \\
&+ \frac{1}{n^2} \sum_{i=1}^{n} \sum_{j=1}^{n} \prod_{k=1}^{s} (1 + \frac{1}{2}|x_{ik} - 0.5| - \\
&\frac{1}{2}|x_{jk} - 0.5| - \frac{1}{2}|x_{ik} - x_{jk}|)
\end{aligned}
$$ (2.12)

2.4.1.2.5. *Maximum entropy design*

Shanon used entropy to quantify the amount of information. The lower the entropy, the more precise the knowledge is. Minimizing the posterior entropy is equivalent to finding a set of design points on which we have the least knowledge. It has been further shown that the entropy criterion is equivalent to maximizing the following;

maximize $\log|R|$, $R_{ij} = \exp\left\{\theta \sum_{k=1}^{s} (x_{ik} - x_{jk})^2\right\}$ (2.13)

2.4.2. The Validity of Measurement Point Positioning Using Space Filling Design

2.4.2.1. Conventional technique

Simulation is done under identical conditions with Nakano's dissertation. The sound source is a 2 dimension flat plane of 600mm×600mm. The flat plane is further divided into 25 120mm×120mm flat plane elements and a point sound source is placed on the center of the flat plane elements. The sound pressure measurement points on a 2-dimension surface are placed 300mm directly above the flat plane. 25 of sound pressure measurement points are placed above the monopole sound source for the square lattice shape arrangement method[7].

On the other hand, for circular shape measurement points' arrangement method, the monopole's position coincides with the circle's origin point, 8 measurement points on 150mm radius, and 16 points on 300mm radius. We implemented one the most common Latin hypercube design of space filling design, where 25 measurement points in 600mm×600mm area, 300mm directly above the flat plane sound source.

Figure 2.14 shows the monopole sound sources' positioning on the flat plane, Figure 2.15 shows the sound pressure measurement points placement method of square lattice, circular and space filling design which is implemented using Latin hypercube. The origin point between sound source and sound pressure measurement points, x-axis and y-axis is the same for every method.

Assuming the sound velocity c=340m/s and the air density ρ=1.2kg/m^3. Figure 2.16 shows the results of the ratio between minimum and maximum singular values of the acoustic transfer function [H] for the frequency 10Hz to 5000Hz with interval of 10Hz. Based on the Tolerance from Equation (2.5), the larger the ratio between minimum and maximum singular value, the smaller the error effect of {p}.
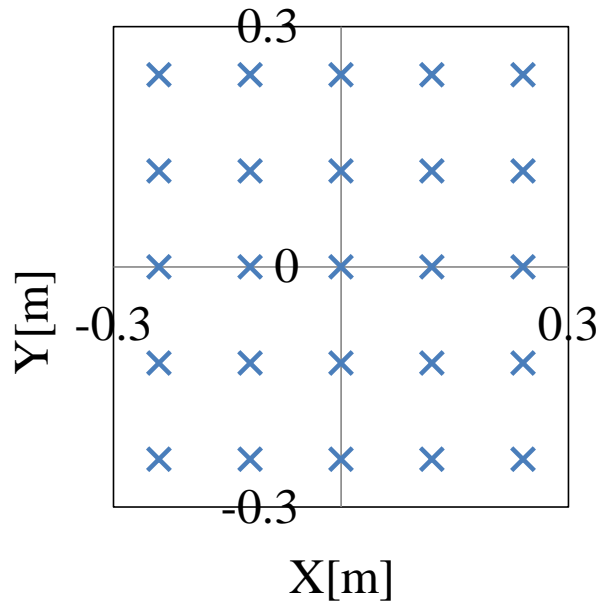
Figure 2.14 Monopole sound source for *n*=25

(a) Square

(b) Circle
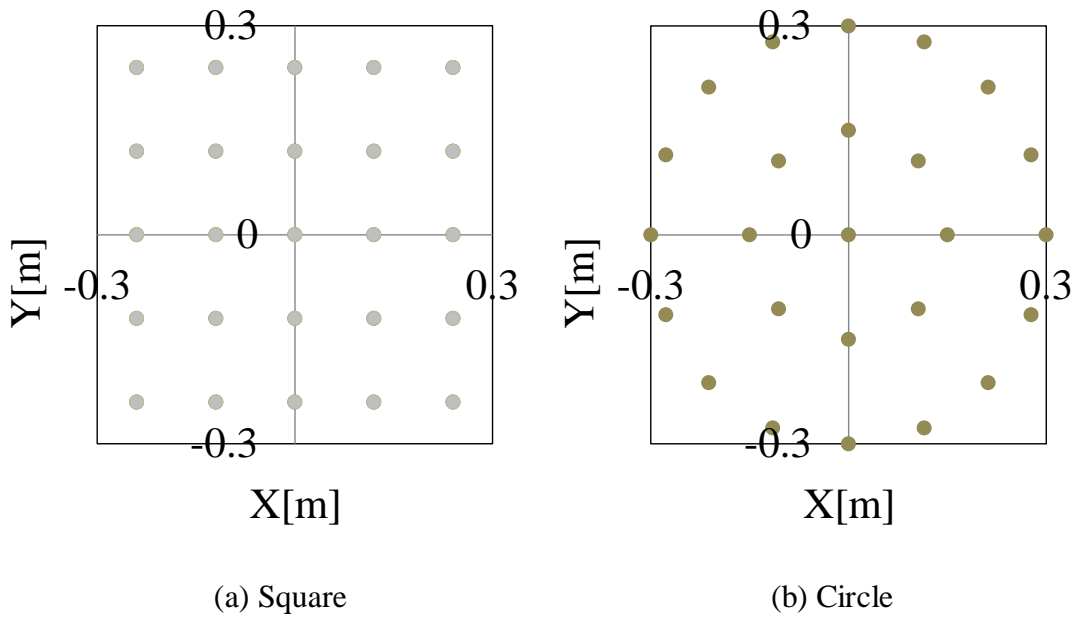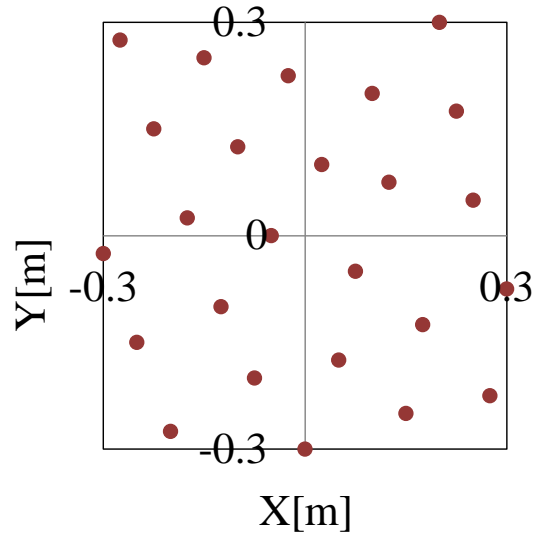
(c) Latin hypercube design

Figure 2.15 Measurement points' placement for *m*=25

The threshold value is assumed as 0.01 as Nakano et al., and the existence of frequency values above the region of 1400Hz, which are below the threshold that can cause the inverse acoustic analysis to be unstable, is observed. For the square lattice method, around 3350Hz were below the threshold, while 2570Hz, 4550Hz and 4830Hz were near the threshold. Moreover, for the circular method, only around 3700Hz were below the threshold. On the one hand, with space filling design, around 2420Hz, 2580Hz, 2810Hz, 4240Hz and 4960Hz were below the threshold, especially for the frequency values from 4090Hz to 4500Hz. Therefore, even though the space filling design has a merit where the number of measurement points can be determine arbitrarily, the stability was worse than the method proposed by Nakano et al.[7].

2.4.2.2. Changes in the number of sound sources

According to Nakano et al., the numbers of surface vibration sound sources and sound pressure measurement points are the same. However, generally in inverse acoustic analysis, the numbers of surface vibration sound sources are more than the measurement points. Therefore, in order to simulate the general condition, the flat plane element of surface vibration is designated as 100mm×100mm, and the 600mm×600mm flat plane is divided into 36 elements and 36 monopole sound sources with 25 measurement points (Figure 2.17). Other conditions were set as identical to Nakano et al., and the results of σ_{25}/σ_1 are shown in Figure 2.18.
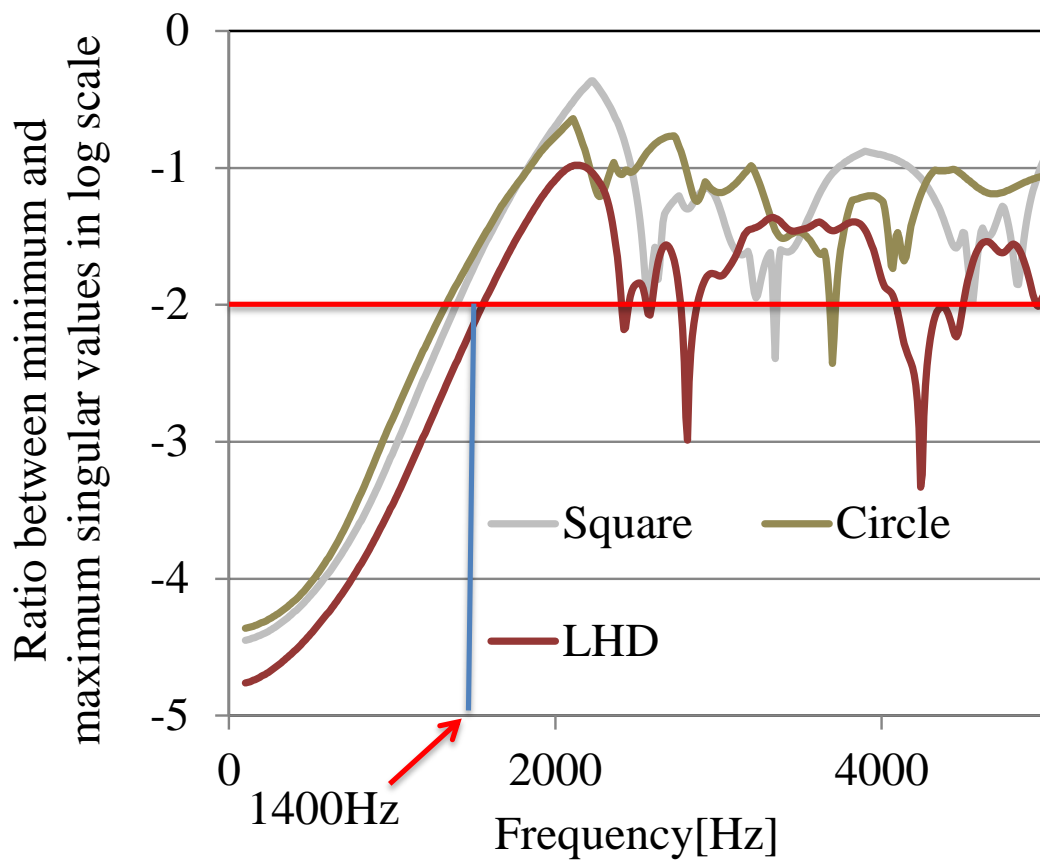
Figure 2.16 Singular value ratio of acoustic transfer function for *n*=25
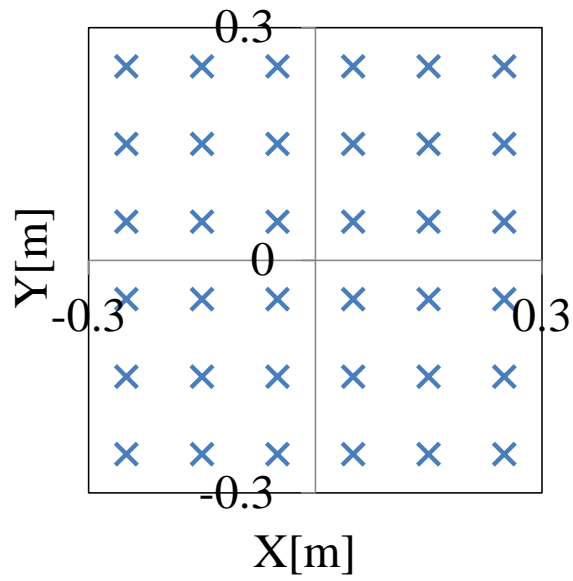
Figure 2.17 Monopole sound sources for *n*=36
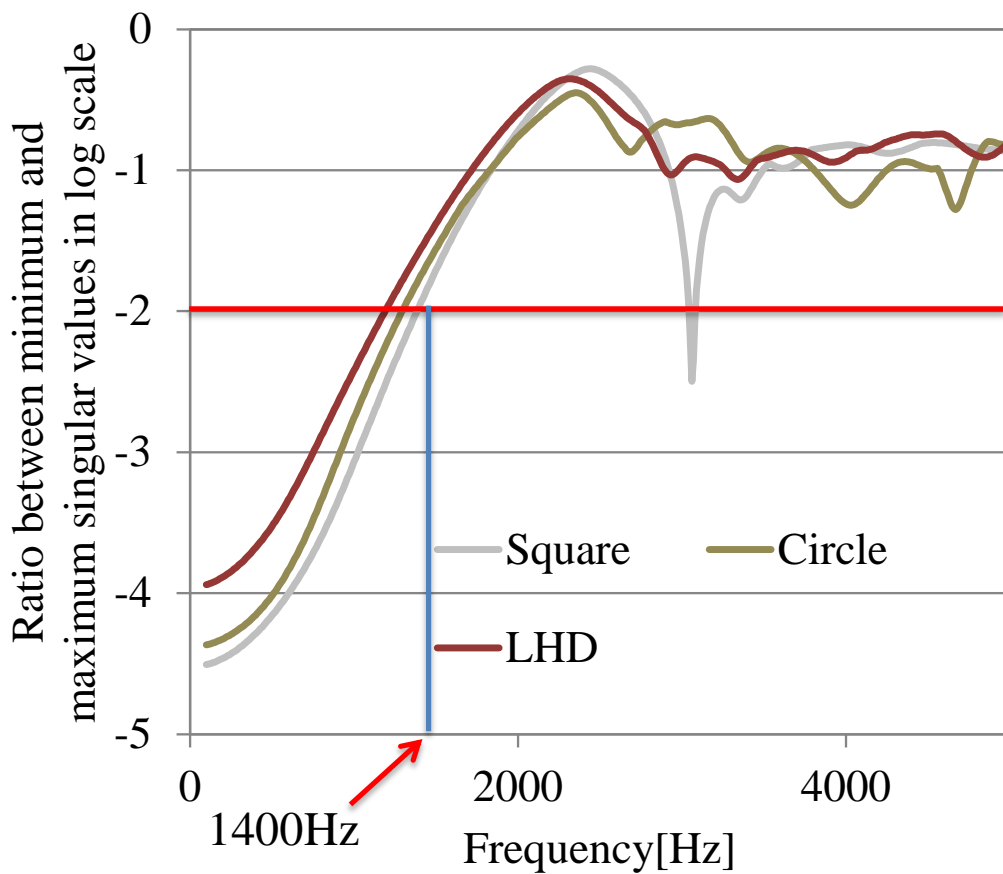
Figure 2.18 Singular value ratio of acoustic transfer function for *n*=36

Based on Figure 2.18, around 3060Hz for square lattice method were below the threshold. However for circular method and Latin hypercube design, there are no frequency values above 1400Hz that are below the threshold value, thus a more stable analysis is possible. Therefore, when the actual conditions of inverse acoustic analysis are considered, the same stability between the placement method of sound pressure measurement points using space filling design and the method proposed by Nakano et al. was verified.

2.4.3. Space Filling Designs' Comparison

There are various methods proposed in space filling design. In this chapter, we investigates the validity for sound pressure measurement points positioning of 5 most common methods from the space filling design which were introduced in previous chapter.

2.4.3.1. Comparing the space filling design criterion

5 types of methods, which are SOBOL, maximin design, Latin hypercube design, uniform design and maximum entropy design, are constructed and evaluated using maximin criteria, discrepancy and entropy. Figure 2.19 shows examples arrangement strategy of 25 points inside 2 dimensional square space of 1 side of 1 length. SOBOL was constructed using MATLAB's sobolset command. Other designs were optimized using possible global optimization of genetic algorithm with tournament selection and uniform crossover.

Figure 2.20 shows the maximin criteria, discrepancy and entropy of the points' arrangement strategies based on Equation (2.11) to Equation (2.13). For maximin criteria and entropy criteria, the larger values are preferable, whereas for discrepancy, the smaller values are preferable. Based on Figure 2.20, maximin criteria and entropy shows similar tendency. Therefore, it is understood that based on these two criterion, the order of maximin design and maximum entropy design is more preferable. On the other hand, discrepancy shows opposite tendency compared to maximin criteria and entropy. When evaluated with discrepancy, uniform design and SOBOL are more superior, while Latin hypercube takes the center value between the 3 evaluation criteria.
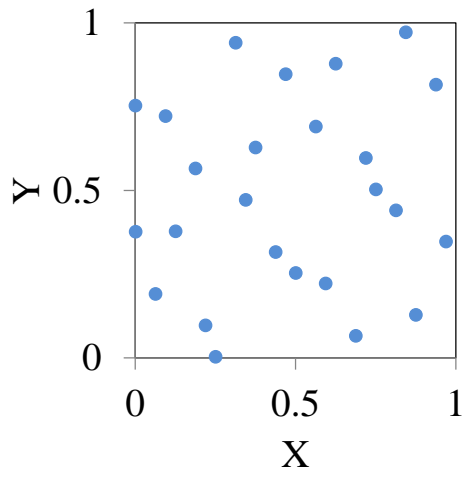
(a) SOBOL sequence
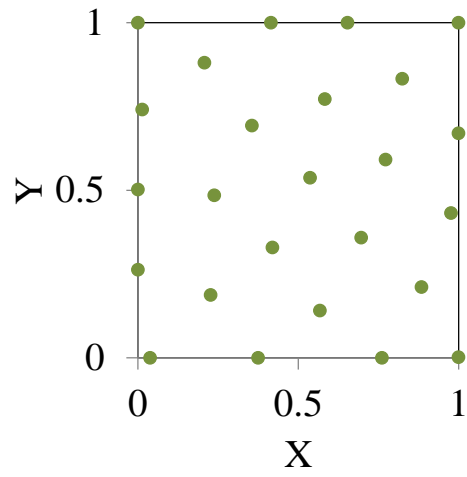
(b) Maximin design
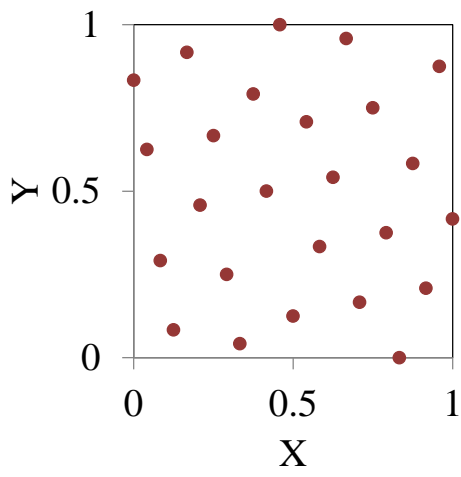
(c) Latin hypercube design
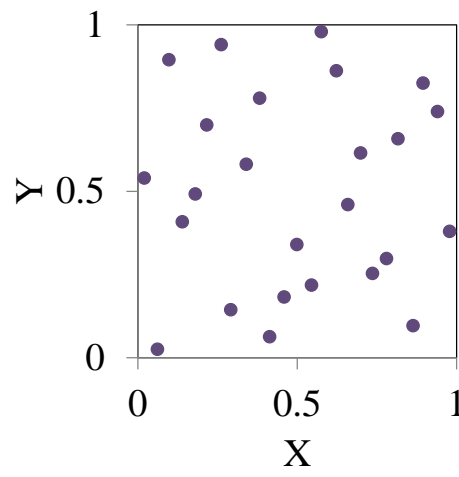
(d) Uniform design
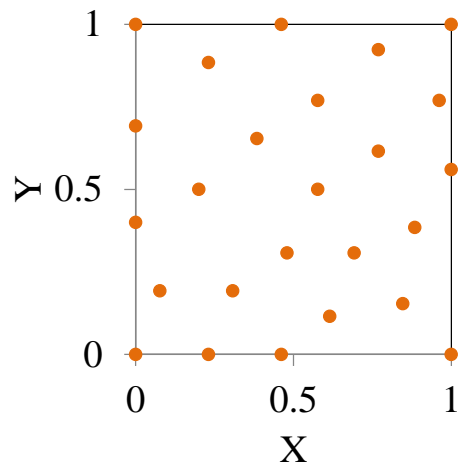
(e) Maximum entropy design

Figure 2.19 Space filling designs
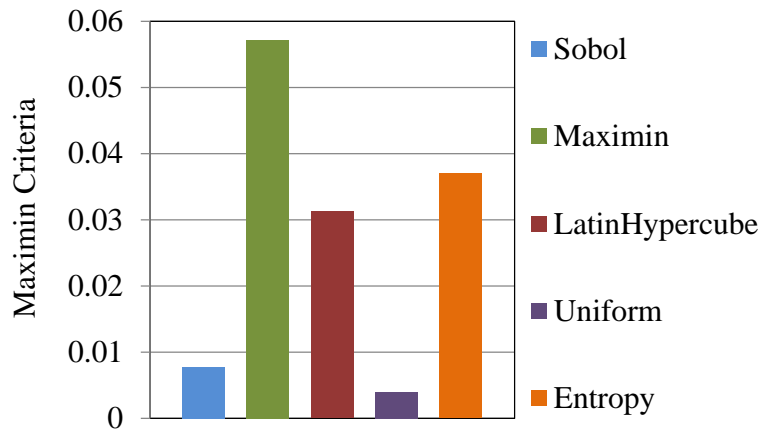
(a) Comparison with Maximin criteria based on Equation (2.11). The large maximin criteria shows good design
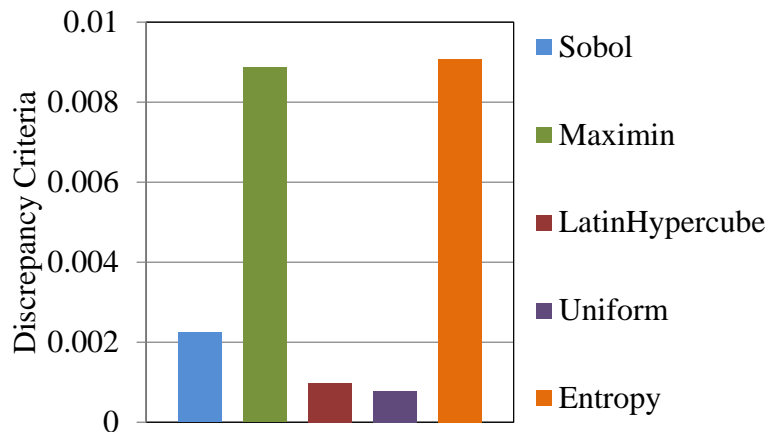
(b) Comparison with discrepancy criteria based on Equation (2.12). The low discrepancy criteria value shows good design
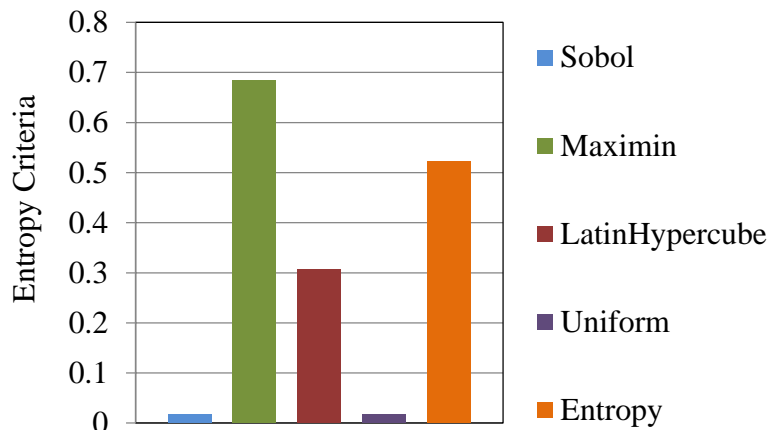
(c) Comparison with entropy criteria based on Equation (2.13). The large entropy criteria value shows good design

Figure 2.20 Evaluation of space filling design

2.4.3.2. Comparison with conventional method

In order to validate which space filling design are valid for the placement of sound pressure measurement points, we construct the transfer function matrix [*H*] of the sound pressure measurement points from the 5 methods of the space filling design, and we evaluated using the same method as Nakano et al.[7].

The ratio of the minimum singular value and maximum singular value for surface vibration in 36 elements of square lattice method and 25 sound pressure measurement points from Figure 2.19 are shown in Figure 2.21.

Based on Figure 2.21, all methods of space filling design shows no values below the threshold of over 1400Hz, thus it satisfies the conditions for the construction of sound pressure measurement points. In addition, maximin, Latin hypercube and maximum entropy design have wider stability range than the other space filling designs because it has the wider frequency range above the threshold value. Therefore, from these results, maximin, Latin hypercube and maximum entropy design is deemed as the most preferable for the sound pressure measurement points' placement method of inverse acoustic analysis for the square plate.
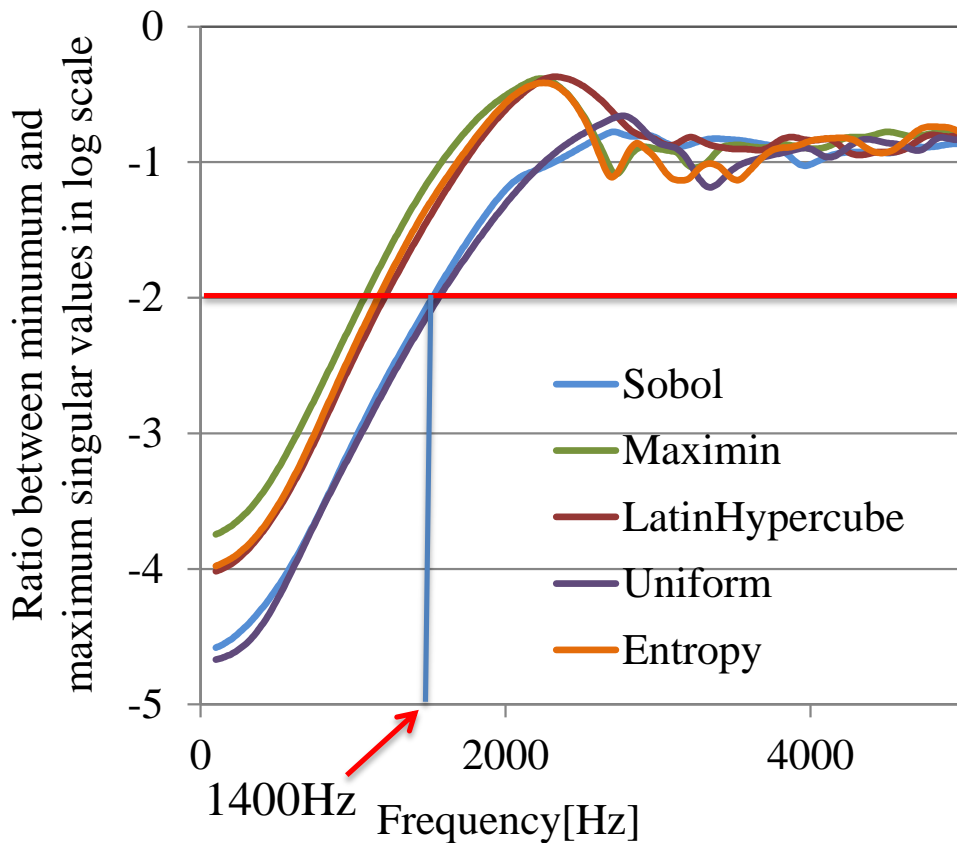
Figure 2.21 Stability of space filling design

2.4.4. Experimental Verification

The surface vibration and the sound pressure of the rectangular plane are measured and the validity of the proposed technique is verified.

2.4.4.1. Stability analysis

Figure 2.22 shows the calculation result of ratio between minimum and maximum singular value of every 10Hz from 10Hz to 5000Hz using the Equation (2.5) as in the case of rectangular plate. 180 points of sound source are placed on the 340mm×180mm rectangular plate with 20mm intervals each between them. 32 sound pressure measurement points were placed on a flat plane surface 25mm from the sound source using square lattice method, maximin design and maximum entropy design based on Equation (2.11) and Equation (2.13). Circular design, SOBOL, Latin hypercube design and uniform design were not compared, as they are incompatible for placement in rectangular space. Because these space filling designs deal with unit hypercube.

As in Figure 2.22, there are no significant difference in stability between conventional method and proposed method. The proposed method of maximin design and maximum entropy design is slightly more stable at below 3000Hz compared to the conventional method. When the stability threshold is assumed at 10^{-2}, at above 500Hz where the least stable square lattice method at low frequency band was above the threshold value. Therefore in this paper we deal with above 500Hz as analysis target. Although the stability is at the same level with the conventional method and proposed methods, the number of measurement points could be arbitrarily determined using the proposed methods.
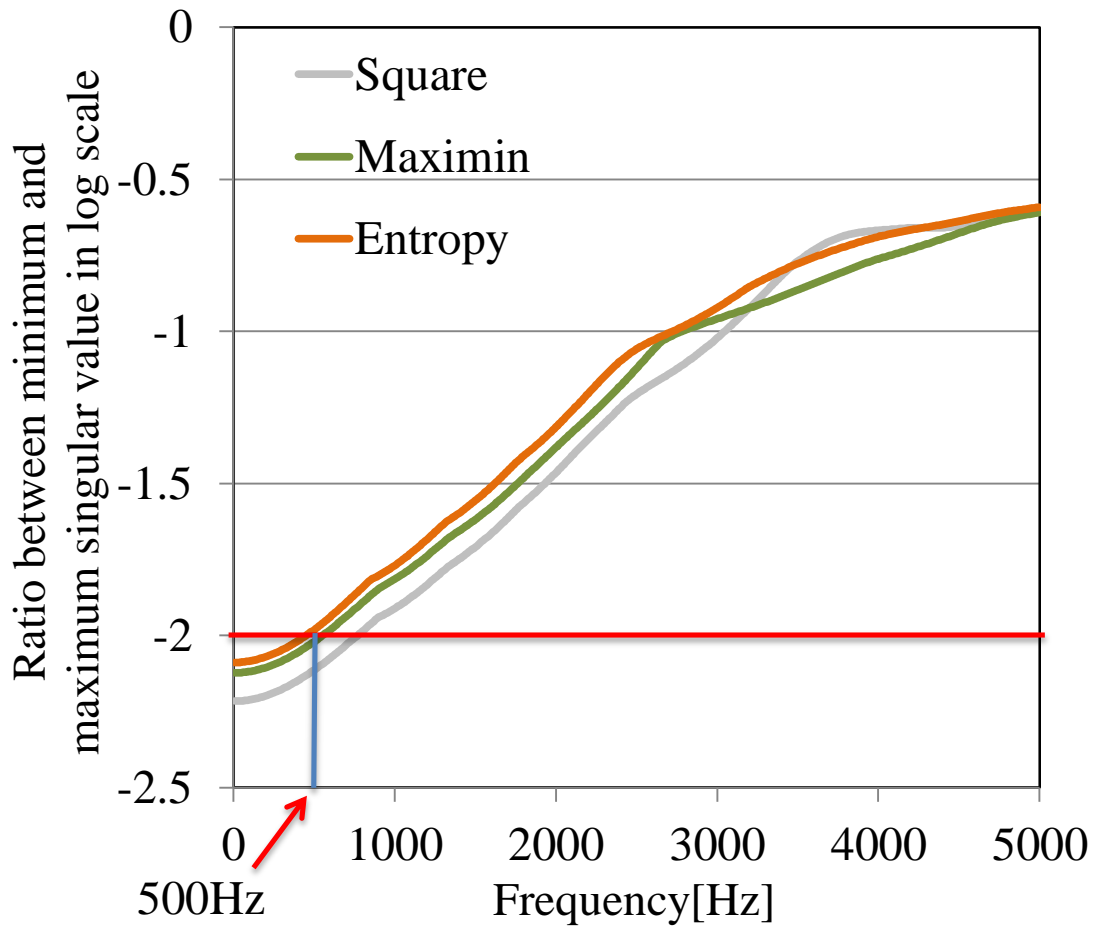
Figure 2.22 Stability of space filling design on rectangular plate

2.4.4.2. Experimental method

In the experiment, the sound source is a steel (SPCC) plate of 340mm×180mm with the thickness of 3.2mm, excited with a shaker on the reverse side center, and excited from 20Hz to 4000Hz with the resolution of 1Hz. In order to compare with the results of inverse acoustic analysis, the plate's surface acceleration is measured at 20mm interval for 180 points and converted into vibration velocity. The sound pressure is measured in a semi-anechoic room with microphones positioned 25mm from the surface of the plate. 15×8 sound pressure measurement points are placed evenly with respect to the plate's surface of 340mm×180mm where the central point corresponded with the x-axis and y-axis. The microphone 4190 (Brüel & Kjaer) and the accelerometer 353B18 (Piezotronics) were used.

2.4.4.3. Experimental results

Figure 2.23 shows the mean square sound pressure of all measurement points in logarithmic scale. From Figure 2.23, the highest peak of the mean square sound pressure is at 654Hz. Therefore, we consider the vibration at 654Hz as the analysis target because it is within the target frequency range from the stability analysis based on Figure 2.22.

Figure 2.24 shows the absolute value of the plate's surface vibration distribution amplitude during excitation at 654Hz.
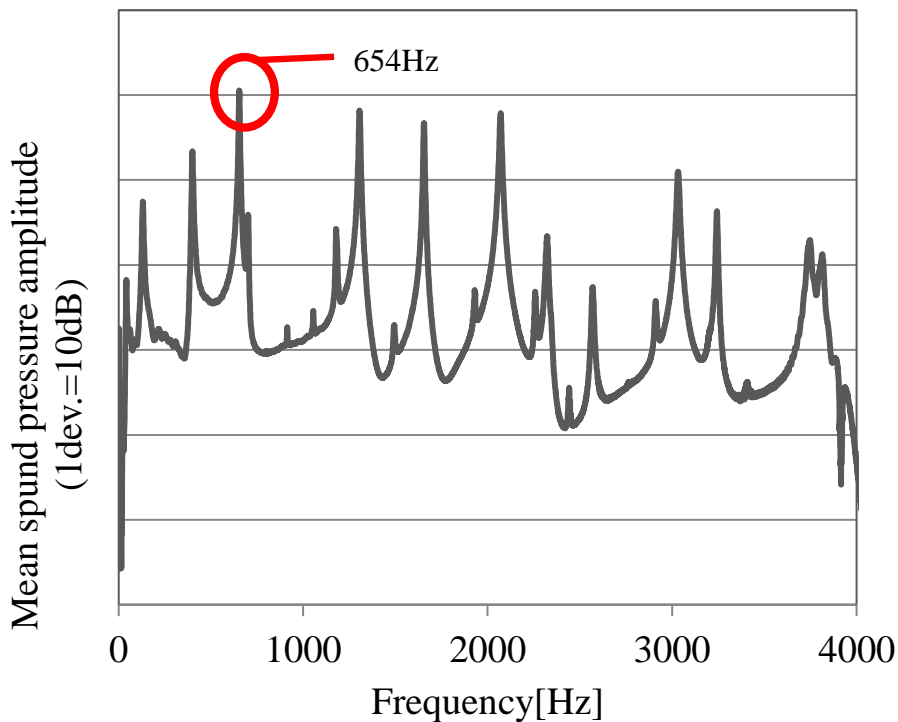
Figure 2.23 Sound pressure level
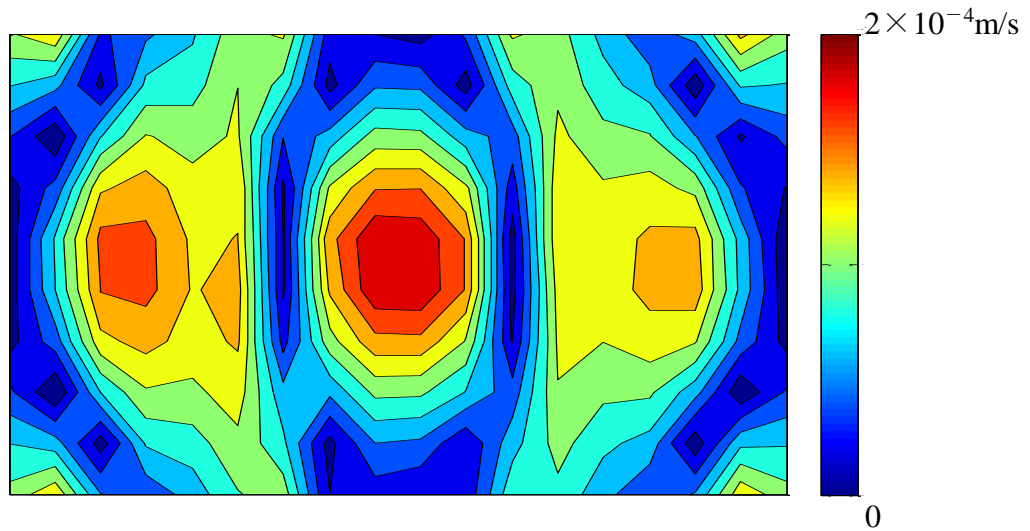
Figure 2.24 Surface vibration measurement distribution from experiment at 654Hz

2.4.4.4. Transfer matrix

The transfer function matrix at 654Hz is calculated with the BEM of LMS Virtual.LAB. The sound source model is a 340mm×180mm steel rectangular plate with the thickness of 3.2mm. The sound source model's number of elements is 7×9=153, element's size is 20mm×20mm, and the number of nodes is 18×10=180. The measurement points' position of the BE model is identical to the experiment.

2.4.4.5. Surface vibration prediction

Figure 2.25 and Figure 2.26 show the predicted surface vibration distributions agree qualitatively with experimental results. From Figure 2.25 and Figure 2.26, it is understood that the surface vibration can be predicted from the measurement results of the sound pressure measurement points determined by maximin design. Therefore, it is possible to determine the number of sound pressure measurement points arbitrarily using maximin design and it is applicable even for rectangular shaped structures or objects.
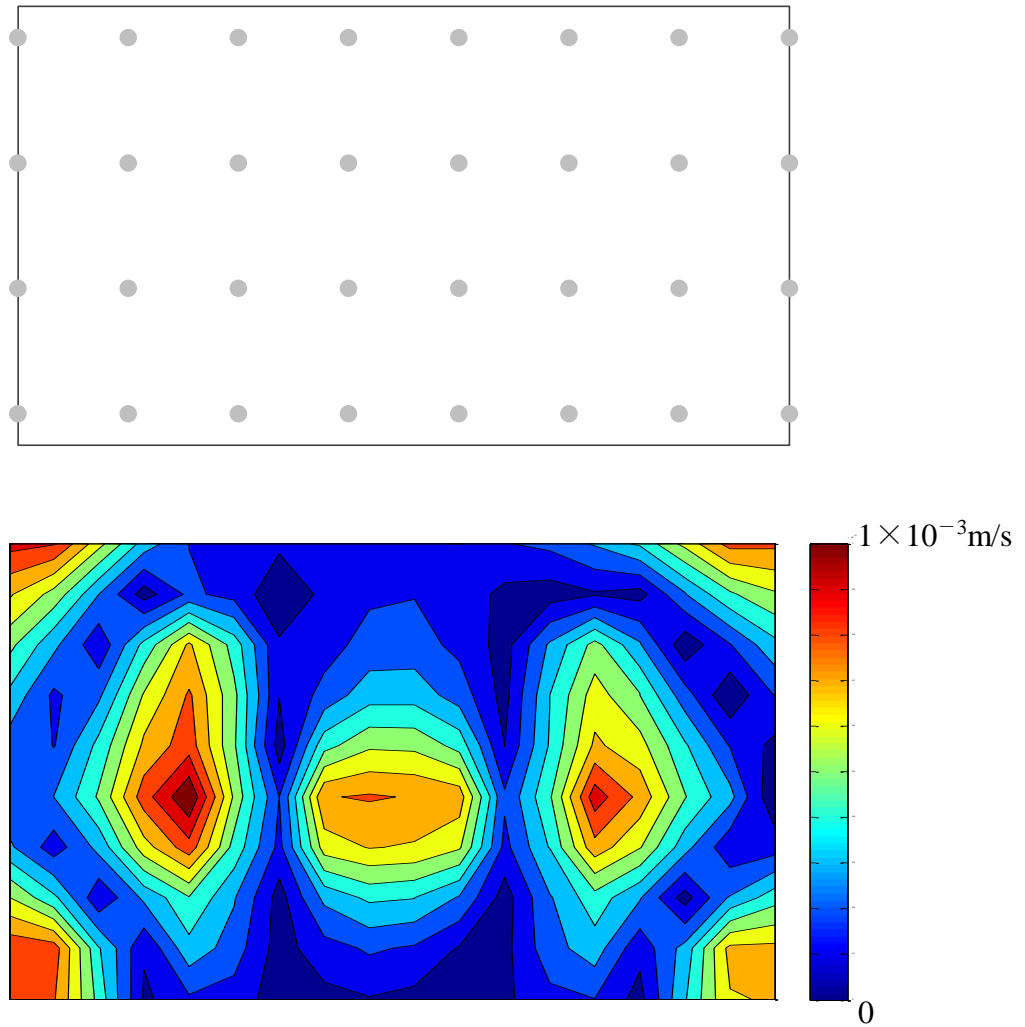
Figure 2.25 Placement of 32 square lattice measurement points and surface velocity distribution predicted from the experimental result
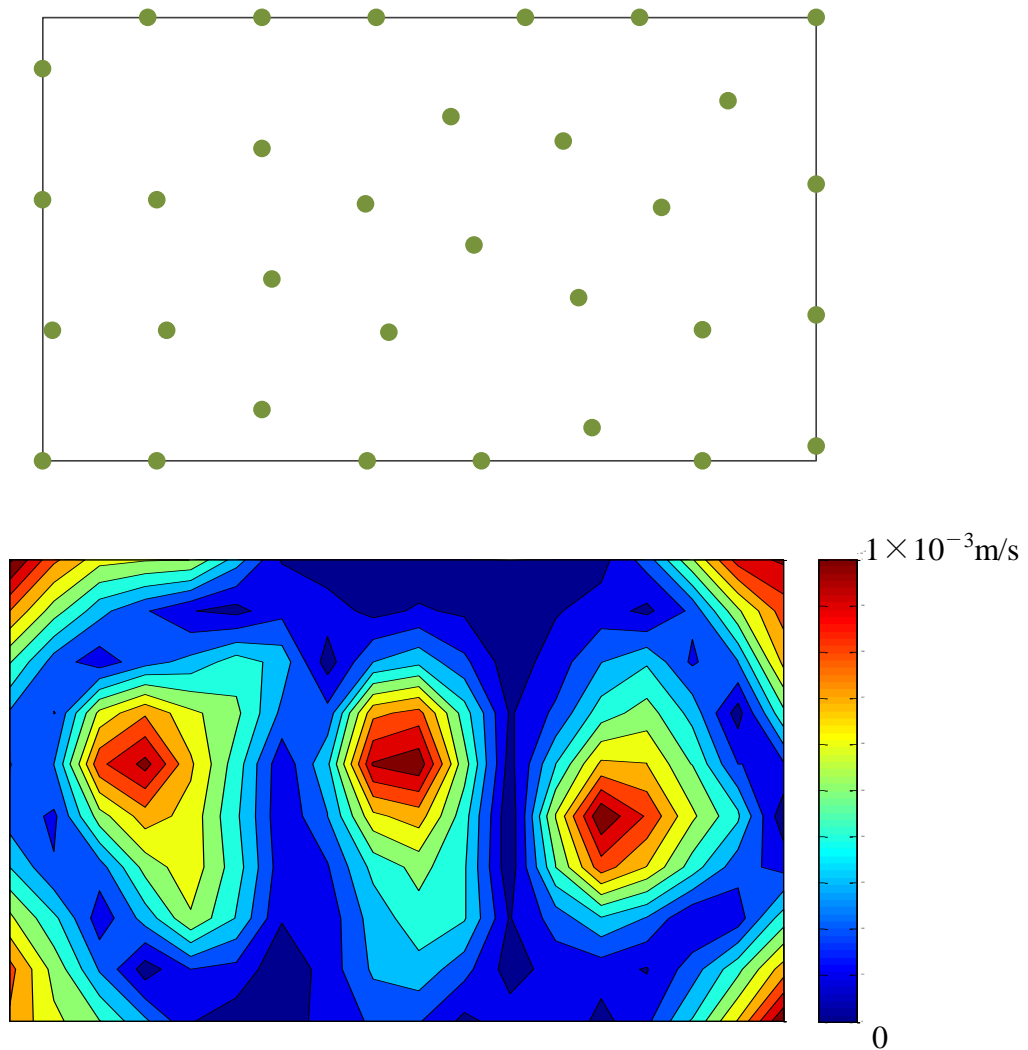
Figure 2.26 Placement of 32 measurement points using maximin design and surface
velocity distribution predicted from the experimental result

2.5. Conclusion

In this study, with the aim to verify the influence of noise source form on the accuracy
of INA, the following conclusions can be drawn from the research;

1) In acoustic input, when the influence of the transmitted sound is large conditions
occur in which we cannot assume that the surface vibration of the object to be the
sound source.

2) When the identified vibration was applied as the boundary condition in the
prediction of sound source, the prediction values have good agreement with the
actual measured values.

3) In order to predict the sound pressure of sound sources, we verified that it is more suitable to use the identified vibration rather than the actual vibration measurement as the boundary condition.

Furthermore, sound pressure measurement points placement method using space filling design for inverse acoustic analysis was proposed, and its validity was verified by experiment and simulation. The following conclusions can be drawn from the research;

1) The number of sound pressure measurement points for inverse acoustic analysis could arbitrarily be determined with space filling design. Furthermore, it can be applied to a sound source with different aspect ratio such as rectangular shape.

2) The surface vibration prediction result of a vibrating body by inverse acoustic analysis is more stabilized using space filling design as the measurement points' placement method, compared to the conventional square lattice shape when the number of surface vibration sound sources is greater than the number of sound pressure measurement points. It has the same stability as the surface vibration prediction results of circular shape measurement points' arrangement method.

3) Among the various space filling designs, maximin design and maximum entropy design are applicable to the sound source with the different aspect ratio. And these two space filling designs are stable when the sound source is square and rectangle.

4) The vibration prediction of a rectangular shape sound source was possible from the sound pressure measurement result which is obtained from arbitrary numbers of measurement points created by the space filling design, and the transfer function calculated by the boundary element method.

References

[1]   Williams, E. G., 1999, Fourier Acoustics, Academic Press, Washington.

[2]   Gardner, B. K. and Bernhard, R. J., 1988, "A Noise Source Identification Technique Using an Inverse Helmholtz Integral Equation Method," Journal of Vibration and Acoustics, ASME, **110**(1), pp. 84-90.

[3]   Tournour, M., Brux, P., Mas, P., Wang, X., McCulloch, C., and Vignassa, P., 2003, "Inverse Numerical Acoustics of a Truck Engine," SAE Technical Paper, (2003-01-1692).

[4]   Kobayashi, A., 2011, "Verification of Coverage of Inverse-numerical Acoustic Analysis," Proceedings of the 29th IMAC A Conference on Structural Dynamics, **9**, pp. 73-80.

[5]   Hilmi, H. L., Koizumi, T., Tsujiuchi, N., Maruo, K., and Uehara, H., 2013, "Construction of Sound Source Model of Gas Engine Using Inverse-Numerical Acoustic Analysis," Proceedings of the 5th International Operational Modal Analysis Conference, pp. 370-377.

[6]   Hilmi, H. L., Koizumi, T., and Tsujiuchi, N., 2013, "Sound Source Model Identification Using Inverse-Numerical Acoustic Analysis (Experimental Verification)," Proceedings of The 3rd Japan-Korea Joint Symposium on Dynamics & Control 2013, **13**(204), pp. 151-154.

[7]   Nakano, Y., and Yoshimura, T., 2013, "Precision Improvement of Identification of the Sound Source by Inverse Acoustic Analysis (In Japanese)," Transactions of the JSME©, **79**(801), pp. 1495-1504.

[8]   Oshima, H., Hilmi, H. L., Tsujiuchi, N., and Ito, A., 2015, "Placement Technique of Measurement Points for Inverse Acoustic Analysis", SAE Technical Paper, (2015-32-0747).

[9]   Chen, X., 2006, "Comparison of Numerical Methods for Noise Source Identification", Noise Control Engineering Journal, **54**(6), pp. 420-428.

[10]   Morkholt, J., 2003, "Hotspot Identification Methods for the Derivation of Acoustic Equivalent Source Models", SAE Technical Paper, (2003-01-1631).

[11]   Suzuki, K., Nishida, K., Maruyama, K., and Watanabe, T., "Vibration and Acoustics for Mechanical Engineering (In Japanese)," Science Press, Tokyo.

[12]   Crombecq, K., Laermans, E., and Dhaene, T., 2011, "Efficient Space-filling and Non-collapsing Sequential Design Strategies for Simulation Based Modeling," European Journal of Operational Research, **214**, pp. 683-696.

[13] Jin, R., Chen, W., and Saudjianto, A., 2005, "An Efficient Algorithm for Construction Optimal Design of Computer Experiments," Journal of Statistical Planning and Interference, **134**, pp. 267-287.

CHAPTER 3

Development of Vibration Analysis Method for Damped Structure Using Statistical Energy Analysis Method

3.1. Introduction

In recent years, reciprocating internal combustion engine is widely used as the power source for industrial machinery. This engine produces high level of vibration and noise especially during combustion process, which has been a particular issue. Thus there is a need for a prediction method to efficiently reduce vibration and noise radiation. Prediction method using Finite Element Method (FEM) and Boundary Element Method (BEM) are effective for low frequency vibration analysis. However, in order to analyze structure-borne noise and vibration it is necessary to consider the overall audible frequency range including the high frequency range noise and vibration that could be predicted more effectively using Statistical Energy Analysis (SEA).

SEA method which was first introduced in the 1960's by Lyon et.al, as a response prediction method for acoustic and vibration system of aerospace sector, is an effective method to predict high frequency range of noise and vibration[1]. In order to predict the vibration, it is necessary to estimate the SEA parameters called damping loss factors (DLF) and coupling loss factors (CLF). The loss factors could be experimentally estimated by conducting excitation tests on a single subsystem[2–5]. However, for a complex structure, it is difficult to estimate the loss factors by conducting single subsystem excitation tests. In order to tackle this problem, Power Injection Method (PIM) was proposed where it is possible to evaluate the loss factors for complex structure even when all the subsystems are connected together[6]. When conducting the analysis, a system is divided into simplified subsystems in order to estimate the parameters accurately. In addition, because the numbers of measurement points affects the accuracy of parameters estimation and vibration prediction, multiple points of vibration measurements are carried out during experiments. However, there is no guidance in determining specific measurement points. In addition, when there was a structural modification on a subsystem, parameters had to be estimated again on the entire system, thus increasing the number of experiments that needs to be conducted.

This chapter aims to verify the influence of vibration measurement points on the vibration response prediction results[7]. Furthermore, we proposed and verified the validity of damping loss factors estimation technique for a structure when a single

subsystem was attached with damping materials as an example of structural modification[7][8].

3.2. Statistical Energy Analysis Theory

3.2.1. Power flow balance equation for multiple subsystems

The Statistical Energy Analysis is a prediction method of sound and vibration for complex structures or system that is divided into several subsystems and characterized by quantities of stored vibration energy and modes within narrow frequency bands. The balance equation between input power, power dissipation and transmission power for each two subsystems can be described as power flow balance equation. Furthermore, in order to solve the equation, it is required to analyze the vibration state of the subsystems and calculate the parameters such as loss factors.

The power flow balance equation for N number of subsystems for a particular system can be described in matrix equation which can be written by the following equation[9];

$$
\omega
\begin{bmatrix}
\left(\eta_1 + \sum_{i \neq 1}^{N} \eta_{1i}\right) N_1 & -\eta_{12}N_1 & \cdots & -\eta_{1N}N_1 \\
-\eta_{21}N_2 & \left(\eta_2 + \sum_{i \neq 2}^{N} \eta_{2i}\right) N_2 & \cdots & -\eta_{2N}N_2 \\
\vdots & & \cdots & \vdots \\
-\eta_{N1}N_N & \cdots & \cdots & \left(\eta_N + \sum_{i \neq N}^{N-1} \eta_{Ni}\right) N_N
\end{bmatrix}
\times
\begin{bmatrix}
E_1/N_1 \\
E_2/N_2 \\
\vdots \\
E_N/N_N
\end{bmatrix}
$$

$$
=
\begin{bmatrix}
P_1 \\
P_2 \\
\vdots \\
P_N
\end{bmatrix}
\tag{3.1}
$$

where ω is the angular frequency, η_i is the damping loss factors, η_{ij} is the coupling loss factors, N_i is the mode number, E_i is the subsystem energy and P_i is the input power. The energy of each subsystem can be obtained by this equation if the loss factors matrix, which is the second term on the left-hand side, is given. Therefore obtaining an accurate loss factors is significant.

The structure subsystem energy is calculated by the following equation by the spatial average of vibration velocity v and mass M;

$$
E = M\langle v^2 \rangle
\tag{3.2}
$$

Here, $\langle v^2 \rangle$ is the spatial root mean square of vibration velocity. With Equation (3.2), the subsystem's vibration can be calculated if energy is obtained from a power balance Equation (3.1).

3.2.2. Calculation of loss factors using power injection method (PIM)

PIM simultaneously estimates damping and coupling loss factors[10]. In this method, vibration power is injected into each subsystem to measure the vibration energy in each subsystem. Each loss factors is estimated by using these experimental data. The coupling loss factors are estimated by the following equation;

$$\eta_{ij} \cong \frac{1}{\omega} \frac{\langle E_{ji} \rangle}{\langle E_{ii} \rangle} \frac{P_j}{\langle E_{jj} \rangle} \tag{3.3}$$

where $\langle \rangle$ shows the root mean square value. This equation is constituted by the energies of the focused and conterminous subsystems. The damping loss factors are estimated using the following equation;

$$\eta_i = \frac{P_i/\omega - (\sum E_{ii}\eta_{ii}) + (\sum E_{ji}\eta_{ji})}{E_{ii}} \tag{3.4}$$

3.2.3. Calculation of loss factors using decay ratio method (DRM)

The decay ratio method calculates the time history of the damped vibration[10]. The subsystem is excited and after the excitation stops, the damping vibration is measured. The logarithmic decrement is calculated from the measured signal. The damping loss factors can be calculated from the following equation using the reverberation time, which is defined as the time at which the energy decays by 60dB;

$$\eta = \frac{2.2}{T_{60} \cdot f} \tag{3.5}$$

Where η is the damping loss factors, f is the frequency, and T_{60} is the reverberation time.

3.3. Loss Factor Estimation in Experimental SEA

3.3.1. Test object

Figure 3.1 shows a test model that is constructed of a base, a roof, and four frames with thickness of 2.3mm, and three panels with thickness of 1.6mm. The external size of the test model is 700×500×390mm, and its structural subsystems are fixed with M8 bolts.

The object is divided into some subsystems in SEA based on the following assumptions;

1) The bended part of the subsystems and the shin panels deal with equivalent thickness.

2) Screw holes are neglected.

Figure 3.2 shows the SEA model. Subsystem 1 is the base, subsystem 2 is the roof, subsystems 3-6 are the frames, and subsystems 7-9 are the panels.

Figure 3.1 Picture of box-shaped structure
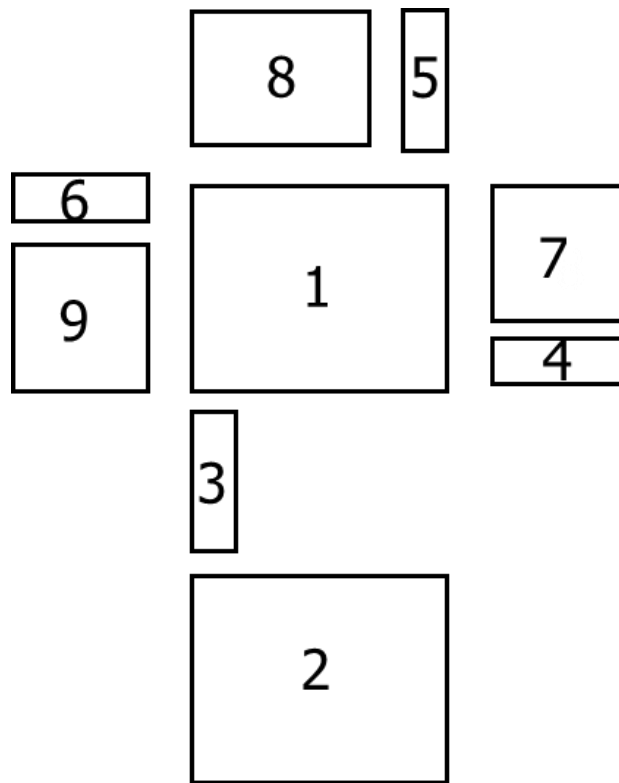
Figure 3.2 SEA model of the box-shaped structure consisting of 9 subsystems

3.3.2. The effect of measurement points to loss factors

3.3.2.1. Experimental method

We conducted an excitation experiments using power injection method in order to calculate the damping loss factors and coupling loss factors. Each subsystem is excited using Wilcoxon Research F3 shaker, and the vibration response is measured using Polytec Laser Doppler vibrometer. One random point on each subsystem was excited using sweep-sine wave signal with the range of 100 to 6000Hz. The measurement points of vibration response for base and roof is 130 points each, frame 19 points each, panel 7 and panel 9 is 80 points each, and panel 8 is 150 points.

3.3.2.2. The variance of mean average values on the change of average measurement points

When identifying the loss factors, several points from the measured points from each subsystem were taken and the averaged values are considered as space average.

The mean average values of the vibration velocity were calculated from the randomly extracted measurement points and the standard deviation of the mean average for the different number of measurements were calculated as variance. As a result, it is confirmed that the variance of the mean average becomes smaller by taking more measurement points. Therefore, it is thought that the average number of measurement points does affect the results of loss factors identification.

3.3.2.3. The change of loss factors for the change of average measurement points

5 random points from the measured values were taken and the damping loss factors are identified. The calculations for the identification of damping loss factors were done 100 times for different random points. The calculated standard deviation of the identified damping loss factors for the base and roof are shown in Figure 3.3. Based on Figure 3.3 we could see that there is variance on the damping loss factors. Therefore, it is clear that the average measurement points can affect the damping loss factors identification result.

3.3.2.4. The relationship between average measurement points and vibration prediction results

A model applied with the identified loss factors was created using the averaged 5 points of the average vibration velocity. Using the model that was created, the response of each subsystem was predicted during base excitation. Figure 3.4 shows the combination of the standard deviation of prediction results for panel 8, actual measurements and calculated results. As shown in Figure 3.4, variance occurs in the analysis result even though the vibration responses are well predicted.

Figure 3.5 shows the variance of analysis results for panel 8 with different average measurement points. As shown in Figure 3.5, there is less variance of analysis results with higher average numbers of measurement points. It could be considered that the

occurrence of variance in the mean average values where the average numbers of measurement points are few will result in the occurrence of variance in the vibration prediction result.
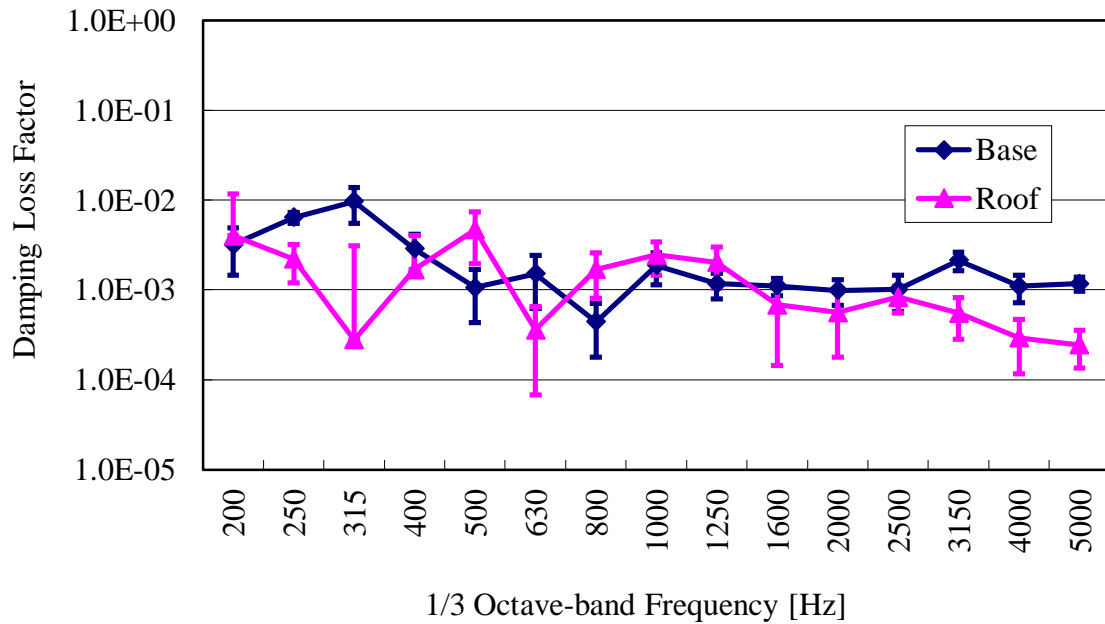
Figure 3.3 Identification results of damping loss factor for Base and Roof
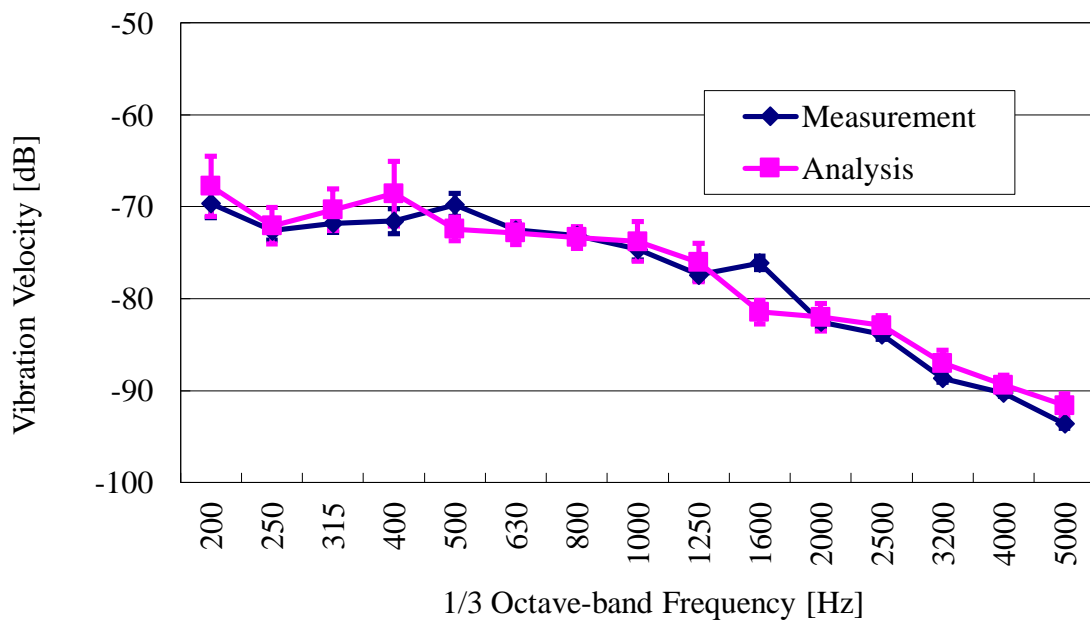
Figure 3.4 Estimation results of vibration response for Panel 8
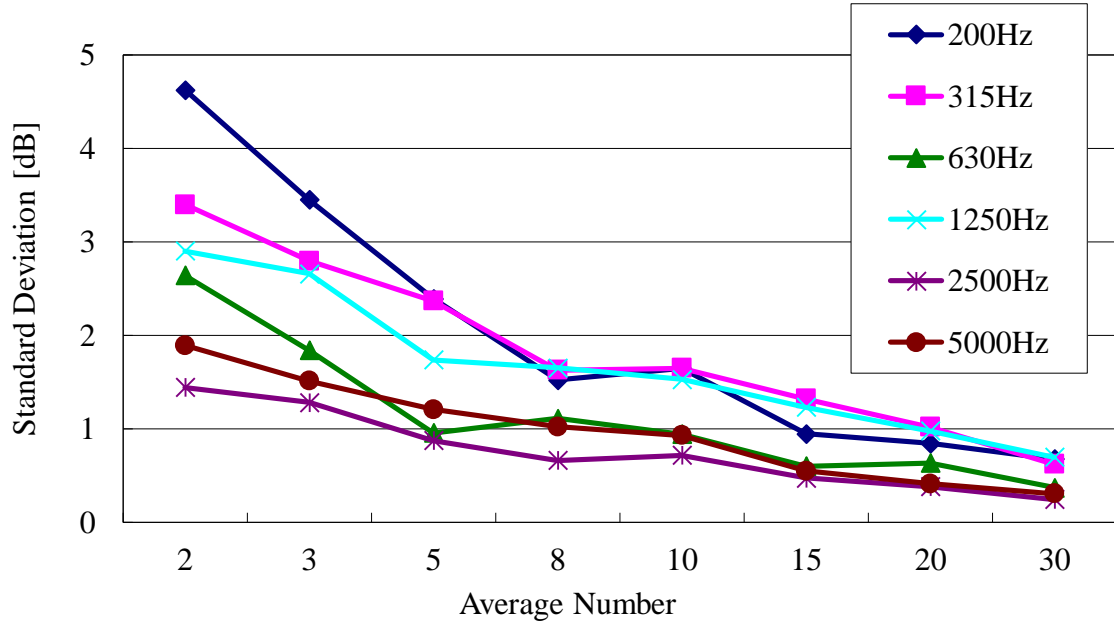
Figure 3.5 Variance in vibration analysis results for Panel 8 with different average numbers of measurement points

3.3.2.5. Predicting the effect of variance in average measurement value on the vibration prediction results

The effect of variance in measurement values for 3 subsystems model analysis on vibration prediction result was predicted. The power flow equation for 3 subsystems can be represented by the following equation,

$$\begin{Bmatrix} P_1 \\ P_2 \\ P_3 \end{Bmatrix} = \omega \begin{bmatrix} \eta_1 + \eta_{12} & -\eta_{21} & 0 \\ -\eta_{12} & \eta_2 + \eta_{21} + \eta_{23} & -\eta_{32} \\ 0 & -\eta_{23} & \eta_3 + \eta_{32} \end{bmatrix} \begin{Bmatrix} E_1 \\ E_2 \\ E_3 \end{Bmatrix} \tag{3.6}$$

where η_i is the damping loss factors, η_{ij} is the coupling loss factors, E_i is the subsystem energy and P_i is the input power. From Equation (3.6), the energy of each subsystem can be calculated from the following formula,

$$\begin{Bmatrix} E_1 \\ E_2 \\ E_3 \end{Bmatrix} = \frac{1}{\omega} \begin{bmatrix} \eta_1 + \eta_{12} & -\eta_{21} & 0 \\ -\eta_{12} & \eta_2 + \eta_{21} + \eta_{23} & -\eta_{32} \\ 0 & -\eta_{23} & \eta_3 + \eta_{32} \end{bmatrix}^{-1} \begin{Bmatrix} P_1 \\ P_2 \\ P_3 \end{Bmatrix} \tag{3.7}$$

Furthermore, by using the equations for calculating damping loss factors and coupling loss factors from the power injection method, each loss factors can be redefined as energy. Therefore, the calculation of damping loss factors for 3 subsystems can be given by the following equation,

$$\eta_i = \frac{P_i/\omega - (E_{ii}\eta_{ij} + E_{ii}\eta_{ik}) + (E_{ji}\eta_{ji} + E_{ki}\eta_{ki})}{E_{ii}} \qquad (3.8)$$

In addition, because the coupling loss factors can only be implemented on two adjacent subsystems, by substituting Equation (3.8) and Equation (3.3) into Equation (3.7), it can be written by the following expression,

$$\{E_a\} = \frac{1}{\omega}[E_m]^{-1}\{P'\} \qquad (3.9)$$

where, $\{E_a\}$ is the energy vector of the analysis results, $[E_m]$ is the energy matrices of measurement results and $\{P'\}$ is the input power vector. In this case, because there is no significant variance in input power, its effect can be ignored and the variance of the measurement values was analyzed. Considering ΔE_{ij} as the variance of each measurement values, the variance of analyzed values $\{\Delta E_a\}$ can be written as,

$$\{\Delta E_a\} = \frac{1}{\omega} \times \left[\frac{\partial}{\partial E_{11}}[E_m]^{-1}\Delta E_{11} + \cdots + \frac{\partial}{\partial E_{ij}}[E_m]^{-1}\Delta E_{ij} \right] \times \{P'\} \qquad (3.10)$$

Here, the effect on vibration prediction result of variance for each measurement values could be analyzed.

Equation (3.10) was applied to 3 subsystems of base, panel 7 and roof. For 2500Hz, the differential coefficient calculation result of Equation (3.10) is shown in Table 3.1. Measurement energy used for the differential coefficient calculation is the actual measured energy.

According to Table 3.1, we could identify the measurement values that have the highest contribution of variance in each energy values. The approximation equation using the measurement values with high contribution of variance can be shown as,

$$\Delta E_1 = \frac{\partial}{\omega \partial E_{11}}[E_m]^{-1}\{P'\}\Delta E_{11} \qquad (3.11)$$

$$\Delta E_2 = \frac{\partial}{\omega \partial E_{71}}[E_m]^{-1}\{P'\}\Delta E_{71} + \frac{\partial}{\omega \partial E_{27}}[E_m]^{-1}\{P'\}\Delta E_{27} \qquad (3.12)$$

The calculated variance of energy values using Equation (3.11) and Equation (3.12), and the variance of analyzed energy values during base excitation using power injection method are shown in Figure 3.6.

Based on Figure 3.6, it is understood that the variance of analyzed values could be estimated accurately from the actual measurement values with high contribution of variance. Therefore, by implementing this approach, the variance of analyzed values could be estimated before conducting power injection method, and the number of measurement points could be determined.

Table 3.1 Partial differential coefficient

	$\triangle E_1$	$\triangle E_7$	$\triangle E_2$
$\dfrac{\partial}{\partial E_{11}}[E_m]^{-1}$	1.0087	0.00890	0.00326
$\dfrac{\partial}{\partial E_{77}}[E_m]^{-1}$	0.0384	0.0183	-0.0774
$\dfrac{\partial}{\partial E_{22}}[E_m]^{-1}$	0.00604	0.00501	0.0042
$\dfrac{\partial}{\partial E_{17}}[E_m]^{-1}$	-0.0750	-0.0442	-0.0161
$\dfrac{\partial}{\partial E_{71}}[E_m]^{-1}$	-0.0849	0.89133	0.32415
$\dfrac{\partial}{\partial E_{72}}[E_m]^{-1}$	-0.0115	-0.0077	-0.0234
$\dfrac{\partial}{\partial E_{27}}[E_m]^{-1}$	-0.0183	0.00560	0.2114
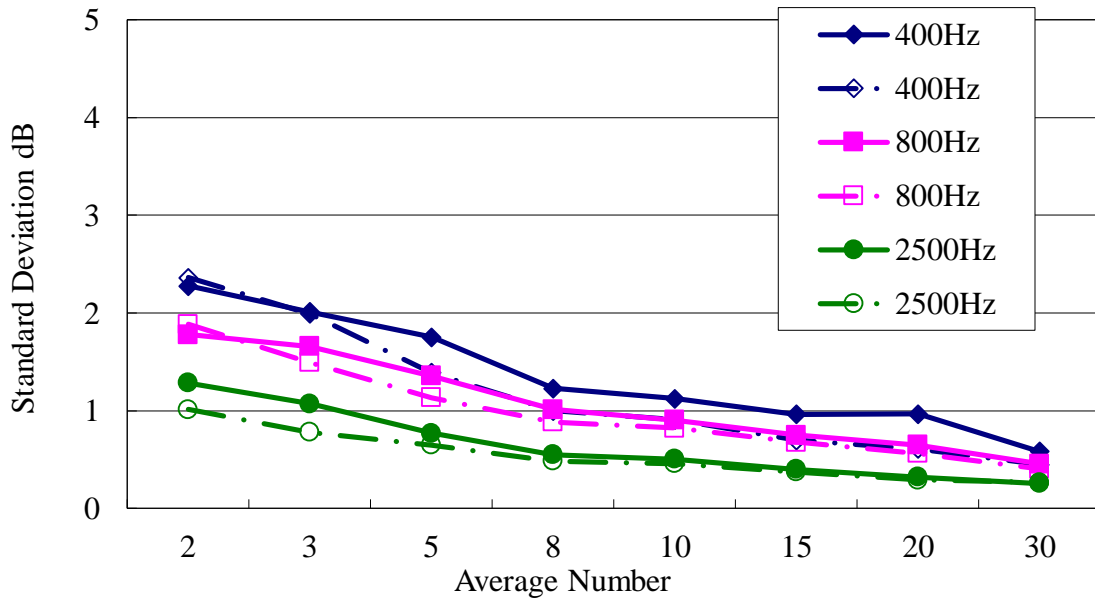
(a) Base
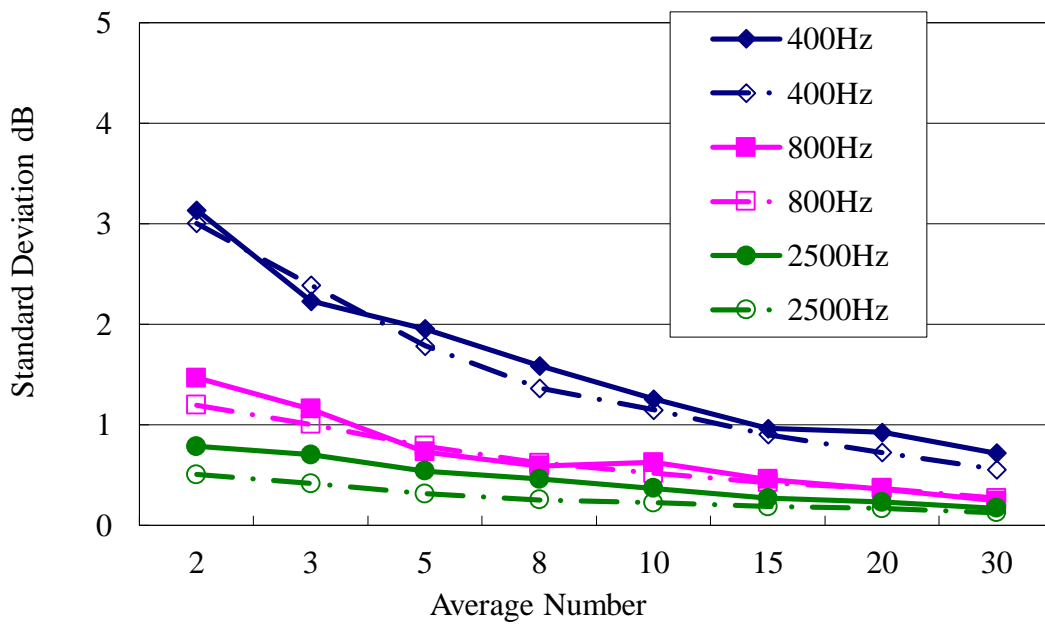
(b) Roof

Figure 3.6 Estimation results of analytical dispersion (●: Variance of analysis results, ○: Prediction result of variance)

3.3.3. Loss factors change estimation method for a single subsystem

It is understood that by attaching damping material on a structure, the damping loss factors of the subsystem would change. However, in order to utilize power injection method to calculate the loss factors, it is necessary to measure the entire structure all over again. Therefore, we conduct excitation experiments only on subsystem that was attached with damping materials and estimated loss factors based on the different amount of attached damping materials. In addition, we also estimated the damping loss factors for mounted structure. The damping loss factors of a single subsystem were estimated using decay ratio method.

3.3.3.1. Experimental method

In order to calculate the damping loss factors using decay ratio method, we conducted hammering test and measured the free vibration. The measurement and excitation points are each 5 points and the panel was hanged to simulate free support condition during experiment.

Rubber material was used for the damping material. The cross-sections and outline of the rubber material is shown in Figure 3.7. The damping material is attached to panel 8 with 2 different ways that are diagonally across the panel and squared around the panel. The lengths for diagonal attachment are 1.0m, 0.5m, 0.25m, 0.12m, and the lengths for squared attachment are 2.0m, 1.64m, 1.36m, 1.0m, 0.76m, and 0.40m. The attachment diagram is shown in Figure 3.8.
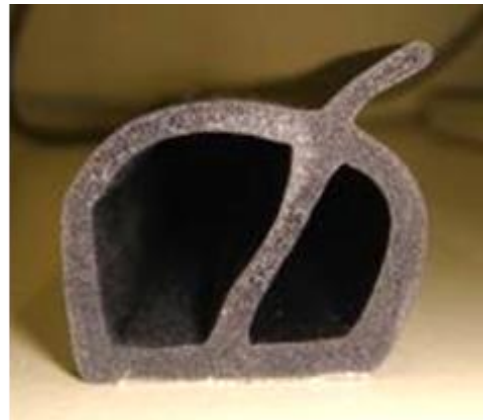
(a) Overview   (b) Cross-sectional view

Figure 3.7 Damping material

| (a) 1.0m | (b) 0.5m | (c) 0.25m | (d) 0.12m |

| (e) 2.0m | (f) 1.64m | (g) 1.36m | (h) 1.0m |

| (i) 0.76m | (j) 0.4m |
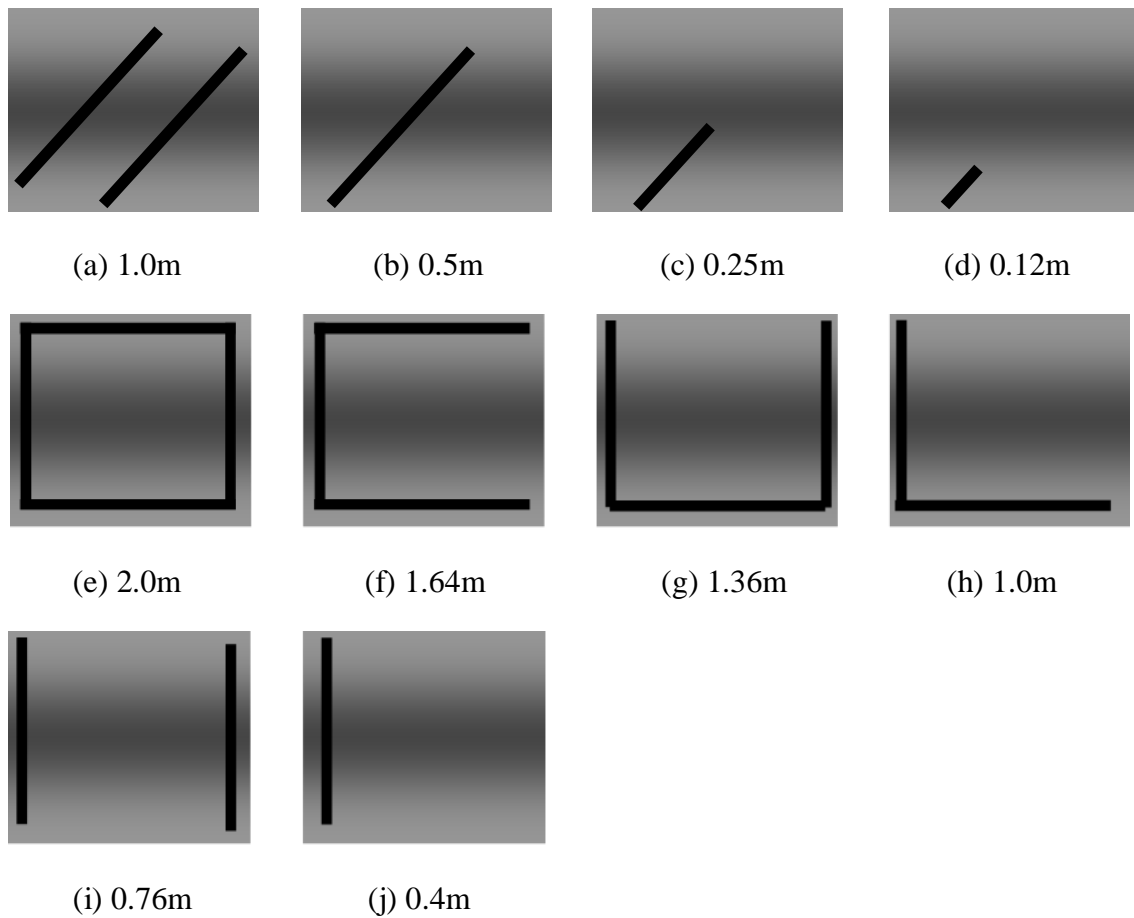
Figure 3.8 Damping material attachment diagrams

3.3.3.2. Loss factors estimation of a single subsystem

In this section will clarify the relationship between the length of attached damping material and the amount of change on damping loss factors. In addition, we derived an estimation equation of damping loss factors for the changes in the length of damping material.

It was reported that the damping loss factors for a flat plate is a constant regardless of the dimension of the plate[9]. In a similar way, it could be considered that the damping loss factors of the damping material are not related to the length. In fact however, the damping loss factors do changes depending on the length of the damping material. This is because when energy was flowing through the panel attached with damping material, the present energy of the damping material also changes. Therefore, we estimated the damping loss factors of the panel attached with damping material based on the energy ratio between the damping material and the panel.

During the energy flow through the panel attached with damping material, the panel and damping material each are assumed as a single subsystem, and the damping energy loss can be represented by the following equation,

56

$$\eta_{all} E_{all} = \eta_1 E_1 + \eta_2 E_2 \tag{3.13}$$

where, η_{all} is the damping loss factors of panel attached with damping material, E_{all} is the energy of panel attached with damping material, η_1 is the damping loss factors of panel, E_1 is the panel's energy, η_2 is the damping loss factors of damping material, E_2 is the energy of damping material. From Equation (3.13) η_{all} can be written as the following equation,

$$\eta_{all} = \frac{\eta_1 E_1 + \eta_2 E_2}{E_{all}} \tag{3.14}$$

where, $E_{all}=E_1+E_2$. η_{all} can be calculated from the ratio between E_1 and E_2.

Next, we could derive the relational equation between E_1 and E_2 from the power flow balanced equation of 2 subsystems when power is injected onto the panel. The power flow balanced equation is shown by the following equation,

$$\begin{Bmatrix} P_1 \\ P_2 \end{Bmatrix} = \omega \begin{bmatrix} \eta_1 + \eta_{12} & -\eta_{21} \\ -\eta_{21} & \eta_2 + \eta_{21} \end{bmatrix} \begin{Bmatrix} E_1 \\ E_2 \end{Bmatrix} \tag{3.15}$$

From Equation (3.15), energy can be expressed as follows,

$$\begin{Bmatrix} E_1 \\ E_2 \end{Bmatrix} = \frac{1}{\omega} \begin{bmatrix} \eta_1 + \eta_{12} & -\eta_{21} \\ -\eta_{21} & \eta_2 + \eta_{21} \end{bmatrix}^{-1} \begin{Bmatrix} P_1 \\ P_2 \end{Bmatrix} \tag{3.16}$$

Here, because the input power to the damping material $P_2=0$, Equation (3.16) can be rewritten as follows,

$$\begin{Bmatrix} E_1 \\ E_2 \end{Bmatrix} = \frac{1}{\omega} \frac{P_1}{\eta_1 + \eta_2 + \eta_2 + \eta_{12} + \eta_1 + \eta_{21}} \begin{Bmatrix} \eta_2 + \eta_{21} \\ \eta_{12} \end{Bmatrix} \tag{3.17}$$

From Eq. (3.17) we could obtain,

$$E_1 = \frac{\eta_2 + \eta_{21}}{\eta_{12}} E_2 \tag{3.18}$$

By substituting Equation (3.18) into Equation (3.13), η_{all} could be calculated from the following equation,

$$\eta_{all} = \frac{\eta_1 \eta_2 + \eta_1 \eta_{21} + \eta_2 \eta_{12}}{\eta_2 + \eta_{21} + \eta_{12}} \tag{3.19}$$

From Equation (3.19), it is possible estimate the damping loss factors of panel attached with damping material if the damping loss factors of panel and damping material, and the coupling loss factors between panel and damping material are known. η_1 was calculated using decay ratio method, whereas a constant value of $\eta_2= 0.1$ which is a common value of rubber material for all frequency range was used because it is difficult to obtain η_2 experimentally[12]. In addition, coupling loss factors can be theoretically calculated from the following equation[13],

$$\eta_{ij} = \frac{C_{gi} L_c \tau_{ij}}{\pi \omega S_i} \tag{3.20}$$

where, C_{gi} is the bending-wave group velocity of subsystem i, which can be represented by phase velocity C_{bi}, where $C_{gi}=2C_{bi}$. Moreover, L_c is the bond length, τ_{ij} is the energy transmittance from subsystem i to subsystem j, and S_i is the area of subsystem i. Even though Equation (3.20) can be used to identify the coupling loss factors, it is theoretically difficult because of the complex cross-section rubber material. Therefore, from the experimental results of diagonal attachment for 1.0m and squared attachment for 2.0m, optimized calculation was conducted. The optimization used the following objective function J,

$$J = \left(\eta_{meas} - \frac{\eta_1 \eta_2 + \eta_1 \eta_{21} + \eta_2 \eta_{12}}{\eta_2 + \eta_{21} + \eta_{12}} \right)^2 \tag{3.21}$$

Where η_{meas} is the identified damping loss factors of the panel attached with damping material from the experiment. In order to minimize Equation (3.21), η_{12} and η_{21} were optimized using quasi-Newton method. The optimization was conducted using ESTECO optimization tool, modeFRONTIER. According to Equation (3.20), η_{12} are proportional to the attachment length and thus it is possible to estimate η_{all} during the change in attachment length.

Figure 3.9 to Figure 3.12 show the estimated results using Equation (3.19) and measured values for diagonal attachment and squared attachment respectively. From Figure 3.9 and Figure 3.12, by using the proposed method the damping loss factors during the change of attachment length could be estimated accurately.
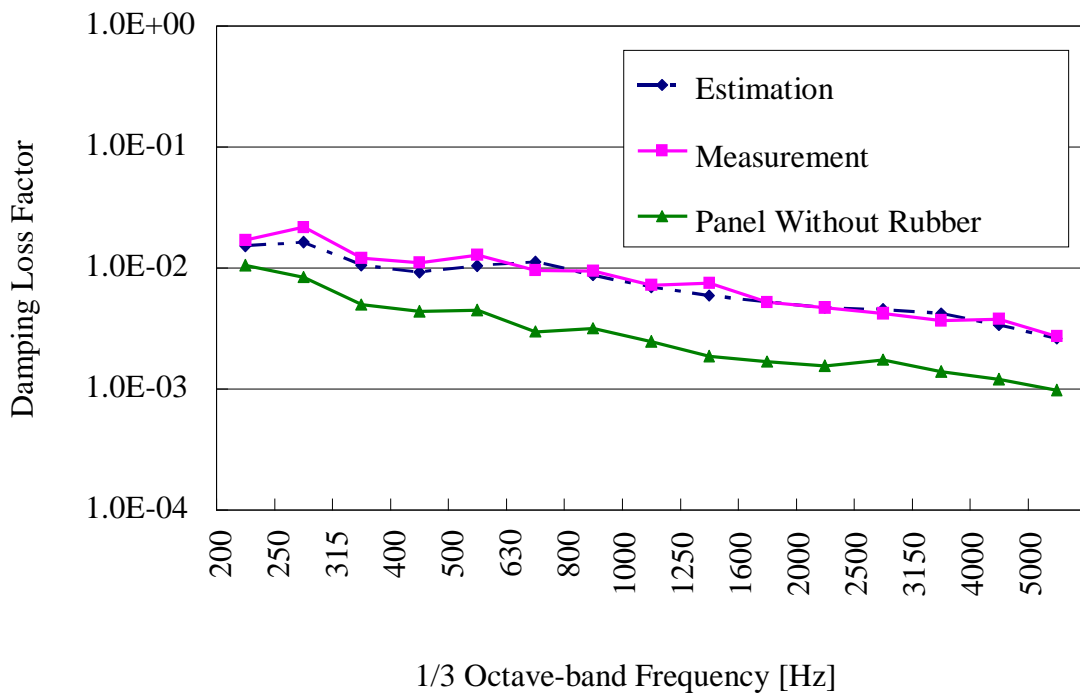
Figure 3.9 Estimation results of damping loss factor for 0.5m diagonal attachment
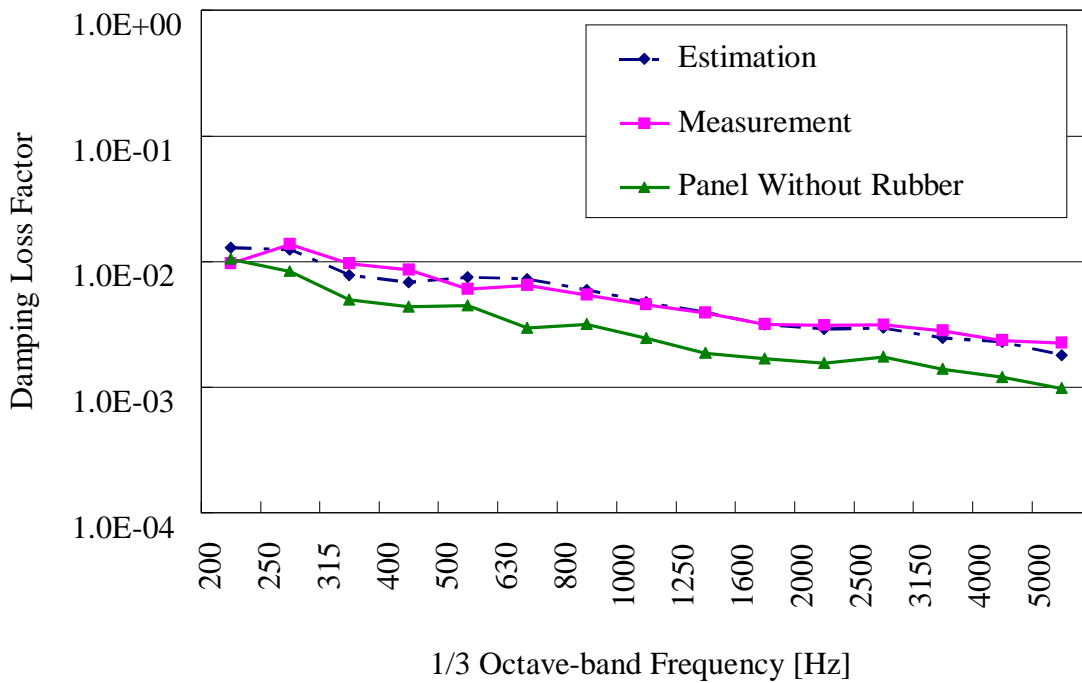
Figure 3.10 Estimation results of damping loss factor for 0.25m diagonal attachment

59
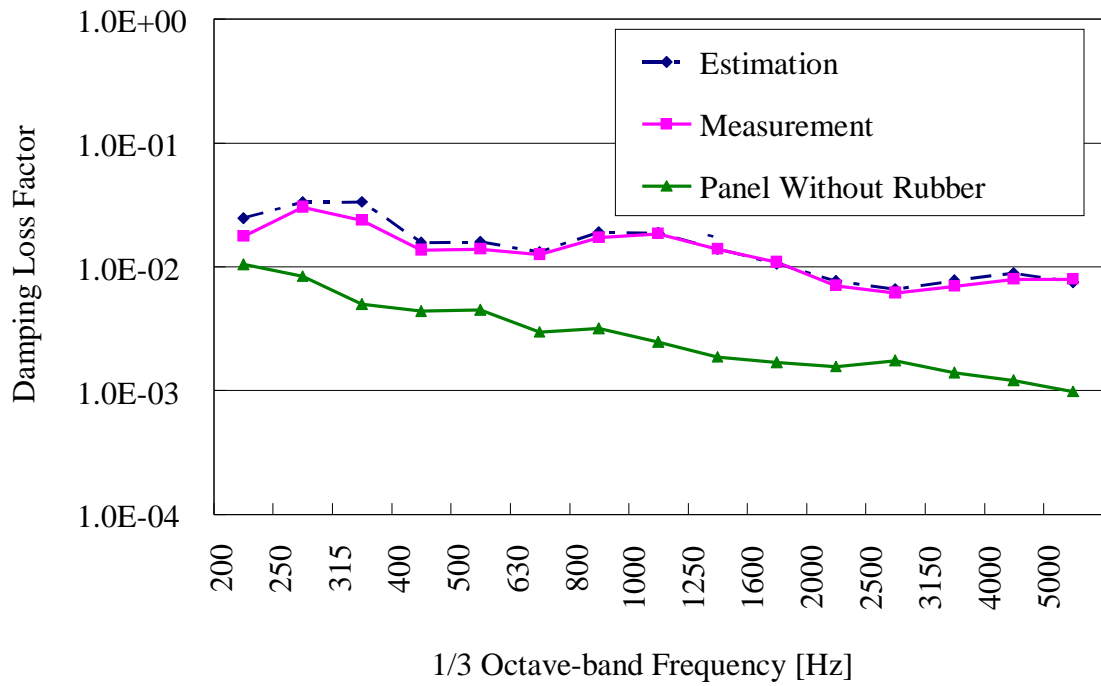
Figure 3.11 Estimation results of damping loss factor for 1.64m squared attachment
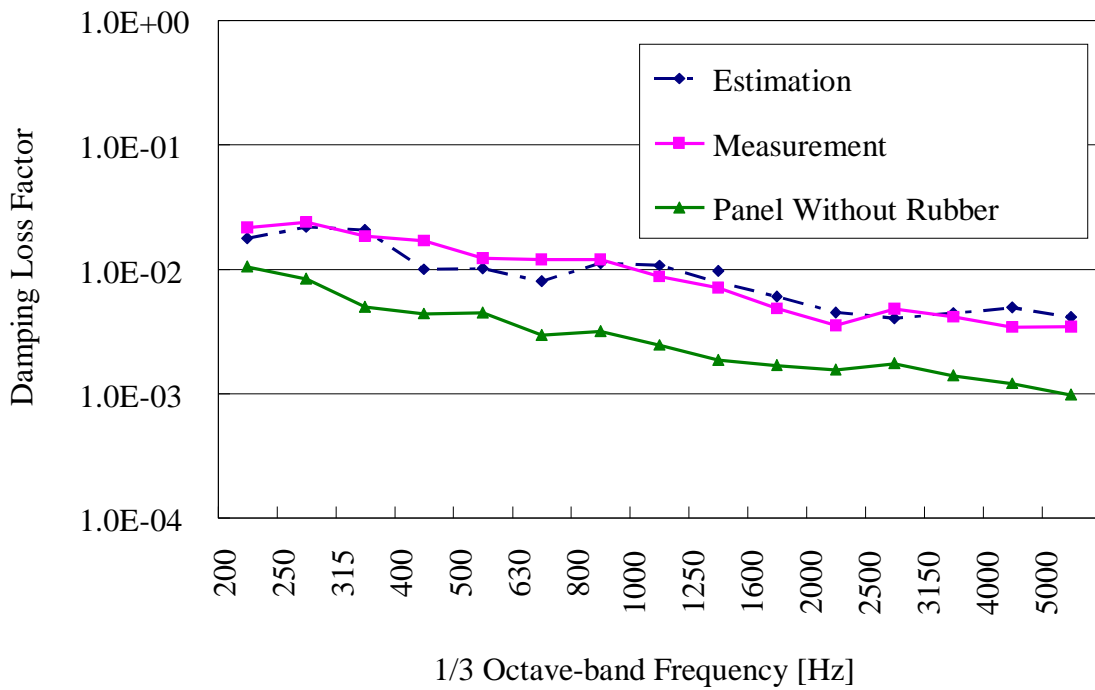
Figure 3.12 Estimation results of damping loss factor for 0.76m squared attachment

3.3.3.3. Application on the actual system

The identified results of internal loss factors for a single panel and the results using power injection method are shown in Figure 3.13. From Figure 3.13 it is understood that the identification result was different for the same when it is in a structure form. Therefore, the identified value of η_1 of Equation (3.18) from the power injection method was used to estimate the damping loss factors of structure form after the attachment of damping material. In addition, the optimized values of η_{12} and η_{21} from the previous section were used. The estimated result of damping loss factors of the structure with diagonal attachment using Equation (3.18) and the identified values using power injection method are shown in Figure 3.14 and Figure 3.15. Based from the figure, the damping loss factors could be estimated accurately. In conclusion, by using the proposed technique, the amount of change in damping loss factors of a structure form when attached with damping material could be estimated.
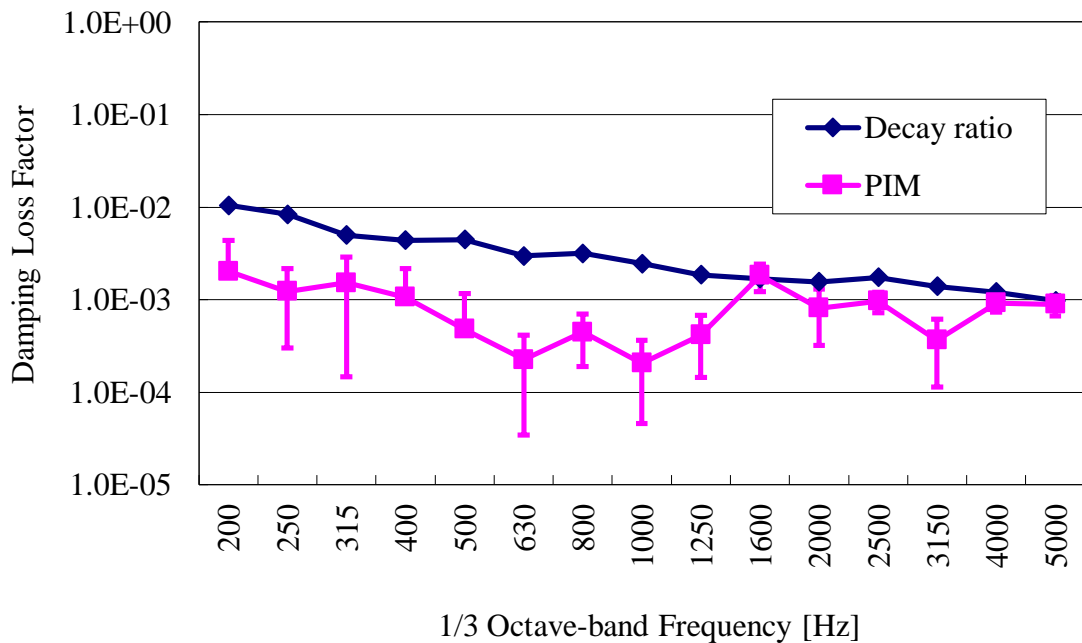
Figure 3.13 Damping loss factor comparison result of decay ratio method and power injection method
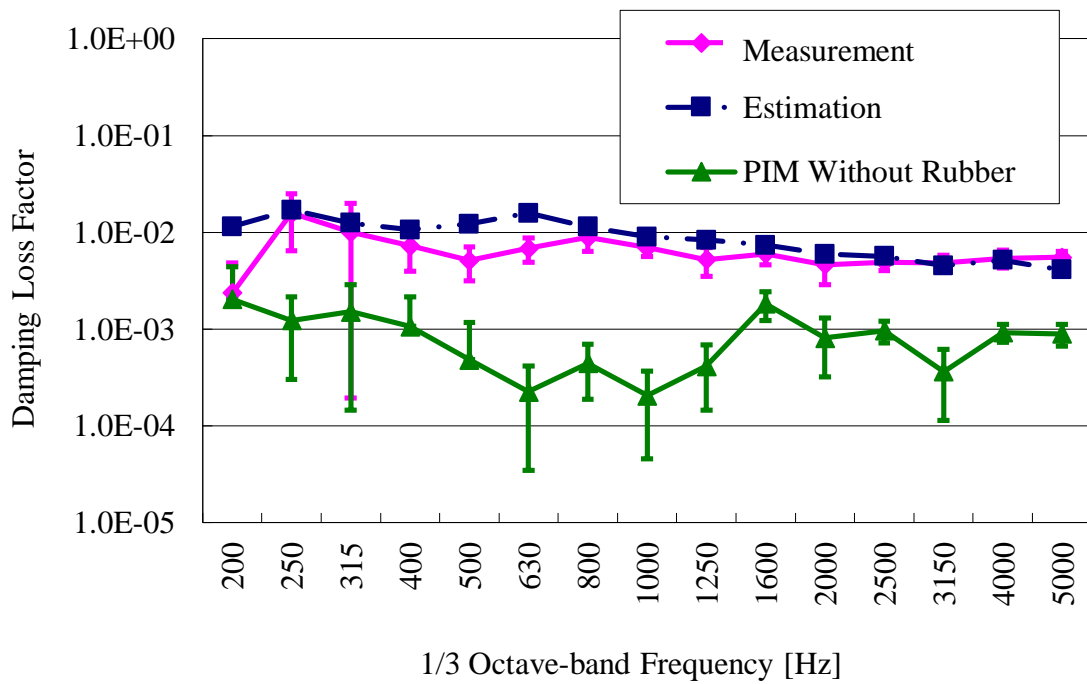
Figure 3.14 Estimation results of damping loss factor for built structure with 1.0m damping material
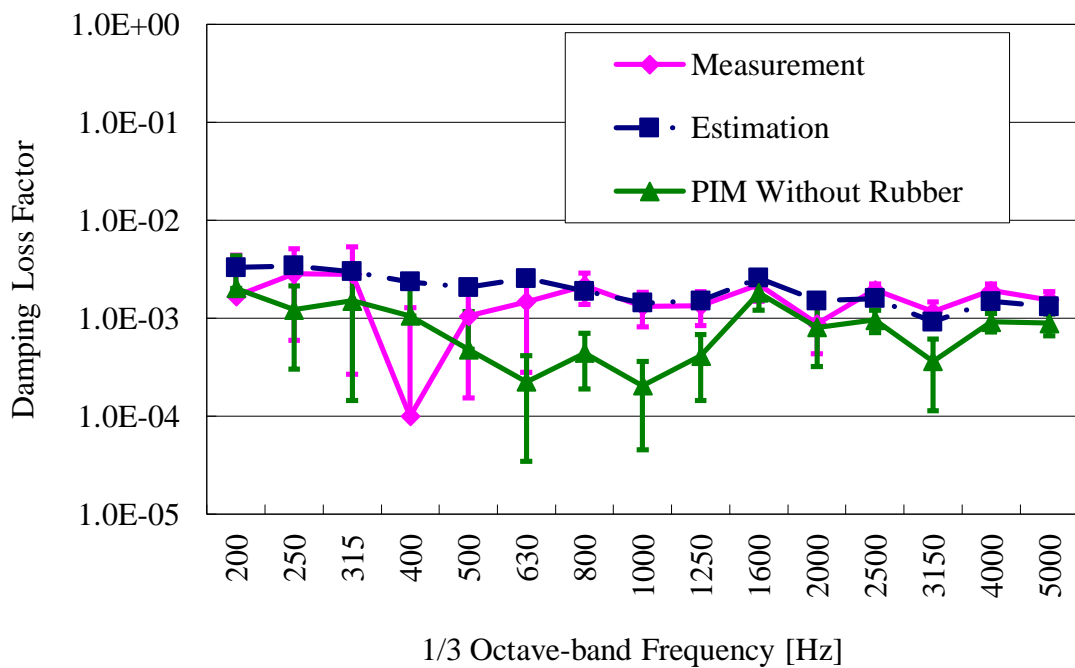
Figure 3.15 Estimation results of damping loss factor for built structure with 0.12m damping material

3.4. Conclusion

In this chapter, we estimated the loss factors using the power injection method. The following conclusions are drawn from this investigation;

1) The variance on the average values using the power injection method shows the influence of the number of measurement points on the loss factors estimation results and the analysis results.

2) By using the variance of the average values from the measurement results of the elements which has the highest contribution, the actual variance of analysis results for the different average numbers were able to be estimated.

3) By estimating the variance of analysis results prior to performing experiments using power injection method, a technique to determine the number of measurement points was proposed.

Furthermore, based on the experiment results of a single element with the attachments of damping materials, a technique to identify the damping loss factors of combined elements with the attachments of damping materials was proposed and validated.

References

[1] Lyon, R. H., and DeJong, R. G., 1995, Theory and Application of Statistical Energy Analysis, Butterworth-Heinemann, Boston.

[2] Lai, H.-Y., 2007, "Experimental Comparison of Test Methods for Structure-borne Sound Power Measurement," SAE Tech. Pap., (2007-01-2169).

[3] Bolduc, M., Atalla, N., and Wareing, A., 2005, "Measurement of SEA Damping Loss Factor for Complex Structures," SAE Tech. Pap., (2005-01-2327).

[4] Pocha, J., 1977, "Acoustic Excitation of Structures Analyzed by the Statistical Energy Method," AIAA J., **15**(2), pp. 175-181.

[5] Crocker, M. J., and Price, A. J., 1969, "Sound transmission using statistical energy analysis," J. Sound Vib., **9**(3), pp. 469-486.

[6] Bies, D. A., and Hamid, S., 1980, "In situ determination of loss and coupling loss factors by the power injection method," J. Sound Vib., **70**(2), pp. 187-204.

[7] Hilmi, H. L., Koizumi, T., and Tsujiuchi, N., 2014, "Loss Factors Estimation of Statistical Energy Analysis Using Power Injection Method", The Science and Engineering Review of Doshisha University, **55**(3), pp. 291-300.

[8] Honsho, K., Hilmi, H. L., Koizumi, T., and Tsujiuchi, N., 2012, "Damping Loss Factor Estimation Method by Using Finite Element Method in Statistical Energy Analysis", The Proceedings of 41st International Congress on Noise Control Engineering, pp. 8330-8341.

[9] Irie, Y., and Nakamura, T., 1984, "Prediction of Structure Borne Sound Transmission Using Statistical Energy Analysis," J. Mar. Eng. Soc. JAPAN, **19**(3), pp. 257-266.

[10] Kamata, M., Lalor, N., and Stimpson, G. J., 1993, "Automotive Noise and Vibration Analysis Using Statistical Energy Analysis Method (In Japanese)," Trans. Soc. Automot. Eng. Japan, **47**(6), pp. 77-83.

[11] Damping Engineering Handbook Editorial, 2008, Damping Engineering Handbook (In Japanese), Corona Publishing Co., Tokyo.

[12] Iizumi, S., 1973, Mechanical Design Handbook (In Japanese), Maruzen Company Limited, Tokyo.

[13] Hiraki, B., 1995, Applied Technology Press (In Japanese), Applied Technology Press, Tokyo.

CHAPTER 4

Development of Comparison Method of Statistical Energy Analysis and Transfer Path Analysis

4.1. Introduction

In the pursuit of efficient ways to analyze the design dynamics of small machines such as a small power generator or a co-generation system, it is important to identify information and dynamics of input power sources during machine operation. On the basis of energy analysis models, such as statistical energy analysis (SEA), we established in previous research an external input power identification technique for simple and practical structure using finite element method[1-3]. The results of the energy analysis models were excellent in cases with unclear input force locations. The identification of input powers was found to be effective and quantitatively accurate if the location and number of excitation and response points could be appropriately distributed within the subsystem. In regards to input power, Kadomatsu et al. discussed the relation between sound power in a car interior and structural input power on the car body[4]. To realize low noise in the car interior, component engineering was required in order to identify the structural input power accurately. Therefore, in the application of small power generator, the identification of input power using SEA is effective even with unknown source location but ineffective when dealing with multiple components.

On the other hand, transfer path analysis (TPA) is based on estimation of a frequency response function (FRF) between the excitation points and response points. Identifying the input forces is trivial when their locations are obvious. The response contributions of transfer paths can then be evaluated after identifying the vibration and noise sources. TPA has been employed in several previous research studies on identifying input forces. Kobayashi et al. proposed a novel approach that used an apparent-mass matrix instead of a matrix inversion method to improve the accuracy of input identification[5]. To improve the accuracy of SEA results, research has also been conducted in which the input power in SEA is calculated by utilizing the force predicted by TPA[6]. However, a study comparing the input powers and contribution rates determined by SEA and TPA are still gathering pace.

Therefore in this chapter, as a basic study to compare both of these methods, we proposed an evaluation method to compare SEA and TPA for multiple excitation input sources and transfer path contributions between excitation sources and evaluation points. We aim to investigate the applicability of the proposed method on a more common

structures consisting of thin plates and frames. The proposed method was validated through numerical analyses using a finite element method (FEM) of thin plate structures consisting two or more subsystems.

4.2. Transfer Path Analysis Theory

4.2.1. TPA by Matrix Inversion Method

In transfer path analysis (TPA), a target system is expressed in terms of a number of systems that act upon it, and the input force and contribution rate are determined as the product of frequency response function (FRF) matrix and input force. The basic equation for predicting the input forces is expressed as[5];

$$\{v_m\} = [H_{mn}]\{F_n\} \tag{4.1}$$

Here, $[H_{mn}]$ is the measured FRF matrix between responses and excitation sources, $\{F_n\}$ is the force vector, and $\{v_m\}$ is the vector of measured responses at the response positions. The subscripts m and n denote the number of responses and excitation sources, respectively. $[H_{mn}]$ is measured by performing an excitation test on the FEM results before conducting the machine operation test in which $\{v_m\}$ is measured. Each response in the $[H_{mn}]$ matrix is expressed through a magnitude and phase response:

$$H_{mn} = \left|\frac{v_m}{F_n}\right| (cos\,\theta + j\,sin\,\theta) \tag{4.2}$$

where j is the imaginary unit and θ is the phase response. Hence, the predicted force evaluated by the matrix inversion method is expressed from Equation (4.1) as;

$$\{F_n\} = [H_{mn}]^{-1}\{v_m\} \tag{4.3}$$

For the contribution rates from excitation sources during machine operation, if p is the evaluation point and $\{F_n{}'\}$ is the identified force from Equation (4.3), then

$$\{v_p\} = [H_{pn}]\{F_n{}'\}$$
$$= \{H_{p1}, \cdots, H_{pn}\}\{F_n{}'\} = H_{p1}F_1{}' + \cdots + H_{pn}F_n{}' \tag{4.4}$$

and the contribution rates from the excitation sources are expressed as;

$$C_{pn} = \left\{\frac{H_{p1}F_1{}'}{v_p}, \cdots, \frac{H_{pn}F_n{}'}{v_p}\right\} \times 100[\%] \tag{4.5}$$

4.3. Comparison Method for SEA and TPA

4.3.1. Excitation Sources

For the TPA input power evaluated by the matrix inversion method, in accordance with the input force in Equation (4.3) and the measured response on the excitation point;

$$P_n = \frac{1}{2} Re[F_n' V_n^*] \tag{4.6}$$

Here, $Re[\cdot]$ represents the real part of a given number, V_n is the response velocity at excitation point n, and * denotes a conjugate complex number.

The SEA input power in Equation (3.15) is expressed in a space averaged over the subsystem, and TPA input power in Equation (4.6) is expressed at the excitation point.

4.3.2. Contribution Rates at Excitation Sources

In SEA, the transfer contribution rates are defined as the power flow rates between subsystems, which;

$$C_{i,j} = \frac{\omega \eta_{i,j} E_i}{\omega(\eta_{i,j} E_i + \eta_{j,i} E_j)} \times 100[\%]$$

$$= \frac{\eta_{i,j} E_i}{\eta_{i,j} E_i + \eta_{j,i} E_j} \times 100[\%] \tag{4.7}$$

According to our earlier paper [1], in experimental SEA model there are cases when the loss factors shows negative values, and thus it is impossible to compare with TPA using Equation (4.7). Therefore, we propose Equation (4.8) where contribution rates will not be negative values.

$$C_{i,j} = \frac{E_j/P_i}{(E_j/P_i + E_i/P_j)} \times 100[\%] \tag{4.8}$$

In contrast, Equation (4.4) and Equation (4.5) are transformed into the power dimension, and the following equation defines the TPA transfer contribution rates;

$$C_{pr} = \left\{ \frac{H_{p1} F_1' F_1'}{p_p}, \cdots, \frac{H_{pn} F_n' F_n'}{p_p} \right\} \times 100[\%] \tag{4.9}$$

$$p_p = \{H_{p1}, \cdots, H_{pn}\}\{F_n'\}\{F_n'\}$$

$$= H_{p1} F_1' F_1' + \cdots + H_{pn} F_n' F_n' \tag{4.10}$$

Since the value of the TPA contribution rates evaluated by Equation (4.9) may exceed 100% because phase response is utilized, comparing this result with the SEA contribution rates given by Equation (4.8) and Equation (4.9) is difficult. Therefore, the

response H_{pn} at the evaluation point in Equation (4.9) and Equation (4.10) is evaluated by using the following equation;

$$H_{pn} = \left| \frac{v_p}{F_n} \right| \tag{4.11}$$

This allows the SEA contribution rates calculated by Equation (4.8) to be expressed from an input subsystem to an evaluated subsystem, whereas the TPA contribution rates calculated by Equation (4.9) are expressed from an input point to an evaluated point.

4.3.3. Comparison Procedures

The procedures for comparing the input powers and contribution rates given by SEA and TPA involve three steps:

1. Construct experimental models to identify the SEA loss factors in Equation (3.16) and the FRF matrix $[H_{mn}]$ for TPA in Equation (4.1).

2. Perform a machine operation test.

3. Identify the input powers and contribution rates.

4.4. The Validating the Applicability of Proposed Method Through Numerical Analyses

In this section, the proposed method is validated through numerical FEM analyses of a simple structure consisting of one frame and flat plate and a partial car model consisting of seven subsystems.

4.4.1. Test Plate 1 and Analytical Conditions

In this section, as a basic study on the applicability of the proposed method for frame and plate structure, a real simulated engine mount frame and front panel as shown in Figure 4.1 is used as a target structure. The thickness of the steel panel (subsystem 3) is 0.8mm. The width, height and thickness of the rectangular steel pipe frame which is shown as purple line (subsystem 1 and 2) are 50mm, 100mm and 0.6mm respectively. The # symbol in the Figure 4.1 shows the subsystem's number, where the edge of subsystems 1 and 2 are connected to the subsystem 3 at y-axis direction. The boundary of subsystem 3 is simply supported. The mass of subsystem 1 and 2 are approximately 0.7kg, while subsystem 3 is approximately 5.6kg. As for the coupling between the subsystems, because subsystem 1 and 2 are connected through different connection, all the subsystems are considered connected for SEA model. The grey and purple arrows (1 per subsystem), grey cylinders (5 per subsystem) and blue cylinder denote the excitation, response, and evaluation locations, respectively. Figure 4.1 also shows the real operation test according to procedure (2). The input and response locations are placed at locations that are easy to compare the results of SEA and TPA. That is, in order for the contribution rates to be 50% from input locations on subsystem 1 and 2 to

evaluation point on subsystem 3, the input and response locations of subsystem 1 and 2, and the response locations on subsystem 3 should be approximately symmetric, and the input location on subsystem 3 should be approximately center. Approximate locations was used because the when there are distortion on the structure mesh, the automatic mesh function of the PAM-VA One 2010.5 could not be accurately symmetric. The locations and numbers of the excitation and response points are the same when applying SEA and TPA in examination procedures (1) and (2).

The target frequencies are the one-third octave band frequencies from 100Hz to 3.15kHz. Although from the result of the modal analysis to the single piece of frame we can observe the first mode from about 180Hz. The size of each element in the mesh is about 8.5mm×8.5mm, which is sufficient to contain six nodes per bending wavelength up to 4.25kHz. The modal damping ratio is assumed to be two cases for all modes;

(i)   0.1% for subsystem 1 and 2, and 1% for subsystem 3

(ii)   0.1% for all subsystems.

In our research, PAM-VA One is utilized in examination procedures (1) and (2), and the MATLAB software package is utilized in procedure (3). In addition, the magnitude of the excitation force in the model construction and in the machine operation test is set to be a unit force (1N). In the operation test, each unit force on the subsystem is applied during the same phase. To solve the input vector $\{F_n\}$ in Equation (4.3), the MATLAB function for finding the Moore-Penrose pseudoinverse of a matrix is employed.
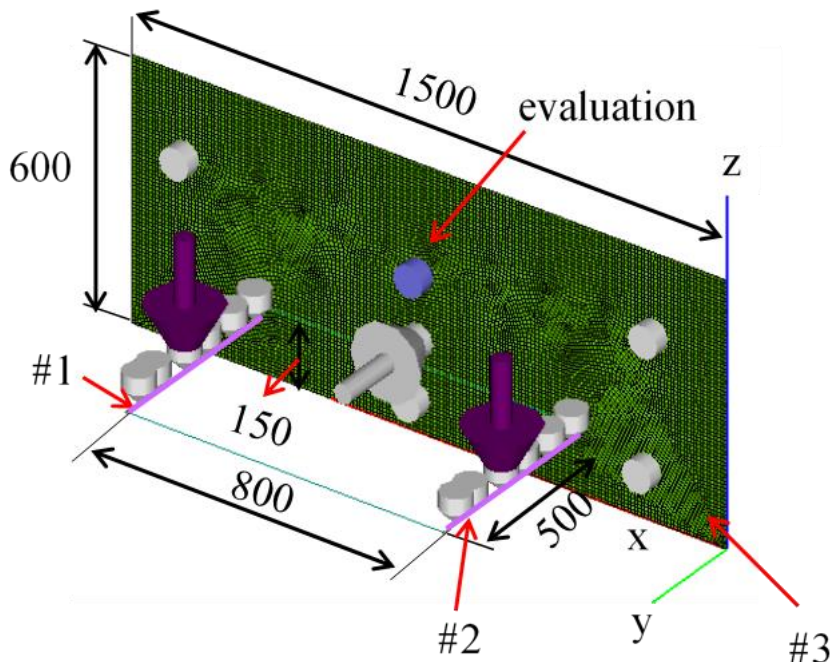
Figure 4.1 Test structure 1

4.4.1.1. Analysis results and discussions

Following procedures (1) and (2), the TPA input force identified from Equation (4.3) by the matrix inversion method is a unit force in all frequency bands regardless of the conditions of the loss factors, and thus shows the validity of the model. In addition, the influences of the modal damping ratio on the input power and the contribution rates, as to the input power are quantitatively similar regardless of the conditions of the loss factors. As to the contribution rates, since there are cases where the SEA coupling loss factor shows negative value in two frequency bands in case (ii), it is difficult to compare SEA and TPA. Except for these frequency regions, contribution rates for the two cases did not show large difference.

4.4.1.2. Identified input power

Figure 4.2 and Figure 4.3 show the comparison results between the input powers predicted by SEA and by TPA for case (i) and case (ii) respectively. A similar trend is obtained as in the case of subsystem 2. Both in Figure 4.2 and Figure 4.3, the prediction results of SEA are quantitatively similar to those of TPA using Equation (4.6) at frequencies above 400Hz. Therefore, the proposed method was also shown to be useful on a simple structure consisting of one frame and flat plate.
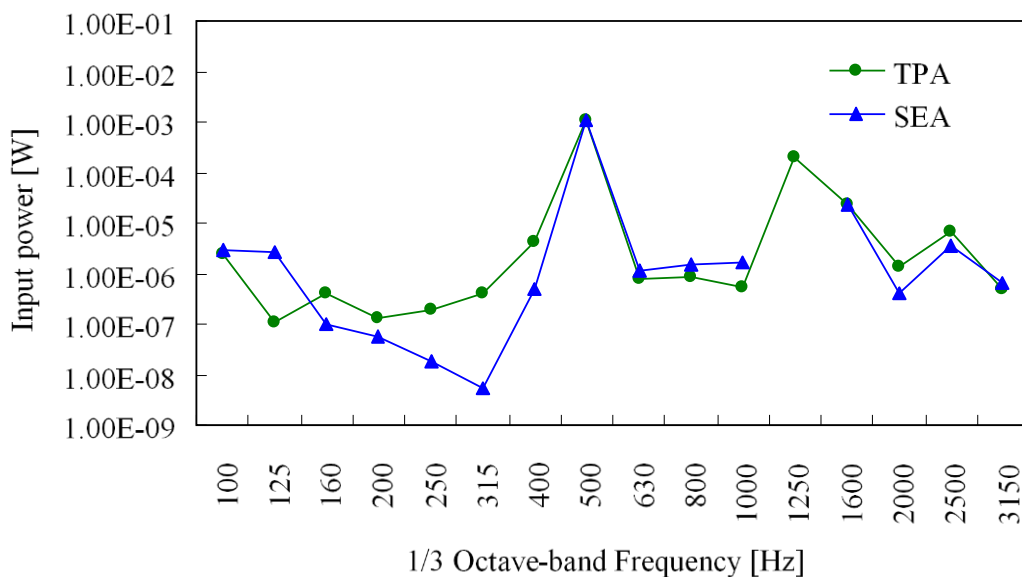
Figure 4.2 Comparison of input power between SEA and TPA of subsystem 1 for case(i)

70
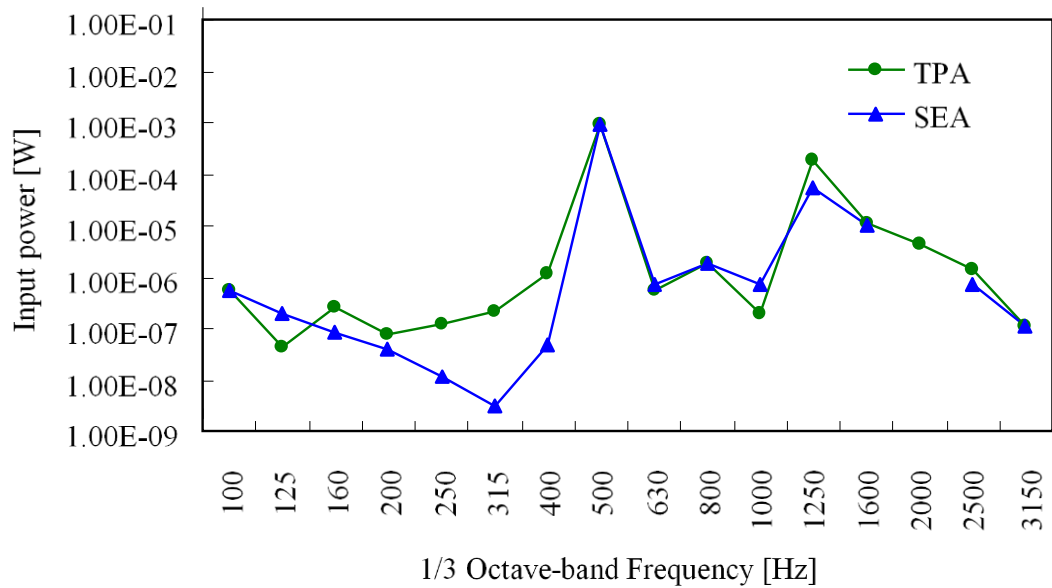
Figure 4.3 Comparison of input power between SEA and TPA of subsystem 1 for case(ii)

4.4.1.3. Contribution rates from power sources

Figure 4.4 and Figure 4.5 show the comparison results of the contribution rates for case (i) and case (ii) respectively. From Figure 4.4 of case (i), the contribution rates by TPA are approximately 50% except for the 1000Hz and 2000Hz bands, and the results by SEA using Equation (4.7) for 160, 250, 1000, 1250, 1600 and 2000Hz bands are away from 50%, whereas the results by SEA using Equation (4.8) are approximately 50%. From procedures (1) and (2), the excitation data of subsystem 2 was replaced by those of subsystem 1 and the results of contribution rates by SEA and TPA are approximately 50%. Namely, it can be said that if the response position of input point and evaluation point are in good condition, then the desired results can be obtained, thus shows the validity of the proposed method for a simple structure consisting of one frame and flat plate. On the other hand, from Figure 4.5 of case (ii), the contribution rates are similar to case (i) accept for between 1000 and 2000Hz bands where the contribution rates by SEA using Equation (4.7) shows value above 100% due to the negative coupling loss factor as stated in section *4.4.1.1*.

71
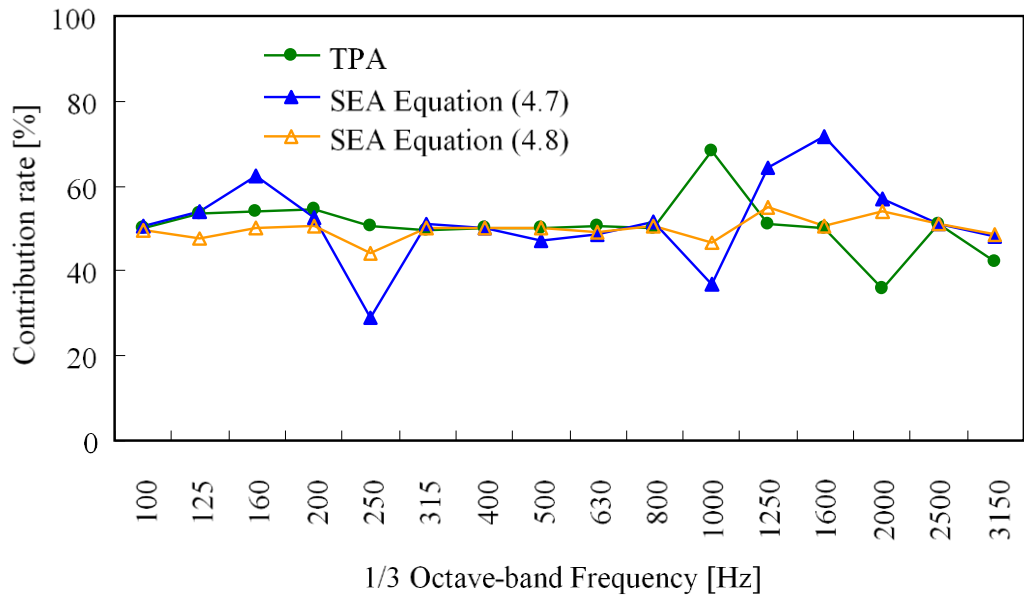
Figure 4.4 Comparison of contribution rates from subsystem 1 to subsystem 3 between SEA and TPA for case(i)
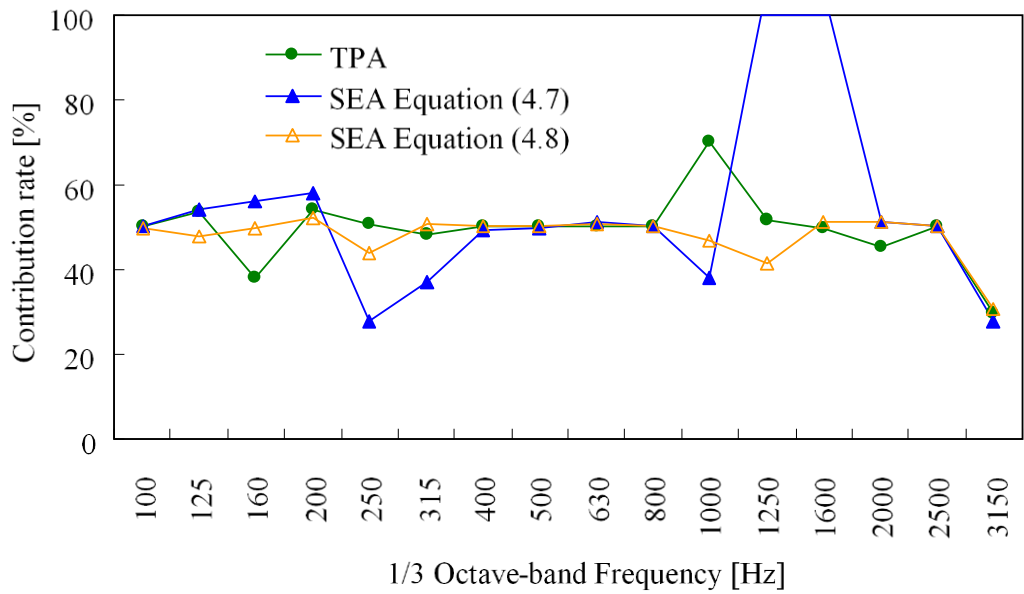
Figure 4.5 Comparison of contribution rates from subsystem 1 to subsystem 3 between SEA and TPA for case(ii)

4.4.2. Test Plate 2 and Analytical Conditions

In order to validate the practicality of the proposed method, an extended version of the structure discussed in the previous section as shown in Figure 4.6 is investigated. The thickness of the panel, cross-sectional dimensions of the frame and material properties are the same as the previous section. The frame of subsystem 1 is connected to subsystems 3, 4 and 5 by the point junction. The frame of subsystem 2 is connected to subsystems 3, 4 and 7 by the point junction. All edges of the plate are pin supported. The information about subsystem is shown in Table 4.1. Figure 4.6 also shows a real operation test. The input and response locations of subsystem 1 and 2 are symmetric, while the locations on the other subsystems are randomized. ED is used instead of SEA as an energy model because the contribution rates from each input subsystem to subsystem 5 are applied as an evaluation point in TPA. The target frequencies are the one-third octave band frequencies from 100Hz to 2kHz. The size of each element in the mesh is about 12.5mm×12.5mm, which is sufficient to contain six nodes per bending wavelength up to 2.6kHz. The modal damping ratio is assumed to be 0.1% for subsystem 1 and 2, and 1% for other subsystem for all modes.
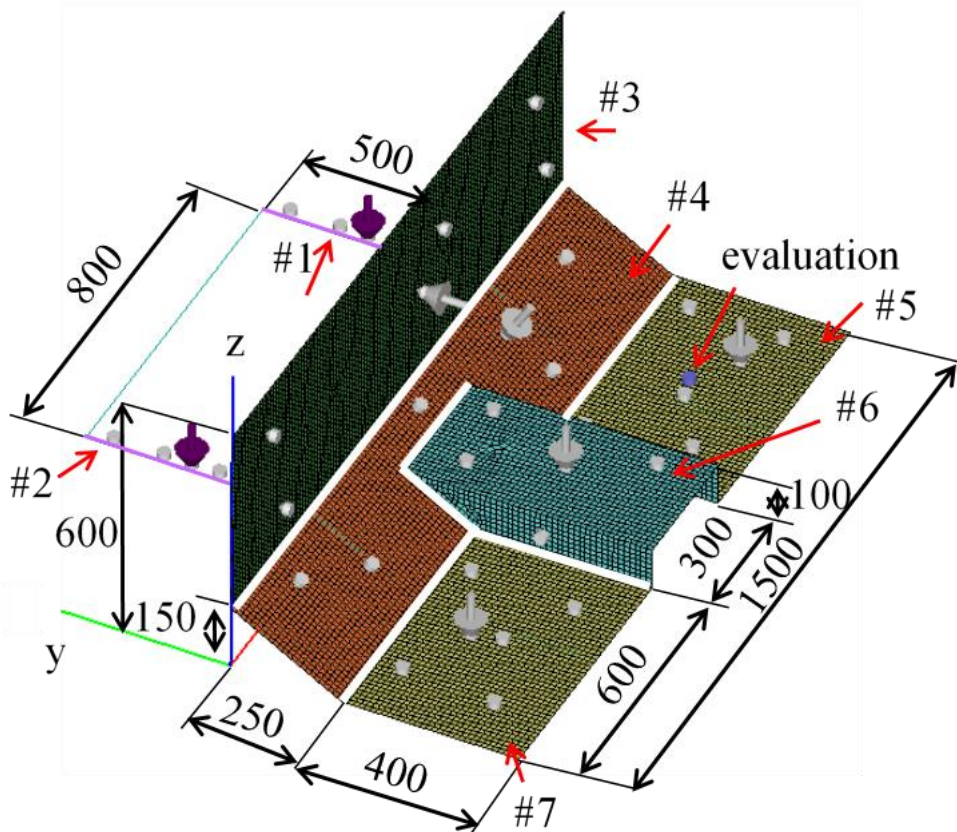
Figure 4.6 Test structure 2 (grey and purple arrows: excitation, grey cylinders: response, blue cylinder: evaluation point)

Table 4.1 Subsystems information for Test Plate 2

Subsystem number and name	Area (m^2)	Weight (kg)
1. Right frame	-	1.673
2. Left frame	-	1.673
3. Dash panel	0.675	4.212
4. Center plate	0.379	2.365
5. Right floorboard	0.240	1.498
6. Center floorboard	0.267	1.664
7. Left floorboard	0.240	1.498

4.4.2.1. Analysis results and discussions

Following procedures (1) and (2), the TPA input force identified from Equation (4.3) by the matrix inversion method is a unit force in all frequency bands, and thus shows the validity of the model.

4.4.2.2. Identified input power

Figure 4.7 shows the comparison results between the input powers predicted by SEA and by TPA of subsystem 1. A similar trend is obtained as in the case of subsystem 2 as shown in Figure 4.8. From Figure 4.7 and Figure 4.8, the prediction results of SEA are quantitatively similar to those of TPA using Equation (4.6) except for the frequency bands from 200 to 400Hz. Therefore, the proposed method was also shown to be useful on a complicated structure consisting of one frame for two subsystems and thin flat plates for five subsystems.
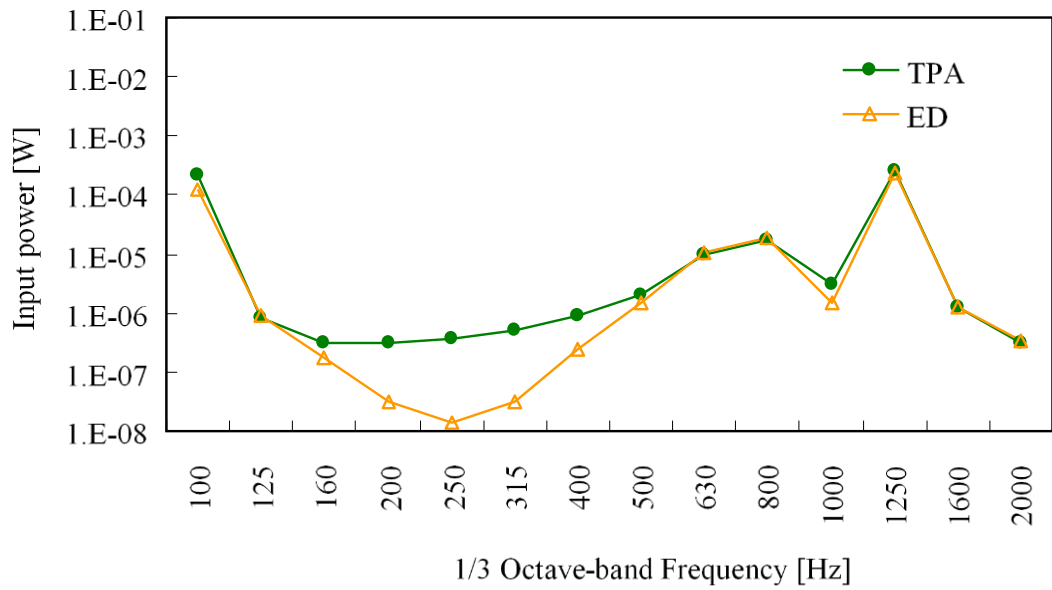
Figure 4.7 Comparison of input power between SEA and TPA of subsystem 1
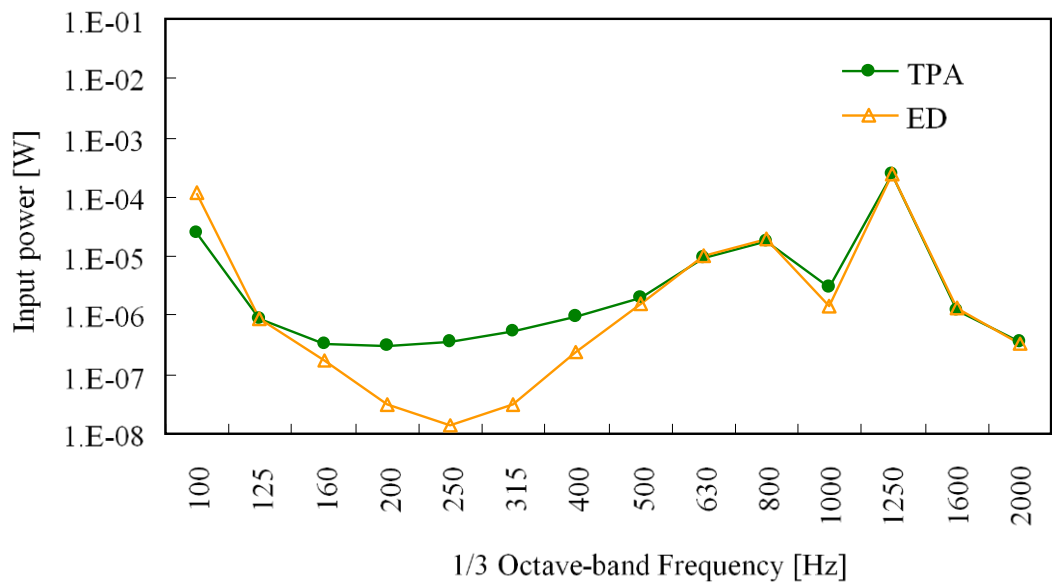
Figure 4.8 Comparison of input power between SEA and TPA of subsystem 2

4.4.2.3. Contribution rates from power sources

Figure 4.9 and Figure 4.10 show the comparison results of the contribution rates between SEA and TPA from subsystem 1 to subsystem 5, and from subsystem 2 to subsystem 5 respectively. In ED, negative values of loss factors were found and thus comparison between SEA predicted from Equation (4.7) and TPA became difficult. Therefore the comparison result by newly proposed Equation (4.8) is shown. From Figure 4.9 and Figure 4.10, there are areas that are quantitatively similar and qualitatively different. However, by applying the Equation (4.8) to make a comparison between the contribution rates from a power source, the effectiveness of the proposed method has been verified for the complicated structure consisting of frame and thin flat plates.
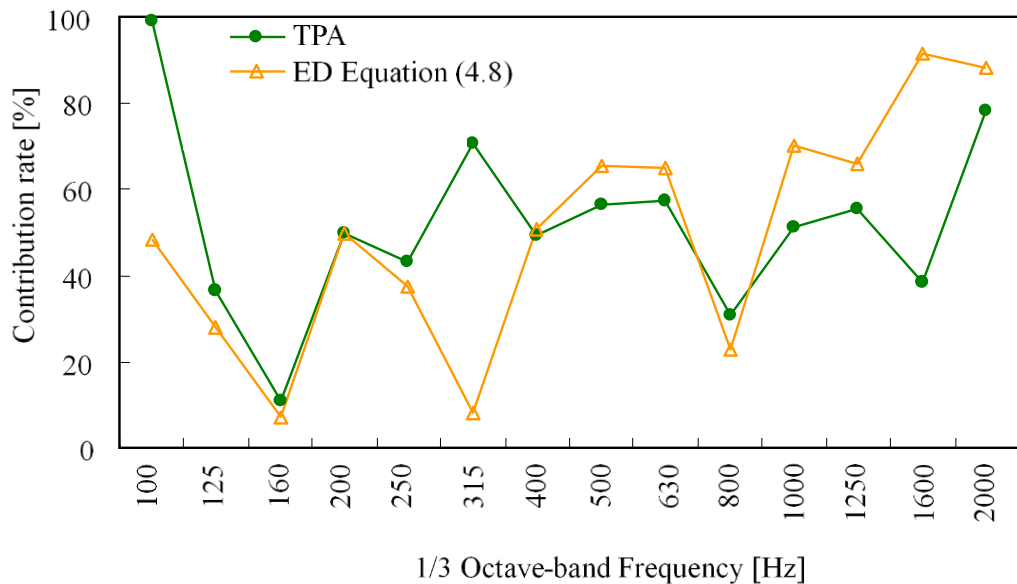
Figure 4.9 Comparison of contribution rates from subsystem 1 to subsystem 5 between SEA and TPA
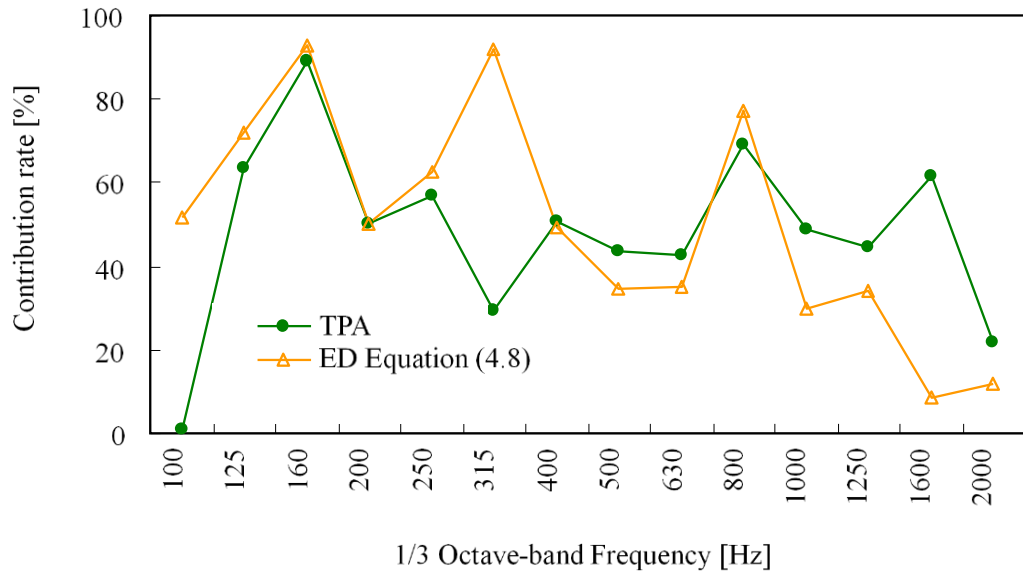
Figure 4.10 Comparison of contribution rates from subsystem 2 to subsystem 5 between SEA and TPA

4.5. Conclusion

In this chapter, with the aim of realizing the utilization of comparison method between input powers and contribution rates from SEA and TPA, the method was extended to the practical structure represented by the thin-walled plane frame structures. The following conclusions were drawn from this investigation;

1) In regards to input source, the identified input power during frame input by SEA relatively and quantitatively agrees with identified input power using TPA matrix inversion method that used the result of response at excitation point. This shows the validity of the proposed equation.

2) In regards to the contribution rates from power sources, it was shown that it is possible to compare contribution rates of new energy model for both SEA and TPA using proposed evaluation equation.

References

[1] Kuroda, K., and Yamazaki, T., 2013, "A Study on Comparison between Input Powers and Contribution Rates from Statistical Energy Analysis and Transfer Path Analysis on a Mechanical Structure," Journal of System Design and Dynamics, **7**(4), pp. 504-515.

[2] Kuroda, K., Yamazaki, T., Hilmi, H. L., and Koizumi, T., 2013, "Comparison between Input Powers and Contribution Rates from Energy Analysis and Transfer Path Analysis on Thin-Walled Plane Frame Structures," Proceedings of 15th Asia Pacific Vibration Control Conference, pp. 1326-1330.

[3] Kuroda, K., Yamazaki, T., 2012, "Comparison of SEA and TPA for Input Source and Contribution Rates," The Proceedings of 41st International Congress on Noise Control Engineering, pp. 8307-8318.

[4] Kadomatsu, K., and Iwanaga, Y., 2002, "Vibro-Acoustic Transfer Function and Driving-Point Conductance for Vehicle Body (in Japanese)," Transactions of the Japan Society of Mechanical Engineers. C, **68**(676), pp. 3561-3565.

[5] Kobayashi, S., and Yoshimura, T., 2009, "Identification of Excitation Force Spectra Using Apparent-Mass Matrix (in Japanese)," Transactions of the Japan Society of Mechanical Engineers. C, **75**(753), pp. 1500-1507.

[6] David, C., Herrin, W. D., Harvind, R., and Jiantie, Z., 2011, "Obtaining Structure-Borne Input Power for a SEA Model of an Earthmoving Machine Cab," SAE Technical Paper, 2011-01-1732.

CHAPTER 5

Experimental Verification of SEA-TPA Comparison Method

5.1. Introduction

As mentioned in Chapter 4, we proposed a method to compare SEA evaluated by power injection method and TPA evaluated by matrix inversion method, and it is validated through numerical analyses, using finite element method (FEM). We extended the application of the proposed method to the practical structure represented by thin-walled plane frame structures, which is a real simulated engine mount frame and front panel as shown in Figure 4.1 and Figure 4.6.

In previous findings, we have verified the validity of the proposed method in various numerical analysis using FEM from simple 2-subsystems structure[1] to complex structures of partial car model[2][3]. However, the validity and practicality of the proposed method could not be sufficiently verified without an actual practical experiment involving real structures.

In this chapter, we extended the application our research on an enclosure model of a 20kW class power generator and simplified it by constructing a partial enclosure model of a simple structure consisting of two L-shaped plate structure with 3-point connection[4]. We aim to verify the practicality of this comparison method proposed in Chapter 4 by conducting an experimental verification using partial model plate structure of the enclosure model of a 20kW class power generator.

5.2. Validating the Proposed Method on Application Structure Through Numerical Analysis

5.2.1. Analytical Overview and Conditions

In this section, the proposed method is validated through numerical analyses using FEM. We focused our research on a small power generator's enclosure, and we simplified it by constructing a partial enclosure model of a simple structure consisting of two L-shaped plate structure coupled with bolts and spacers.

5.2.1.1. Finite element model of panel and base

We constructed the FE models of one of the enclosure's panel and the base. Figure 5.1 and Figure 5.2 shows FE models that were constructed using finite element analysis software I-DEAS. Table 5.1 shows the material properties and dimensions of each model, and Table 5.2 shows the parameters to generate the mesh model of each subsystem. Figure 5.3 and Figure 5.4 shows the comparison results of vibration acceleration at excitation point (indicated by crosses), between FE models and vibration measurement results where the boundary condition was free-free condition. The analysis results show good agreement with measurement results. Moreover, Figure 5.5 and Figure 5.6 shows the number of modes on each subsystem in 1/3 octave band frequency. Therefore, analysis can be done at the same level and conditions as the actual experiment.
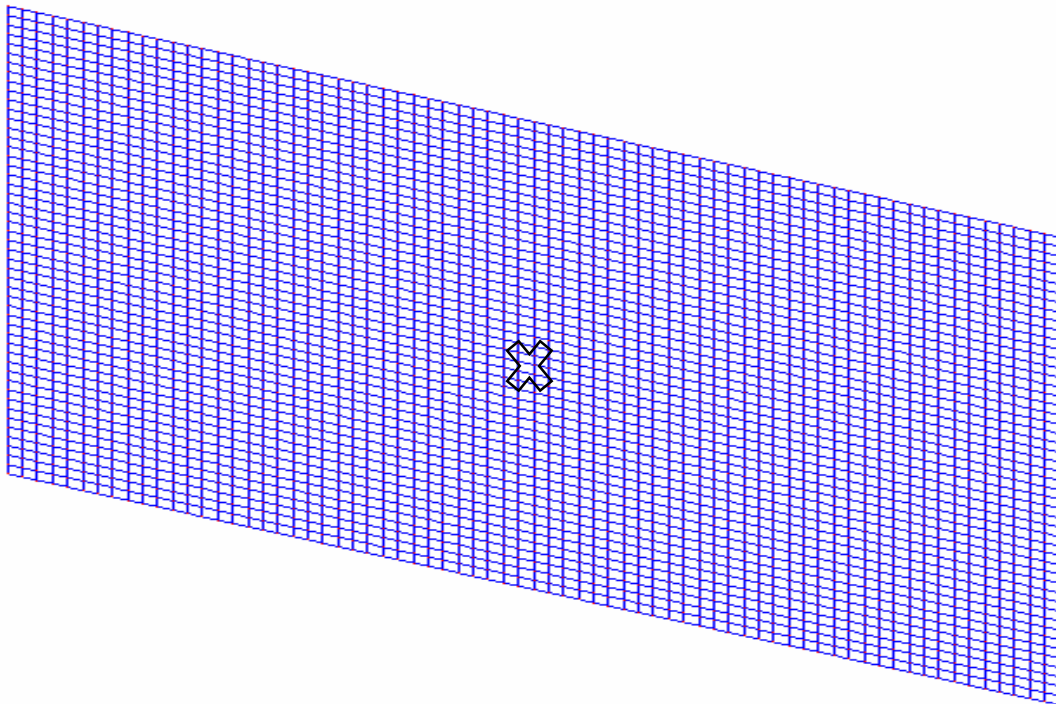
Figure 5.1 Finite element model of the panel
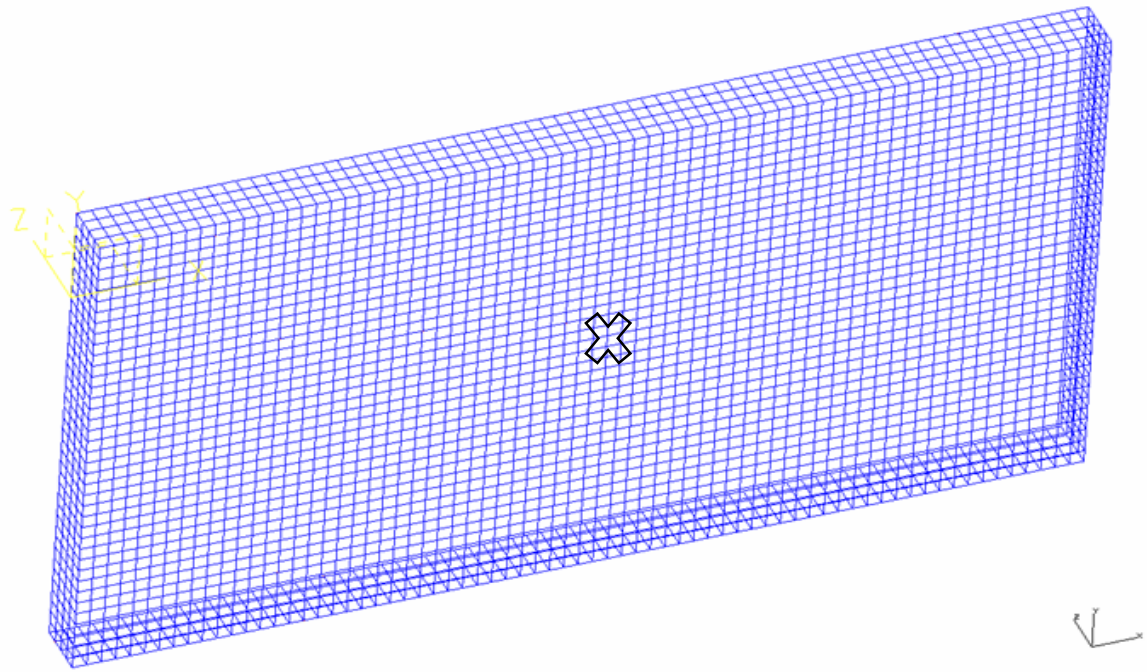
Figure 5.2 Finite element model of the base

Table 5.1 Material properties and dimensions

	Panel	Base
Thickness	1.6mm	2.3mm
Width	500mm	390mm
Length	700mm	
Young's Modulus	205GPa	
Density	7500kg/m^3	
Poisson's Ratio	0.3	
Structural Damping	1%	

Table 5.2 Parameters to generate mesh models

	Panel	Base
Mesh Length	5mm	
Node Count	14382	14627
Element Count	14140	14408
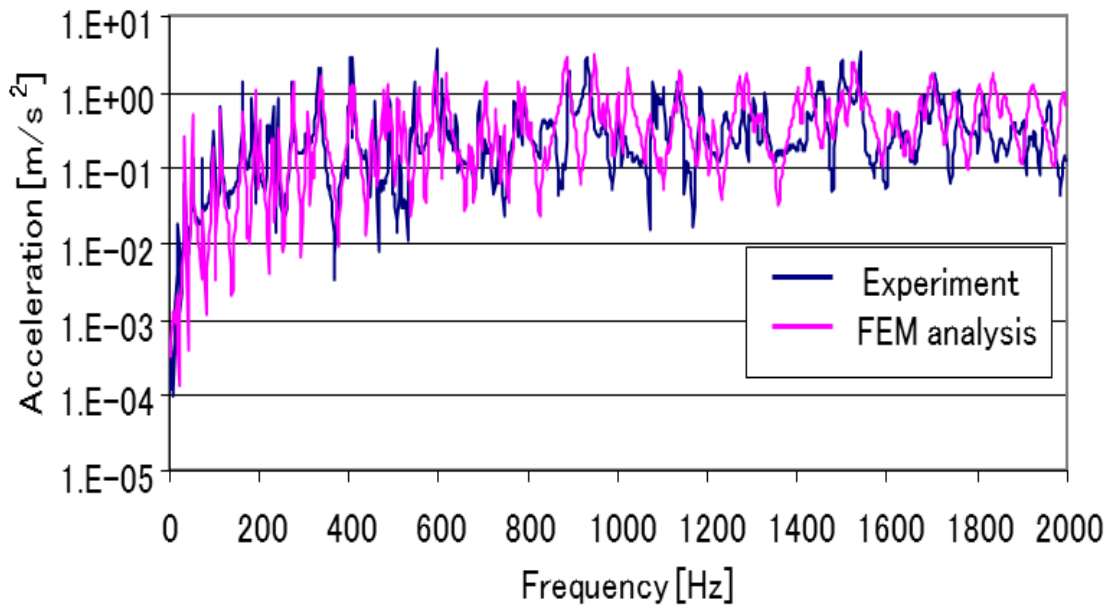
Figure 5.3 Comparison results between the vibration acceleration of experiment and FEM analysis for Panel
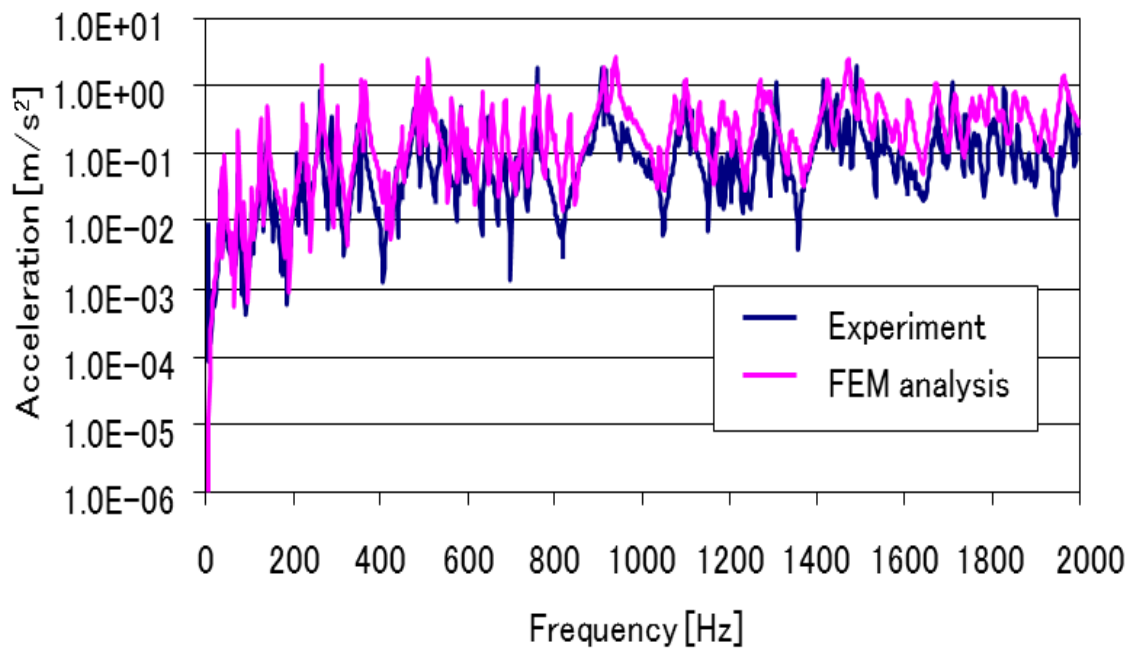
Figure 5.4 Comparison results between the vibration acceleration of experiment and FEM analysis for Base
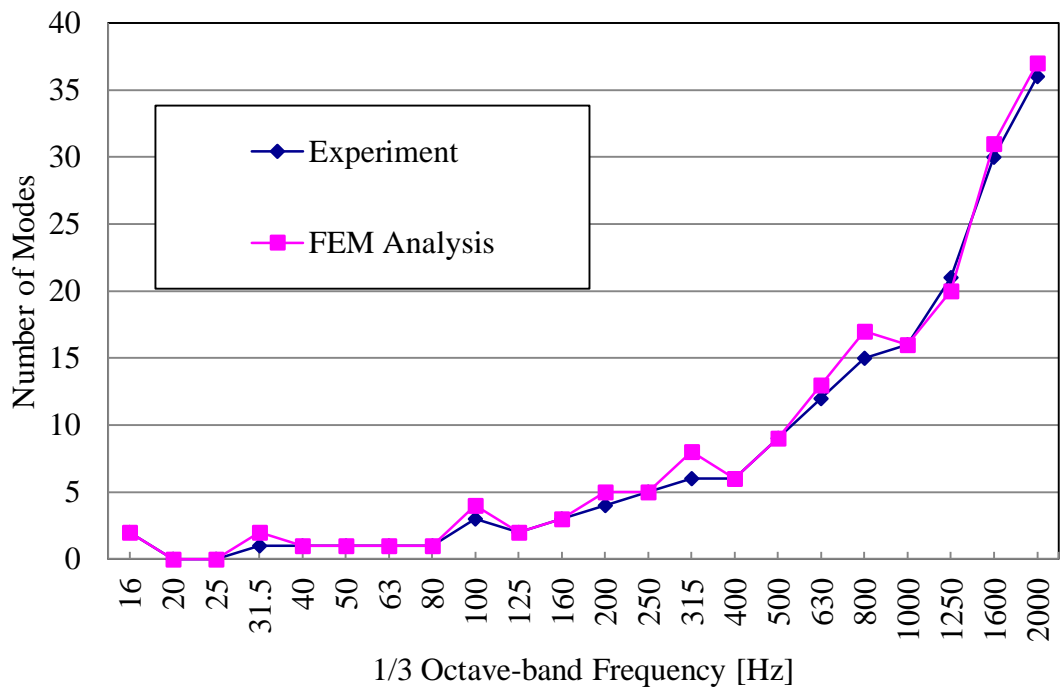
Figure 5.5 Comparison result between experiment and FEM analysis for the number of modes (Panel)
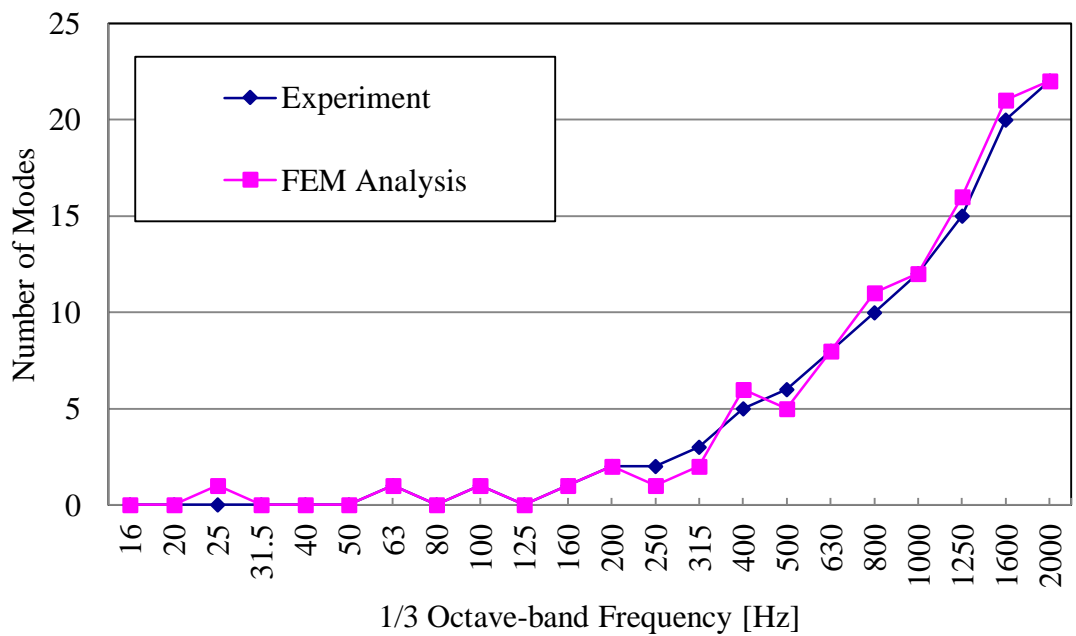
Figure 5.6 Comparison result between experiment and FEM analysis for the number of modes (Base)

5.2.1.2. Finite element model of L-shaped structure

We constructed a free boundary condition FE model of the two subsystems coupled with the three bolts by using the FE models constructed in the previous section. To construct the accurate FE model of the bolts and spacers, we connected each node corresponding to the bolt position with bar elements using the TUBE type. The thickness of the panel is 1.6mm and the distance of the gap between the panel and the base is 15mm. To consider the equivalent stiffness of the contact surface, we connected the nodes surrounding the node corresponding to the bolt positions with rigid bar element (RBE). Figure 5.7 shows the constructed FE model of the coupled subsystems.
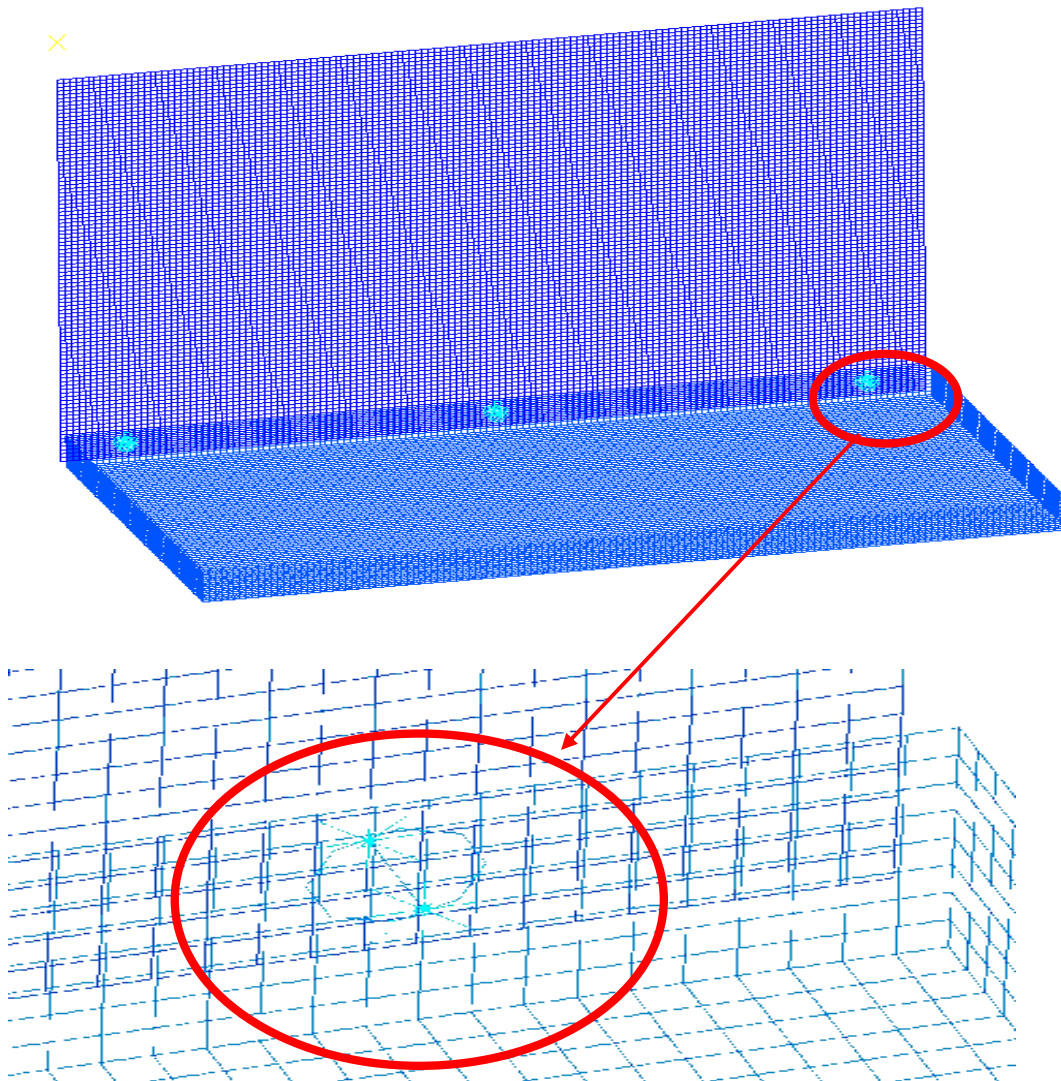
Figure 5.7 FE model of L-shaped structure where the bolt connection is circled in red

Figure 5.8 shows the locations of excitation points, evaluation and response locations on a two-dimensional view of the FE model. The crosses (1 per subsystem), circles (5 per subsystem), triangle, and black hexagon denote the excitation points, response locations, evaluation point and bolts/coupling points respectively. The locations and numbers of the excitation and response points are the same when applying SEA and TPA. However, to calculate the contribution rates from the power source, the TPA evaluation point is located close to the coupling point between the subsystems which is near the bolt, in order to make a comparison with the SEA results in which the power flow rates between subsystems are considered.

We utilized NX-NASTRAN for the finite element analysis. The target frequencies are one-third octave band frequencies from 16Hz to 2000Hz for the evaluation of thin plate structure including for frequency band with low number of modes. Furthermore, the structural damping for the coupled system is set at 6% for the base and 15% for the panel. As for the bolts and spacers, we set the structural damping at 1%. The magnitude of excitation force for the FE model was taken from the actual experimental measurements, which will be explained in the next section.

Excitation �ख , Response point ◯ , Evaluation point △ , Coupling point ⬣
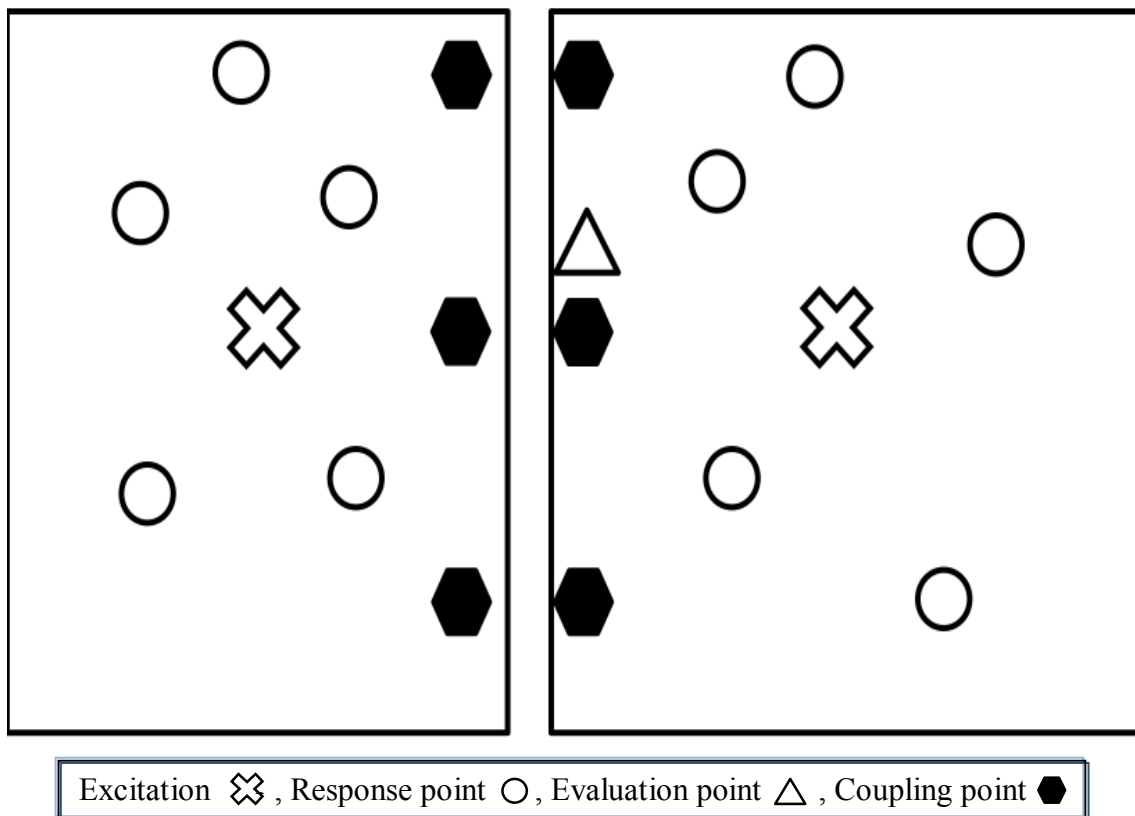
Figure 5.8 L-shaped structure in two-dimensional view (left: base, right: panel)

5.2.2. Examination Procedure

Based from the procedures proposed in section 4.3 of Chapter 4, the procedure for comparing the input powers and contribution rates given by SEA and TPA involves three steps;

1. Construct experimental models to identify the SEA loss factors in Equation (3.16) and the FRF matrix $[H_{mn}]$ for TPA in Equation (4.1).

2. Perform a machine operation test.

3. Identify the input powers and contribution rates.

5.2.3. Results and Discussions

5.2.3.1. Identified input power

Figure 5.9 and Figure 5.10 shows the comparison result of input powers predicted by SEA and TPA. The prediction results of SEA are quantitatively similar TPA for both base and panel. Therefore, the proposed method was shown to be valid on a simple structure consisting two panels with particular coupling. These results also confirms the validity of this method using FEM, as shown in previous studies.
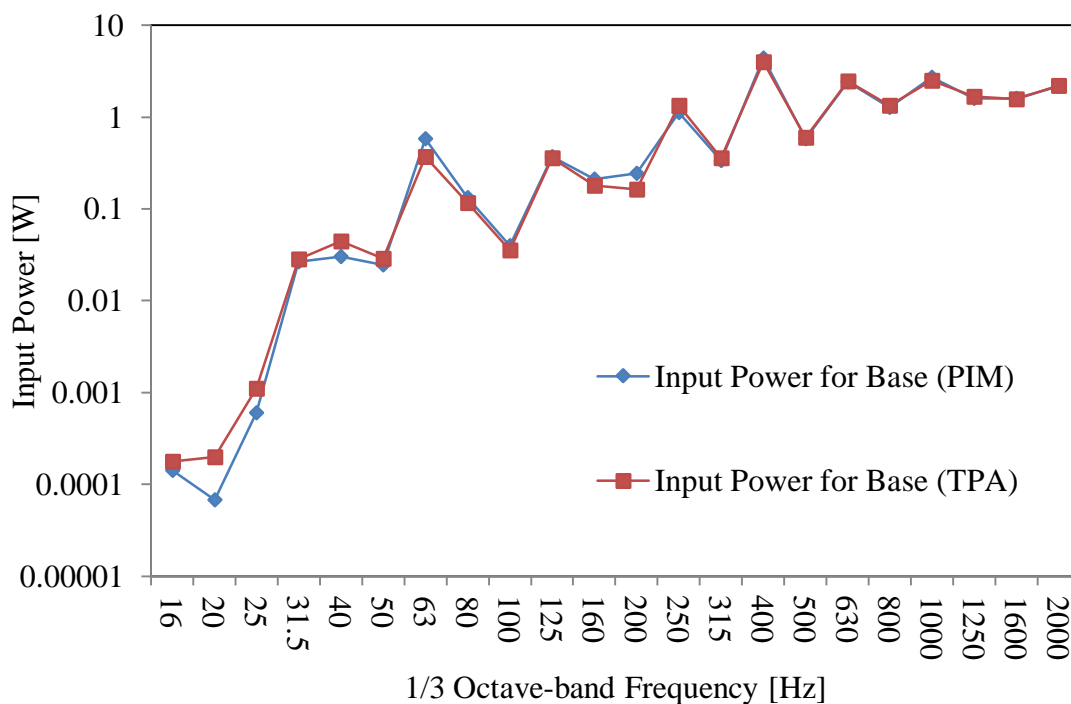
Figure 5.9 Comparison of identified input powers for Base between SEA using PIM and TPA using matrix inversion method
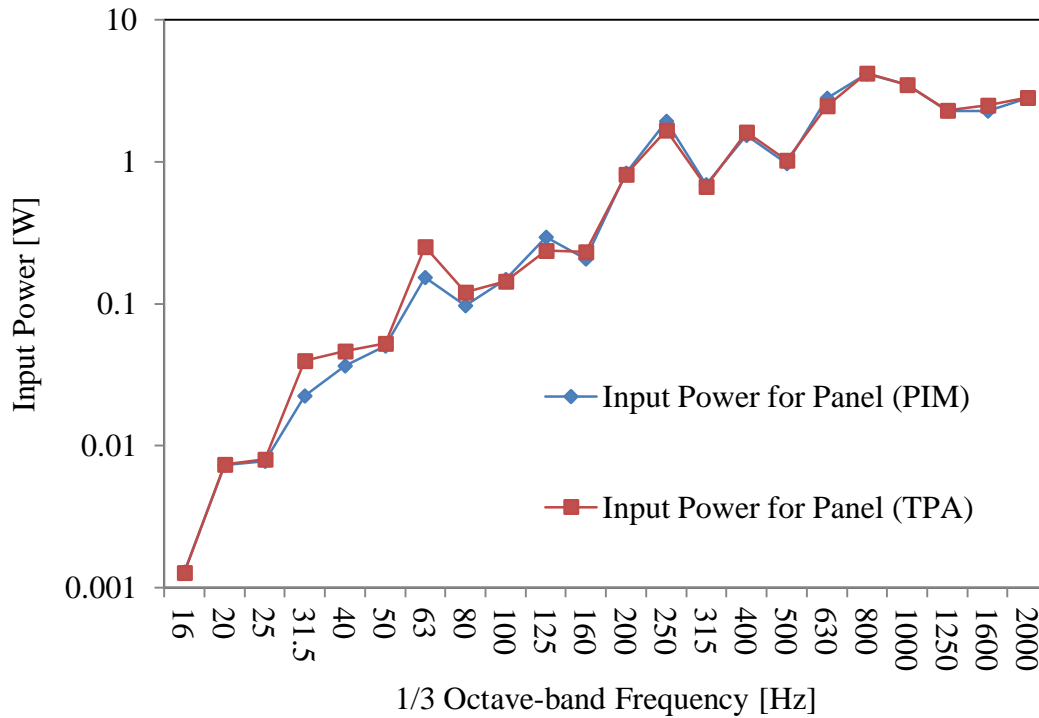
Figure 5.10 Comparison of identified input powers for Panel between SEA using PIM and TPA using matrix inversion method

5.2.3.2. Contribution rates from power sources

Figure 5.11 and Figure 5.12 shows the comparison result of the contribution rates calculated by SEA and TPA. From the results, the contribution rates did not exceed 100% and are always positive when the proposed method for comparing SEA and TPA is applied through Equation (4.8) for SEA and Equation (4.9) for TPA without consideration of the response phase. The SEA and TPA results are qualitatively similar, except for the 40Hz, 125Hz, and 1250Hz bands. We can conclude that the positioning and conditions of excitation points and evaluation point could affect the contribution rates between SEA and TPA.
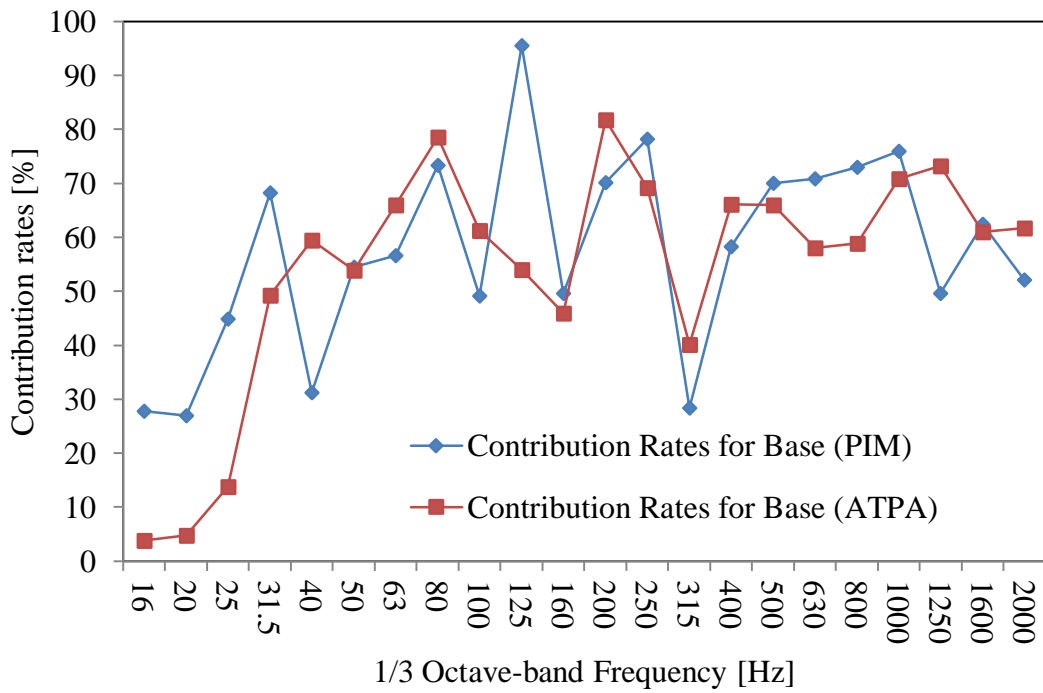
Figure 5.11 Comparison of contribution rates from Base to Panel between SEA using PIM and TPA without considering phase
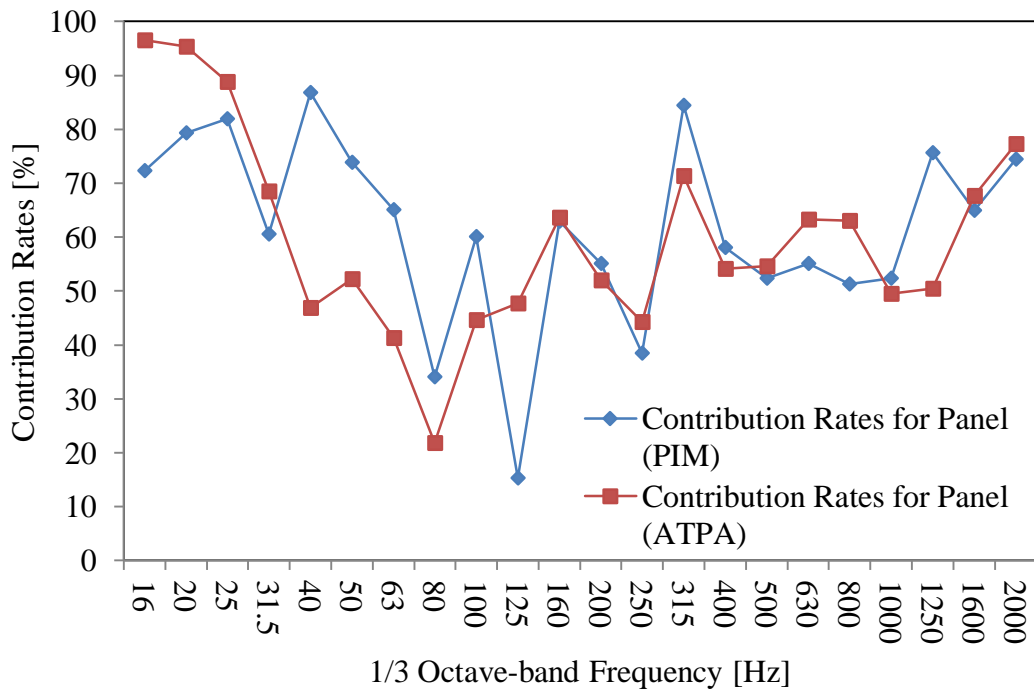
Figure 5.12 Comparison of contribution rates from Panel to Base between SEA using PIM and TPA without considering phase

5.3. Experimental Verification

5.3.1. Test Equipment and Experimental Method

Figure 5.13 shows the outline view of the L-shaped partial structure of the power generator's enclosure. It is coupled with 3 bolts and spacers, which are tightened at standard tightening torque. Figure 5.14 shows the detailed view of one of the bolt and spacer. Table 5.3 shows the dimensions of the structure. Figure 5.15 and Figure 5.16 show the experimental view where the shakers are circled in Figure 5.15. The shakers are fixed with an aluminum dummy stud and mounted on the test structure with strong adhesive. The test structure is suspended on 4 points using rubber ropes to create a free-free boundary condition as circled in Figure 5.16.

Table 5.4 shows the experimental conditions and equipment for the comparison test. We conducted 3 excitation models where each subsystem is excited separately at one point based on SEA's power injection method (PIM), and both subsystems excited simultaneously. Each measured magnitude forces are then utilized for the FE analysis in order to create the same conditions as the actual machine operation. Moreover, the excitation position, response positions and numbers, and evaluation point's position are the same with FE analysis.

Figure 5.13 View of L-shaped partial structure of enclosure

Figure 5.14 Detailed view of bolt and spacer connection

Shaker

Aluminum
dummy stud
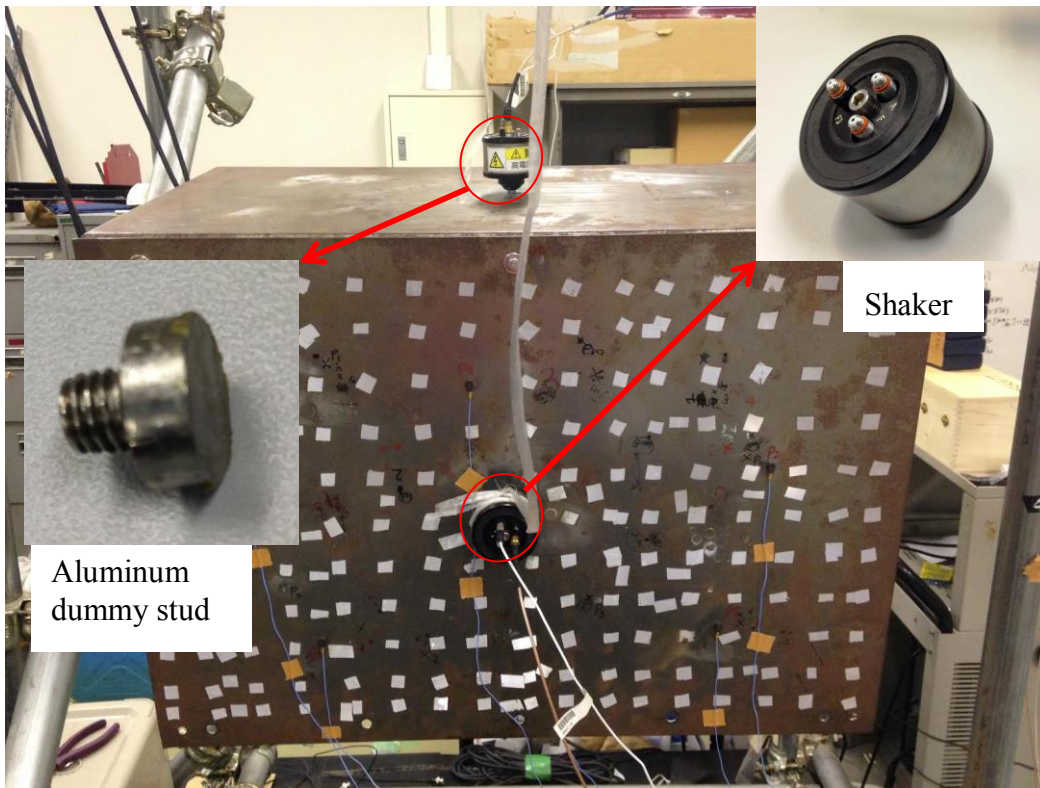
Figure 5.15 Experimental view
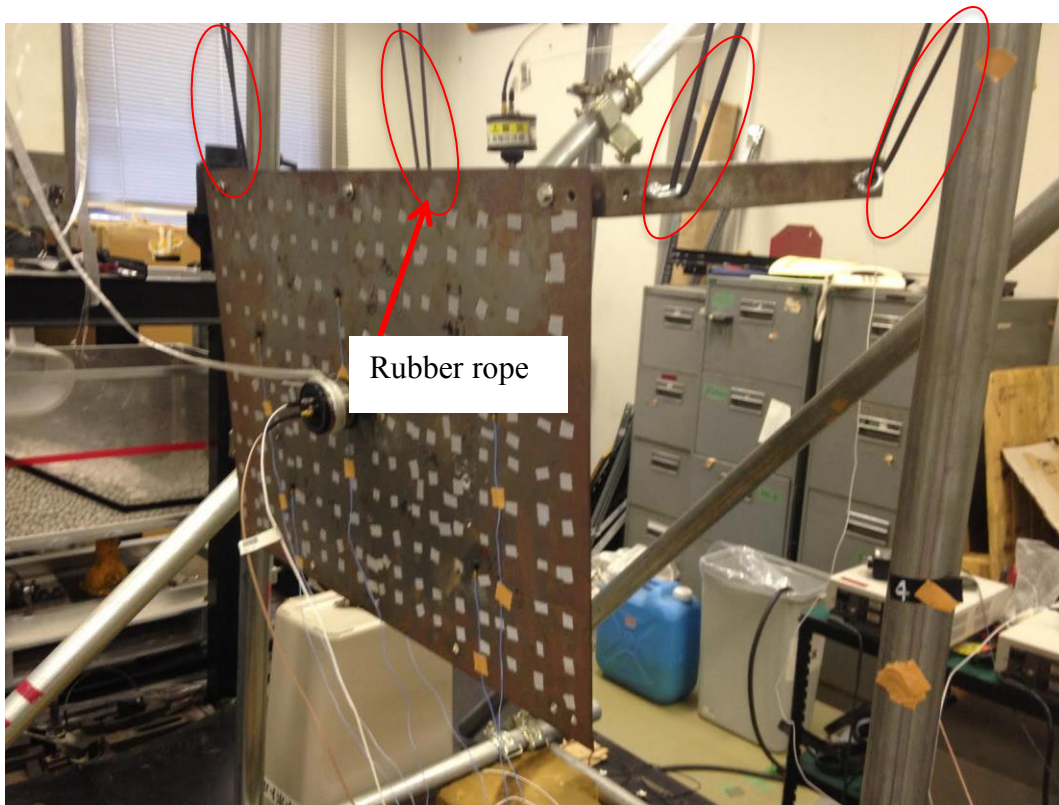
Figure 5.16 Experimental view (free-free boundary condition)

Table 5.3 Structure's information

Dimensions	(500x700x390)mm
Panel's thickness	1.6mm
Base's thickness	2.3mm

Table 5.4 Experimental information

Test analyzer	LMS Test Lab
Shaker	Wilcoxon, F3/Z602WA
Accelerometer	PCB, 352C22
Sampling frequency	8192Hz
Resolution frequency	2Hz
Signal type	Periodic chirp

5.3.2. Results and Discussions

5.3.2.1. Identified input power
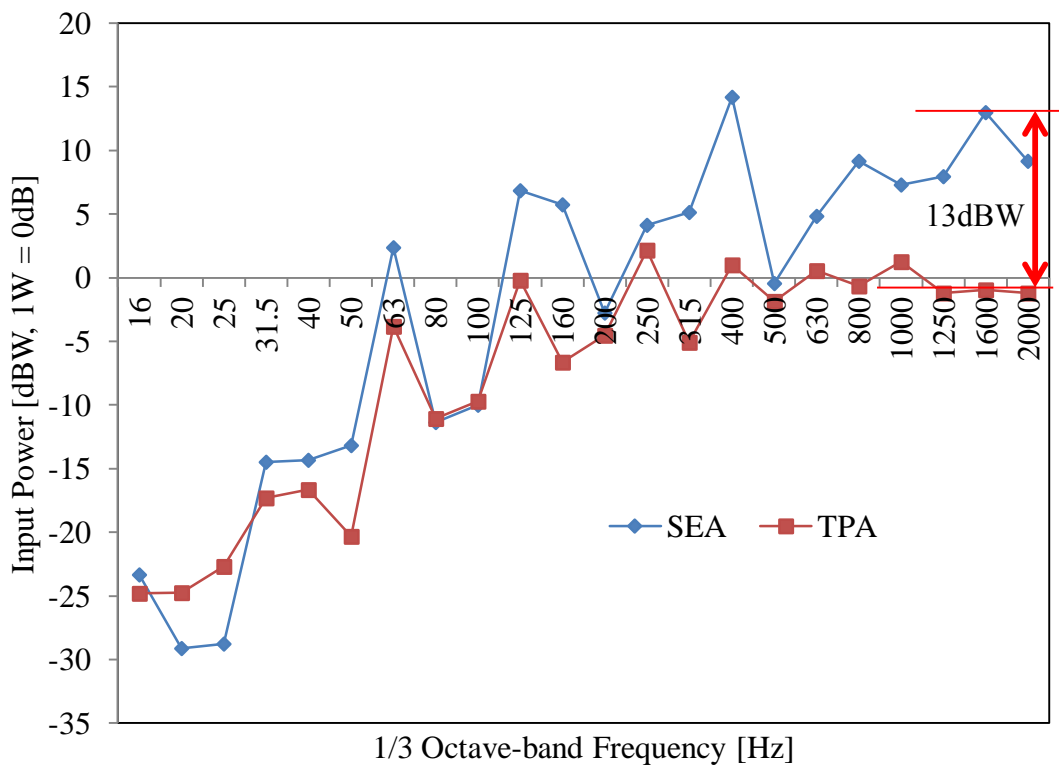
Figure 5.17 Input powers comparison of Base between SEA and TPA

93
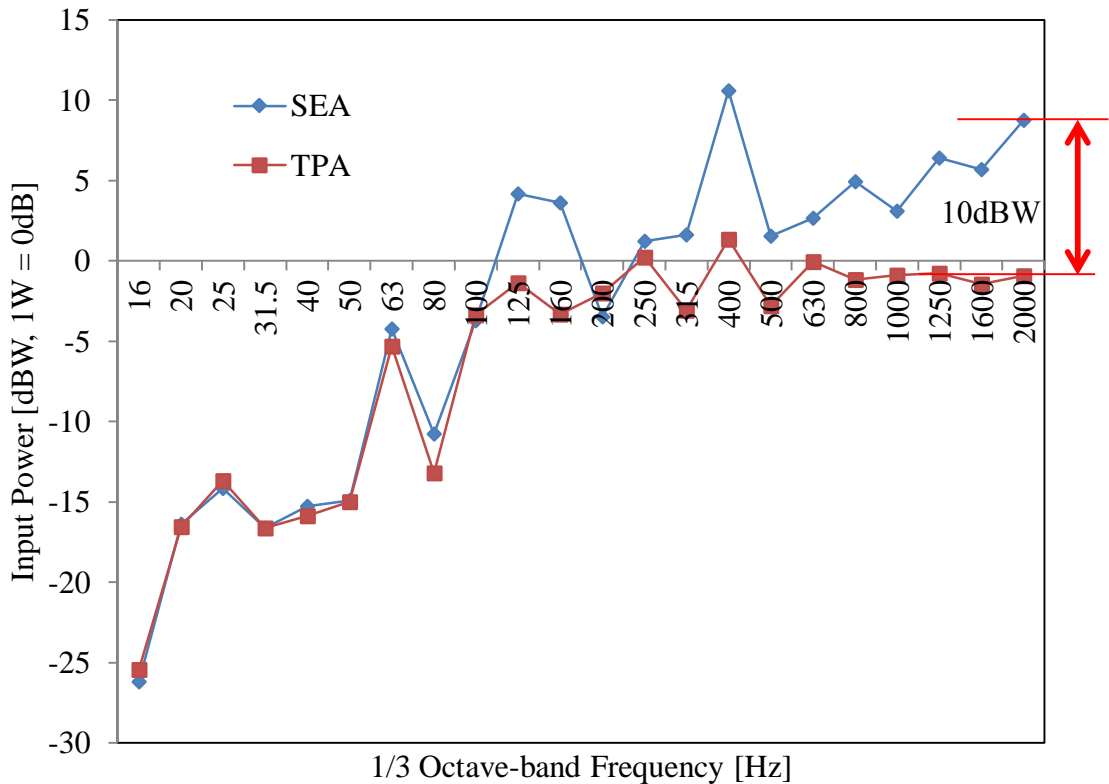
Figure 5.18 Input powers comparison of Panel between SEA and TPA

Figure 5.17 and Figure 5.18 show the comparison result of input powers predicted by SEA and TPA. The prediction results shows similar trend between input powers predicted by SEA and TPA on both the base and panel. However, there are differences up to 10dBW particularly above 630Hz band due to insufficiency in measurements results particularly on excitation level where we could not achieve good excitation on higher frequencies. However, due to the similar tendency of the results, the practicality of the proposed method could be verified when compared to the results shown by FEM analysis previously using the same model.

5.3.2.2. Contribution rates from power sources

Figure 5.19 and Figure 5.20 show the comparison result of the contribution rates calculated by SEA and TPA. From the results, the contribution rates calculated by TPA did not exceed 100% and are always positive when the proposed method for comparing SEA and TPA is applied through Equation (4.9) without consideration of the response phase as in Equation (4.11). The SEA and TPA results are qualitatively similar, except for the 40Hz, 125Hz, and 500Hz bands. This is because, while the evaluation point in TPA is considered as the normalized average response of evaluated component using from excitation point's response, contribution rates in SEA is the evaluation of the coupling loss factor between components. Therefore, in the calculation of contribution rates by SEA by Equation (4.7), damping loss factor was taken into consideration and could affect the differences between SEA and TPA.

94
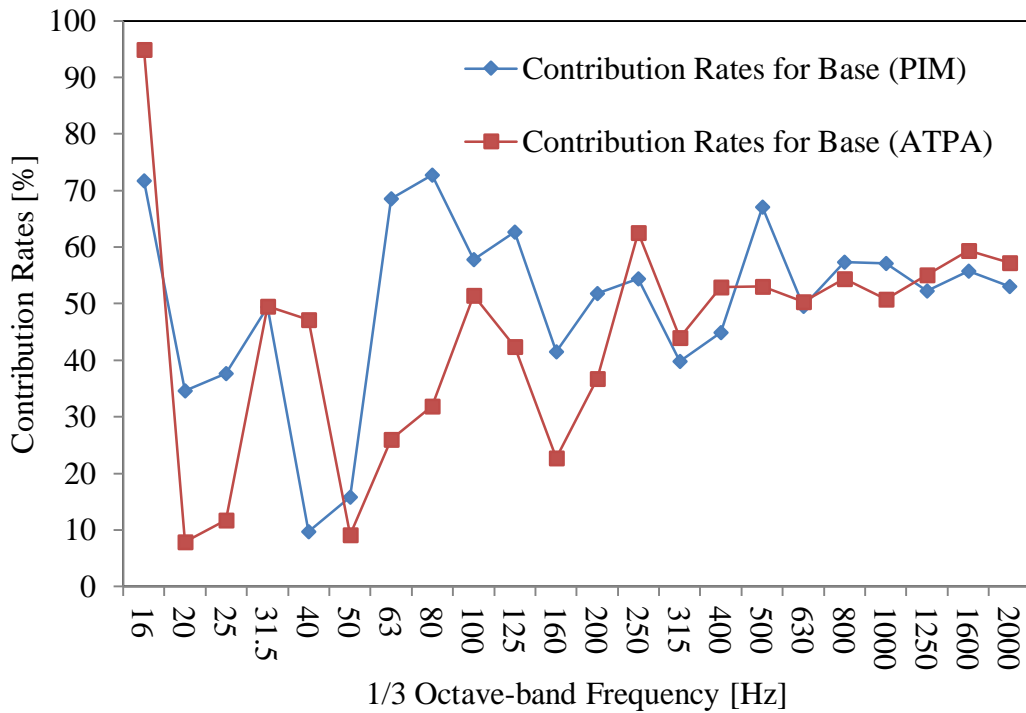
Figure 5.19 Comparison of contribution rates from Base to Panel between SEA using
PIM and TPA without considering phase
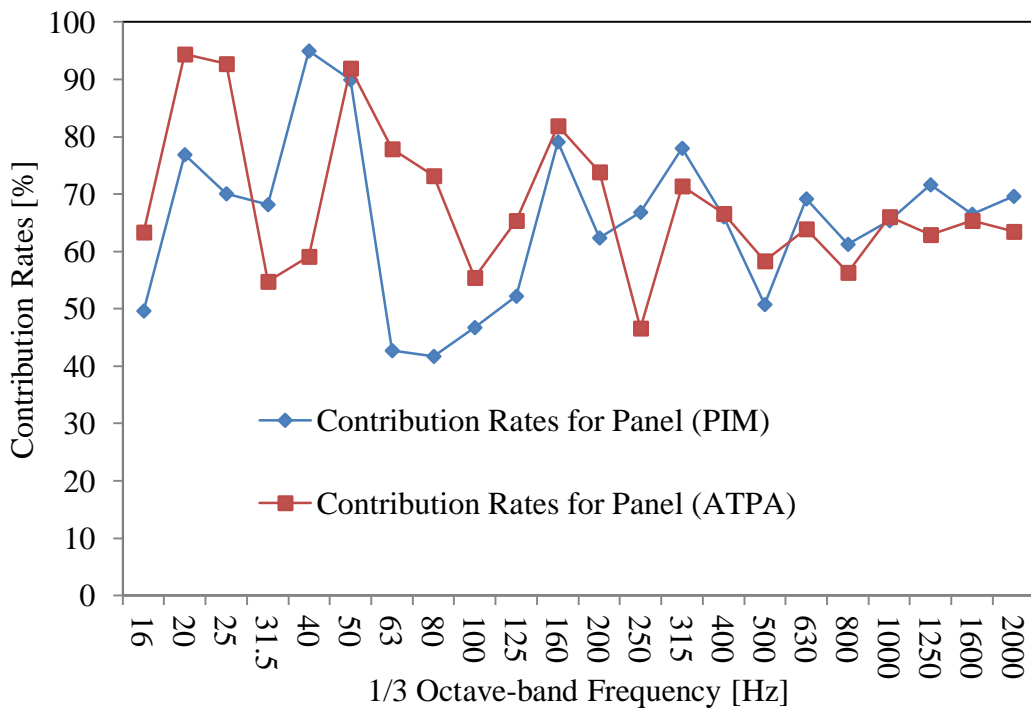
Figure 5.20 Comparison of contribution rates from Panel to Base between SEA using
PIM and TPA without considering phase

95

5.4. Conclusion

The comparison method of input powers and contribution rates between statistical energy analysis method and transfer path analysis method via matrix inversion method was proposed, and it is validated by simulation and its practicality is verified by experiment. The following conclusions can be drawn from this research;

1) The predicted input powers using SEA quantitatively agrees with TPA based on the FE analysis results, thus shows the validity of this method.

2) The experimental results of predicted powers using SEA have similar trend with TPA thus shows the practicality of this method on real structure. However, there are some differences particularly on higher frequencies due to insufficiency in measurement results.

3) When applying the proposed method to make a comparison between the contribution rates from a power source, the SEA and TPA results are qualitatively similar without considering the response phase.

References

[1] Kuroda, K., Yamazaki, T., 2012, "Comparison of SEA and TPA for Input Source and Contribution Rates," The Proceedings of 41st International Congress on Noise Control Engineering, pp. 8307-8318.

[2] Kuroda, K., and Yamazaki, T., 2013, "A Study on Comparison between Input Powers and Contribution Rates from Statistical Energy Analysis and Transfer Path Analysis on a Mechanical Structure," Journal of System Design and Dynamics, **7**(4), pp. 504-515.

[3] Kuroda, K., Yamazaki, T., Hilmi, H. L., and Koizumi, T., 2013, "Comparison between Input Powers and Contribution Rates from Energy Analysis and Transfer Path Analysis on Thin-Walled Plane Frame Structures," Proceedings of 15th Asia Pacific Vibration Control Conference, pp. 1326-1330.

[4] Hilmi, H. L., Kuroda, K., Tsujiuchi, N., and Ito, A., 2015, "Comparison Method of Input Powers and Contribution Rates Between Statistical Energy Analysis and Transfer Path Analysis for Small Power Generator's Enclosure", SAE Technical Paper, (2015-32-0774).

CHAPTER 6

Conclusions and Recommendations

6.1. Conclusions

In this thesis, we have established new theoretical approaches as well as some basic practical applications in the development of noise and vibration analysis for structures involving transfer path and sound source from airborne noise and structure-borne noise. These new approaches were extracted from the existing experimental and analysis technique of noise and vibration for structures, which will improve their efficiency and reliability for noise and vibration reduction on industrial machineries as well as other machines. The following conclusions can be drawn from chapters discussed in this thesis.

1) In chapter 2, we have established new approaches in inverse numerical acoustic analysis, to reduce the identification error of sound source by using different boundary condition and new placement technique of sound pressure measurement points. In acoustic input, when the influence of the transmitted sound is large conditions occur in which we cannot assume that the surface vibration of the object to be the sound source due to the difference occurred between measured surface vibration and identified vibration results. Furthermore, for new placement technique of sound pressure measurement points using space filling design, the surface vibration prediction result of a vibrating body by inverse acoustic analysis is more stabilized, compared to the conventional square lattice shape when the number of surface vibration sound sources is greater than the number of sound pressure measurement points. It has the same stability as the surface vibration prediction results of circular shape measurement points' arrangement method.

2) In chapter 3, we have established new approaches in vibration analysis and prediction of structure-borne noise using statistical energy analysis method. We proposed a damping loss factors estimation technique, which can determine the damping loss factors of a modified structure by estimating the amount of change in damping loss factors of a structure form when attached with damping material. We also proposed and verified a technique to determine the number of measurement points by estimating the variance of analysis results prior to performing experiments using power injection method. By using the variance of the average values from the measurement results of the elements, which has the highest contribution, the actual variance of analysis results for the different average numbers were estimated.

3) In chapter 4, we have established an evaluation method to compare statistical energy analysis method (SEA) and transfer path analysis method (TPA) for multiple excitation input sources and transfer path contributions between excitation sources and evaluation points. We verified the applicability of the proposed method on a more common structures consisting of thin plates and frames through numerical analyses using a finite element method (FEM) of thin plate structures consisting two or more subsystems. The identified input power during frame input by SEA relatively and quantitatively agrees with identified input power using TPA. Moreover, it was shown that it is possible to compare contribution rates of new energy model for both SEA and TPA using proposed evaluation equation.

4) In chapter 5, we have established the application of evaluation method to compare SEA and TPA for multiple input sources on real structure through numerical analysis and experimental evaluation. We extended the application of the proposed method on an enclosure model of a 20kW class power generator and simplified it by constructing a partial enclosure model of a simple structure consisting of two L-shaped plate structure with 3-point connection. The experimental results of predicted powers using SEA have similar trend with TPA thus verifying the practicality of this method on real structure. Moreover, SEA and TPA contribution rates results are qualitatively similar when not considering the response phase.

6.2. Recommendations

Based on the knowledge and experiences gained in this research, the following aspects of future work are recommended.

1) From the new approaches and techniques that we have established from chapter 2 to chapter 5, we have only succesfully established the basic principle and theory. Further study needed to be extended towards establishing the proposed approaches and techniques on real structures with real input. For example, Akei et al. have established the application of noise prediction using inverse numerical acoustic analysis on the enclosure of engine with real noise and vibration input from real engine[1]. This extension of application on real life situation could and should strengthen the validity of proposed methods to be applied in real machines in the future.

2) In statistical energy analysis, being a statistical approach, they give statistical answers which are always subject to some uncertainty[2]. Therefore certain measures including optimization methods have been extensively researched upon in order to optimize the parameters estimation thus giving a more reliable vibration prediction results. In our study, we have established new approaches in experimental and numerical analysis to estimate parameters in SEA, thus in order to develop a more reliable prediction results, it is recommended to extend these approaches to merge with optimization method for example using genetic algorithm (GA) in SEA as done by Horii et al.[3]

References

[1] Akei, M., Tsujiuchi, N., Ito, A., and Yamauchi, T., 2015, "Identification of Sound Source Model Using Inverse-Numerical Acoustic Analysis and Noise Prediction for Engine Enclosure," SAE Technical Paper, (2015-01-2250).

[2] Lyon, R. H., and DeJong, R. G., 1995, Theory and Application of Statistical Energy Analysis, Butterworth-Heinemann, Boston.

[3] Horii, H., Miki, M., Koizumi, T., and Tsujiuchi, N., 2005, "Genetic Algorithm Aided Modeling for Structures' Vibration Response Prediction," Journal of Mathematical Modelling and Application of Information Processing Society of Japan, **46**(SIG2(TOM11)), pp. 76-84.

Acknowledgments

In the name of Allah, the Most Gracious, the Most Merciful.

Firstly and foremost, all praise in the world is to Allah, the All Mighty, for the blessings and strengths to finish this research and thesis.

I would like to take this opportunity to express my deep sense of gratitude and profound thanks to my thesis supervisor Professor Nobutaka Tsujiuchi, Department of Mechanical Engineering at Doshisha University, for his instructive guidance and suggestions during the period of my research work since 2012 when I joined this laboratory, Mechanical Dynamics Laboratory as a senior student.

I would also like to express my deep sense of appreciation and profound gratitude to my thesis supervisor Professor Takayuki Koizumi, Department of Mechanical Engineering at Doshisha University, for his guidance, suggestions, and encouragement during the period of my research work even after he retired.

I also would like to express my deep sense of appreciation to Professor Eiichi Aoyama, Professor Toshiki Hirogaki and Professor Kazuya Okubo of Faculty of Science and Engineering at Doshisha University, for their supervision and opinions.

I would like to express my deep sense of appreciation to Professor Katsuhiko Kuroda of Nagasaki Institute of Applied Science, for his supervision and guidance.

I would also like to express my gratitude to Associate Professor Akihito Ito, Dr. Hiroko Oshima and the members of Mechanical Dynamics Laboratory for their help and guidance to conduct my research work. Gratitude is also extended to the members of the advisory committee for their guidance and suggestions and also to Yanmar Co., Ltd. for their help in conducting my research.

I would like to express my gratitude to Yayasan Pelajaran Mara, International Islamic University Malaysia and Ministry of Higher Education Malaysia, for providing the financial support during the period in which this research work was carried out as well as during my study in Japan since 2008.

I wish to pay my gratitude to all my teachers and friends in the school, S.R.K. St. Agnes, S.M. Sains Labuan and S.M. All Saints, and universities, Japanese Associate Degree, Department of Prime Mover Engineering Tokai University.

I also want to thank my parents and families for their inspiration, in spite of being far away from me. I want to thank my wife Nur Idayu Binti Ayob − without her constant support this work might not come into this shape. Finally to Insyirah Humaira Binti Hilmi, for giving me plenty of motivation and happiness.

Hilmi Bin Hela Ladin, November 2015